Energy management of the embedded hydride tanks considering efficiency degradation and life span on fuel cell vehicles

Dan Zhu

UBFC
UNIVERSITÉ
BOURGOGNE FRANCHE-COMTÉ

utbm
université de technologie
Belfort-Montbéliard

THÈSE DE DOCTORAT DE L'ÉTABLISSEMENT UNIVERSITÉ BOURGOGNE FRANCHE-COMTÉ

PRÉPARÉE À L'UNIVERSITÉ DE TECHNOLOGIE DE BELFORT-MONTBÉLIARD

École doctorale n°37

Sciences Pour l'Ingénieur et Microtechniques

Doctorat de Génie électrique

par

DAN ZHU

Energy management of the embedded hydride tanks considering efficiency degradation and life span on fuel cell vehicles

Thèse présentée et soutenue à Belfort, le 26 May 2020

Composition du Jury :

PERREUX DOMINIQUE	Professeur à l'Université de Franche-Comté	Président
FORGEZ CHRISTOPHE	Professeur à l'Université de Technologie de Compiègne	Rapporteur
HINAJE MELIKA	Professeur à l'Université de Lorraine	Rapporteure
GILLIA OLIVIER	Docteur CEA-Grenoble	Examinateur
SARI ALI	Professeur à l'Université de Lyon 1	Examinateur
DJERDIR ABDESSLEM	Professeur à l'Université de technologie de Belfort-Montbéliard	Directeur de thèse
AIT-AMIRAT YOUCEF	Maître de conférence à l'Université de Franche-Comté	Codirecteur de thèse
N'DIAYE ABDOUL	Ingénieur à l'Université de technologie de Belfort-Montbéliard	Codirecteur de thèse

N° | X | X | X |

école doctorale **sciences pour l'ingénieur et microtechniques**

Title: Energy management of the embedded hydride tanks considering efficiency degradation and life span on fuel cell vehicles

Keywords: metal hydride hydrogen storage, proton exchange membrane fuel cell, state of charge estimation, thermal management, long-term operation

Abstract:

Nowadays, the development of alternative energy sources becoming particularly important due to the effect of climate change and fossil fuels depletion. Hydrogen holds great promise thanks to its unlimited resources, high energy density, large technological flexibility and the environmentally friendly nature. With high potential of safety, storing hydrogen with metal hydrides (MH) is considered to be the optimal on-board hydrogen storage method for the future hydrogen vehicle. This thesis therefore contributes to analyzing the performance and proprieties of embedded MH hydrogen storage systems, including the characteristic estimation, dynamic modeling and thermal management coupling with fuel cells.

Firstly, statistical models are proposed for dynamic performance analysis and state of charge (SOC) calculation. The online SOC estimation process is then realized combining a multi-joint state classifier. The dynamic model of the embedded MH tank considering mass and energy conversion is proposed using optimized parameters identified through particle swarm optimization (PSO) algorithm. Moreover, the dynamic behavior of the fuel cell system integrating proton-exchange-membrane fuel cell (PEMFC) and MH hydrogen storage tank is simulated with a mathematical model set and validated using a database from the real operation vehicles. A thermal management strategy with PID controller is proposed to reduce the degradation and extend the lifespan of PEMFC. Finally, a test bench is designed in laboratory and experiments are carried out to validate the proposed models and strategies.

Titre : Energy management of the embedded hydride tanks considering efficiency degradation and life span on fuel cell vehicles

Mots-clés : stockage d'hydrogène à hydrure métallique, pile à combustible à membrane échangeuse de protons, estimation de l'état de charge, gestion thermique, fonctionnement longue durée

Résumé :

Le développement des sources d'énergie alternatives devient très important en raison de l'effet du changement climatique et de l'épuisement des combustibles fossiles. L'hydrogène est prometteur grâce à sa ressource illimité, sa densité énergétique élevée, sa grande flexibilité technologique et sa nature respectueuse de l'environnement. Avec un potentiel élevé en matière de sécurité et de fiabilité, le stockage d'hydrogène avec des hydrures métalliques (MH) est considéré comme la meilleure méthode. Cette thèse contribue à l'étude des performances des systèmes de stockage de l'hydrogène MH embouqué, plus particulièrement l'état de charge, la modélisation dynamique et la gestion thermique la pile à combustible.

Tout d'abord, des modèles sont proposés pour l'analyse dynamique des performances et le calcul de l'état de charge (SOC). Le processus d'estimation SOC en ligne est ensuite réalisé en combinant un classifieur d'états multi-joint. Le modèle dynamique du réservoir prenant en compte la conversion de masse et d'énergie est proposé à l'aide de paramètres optimisés identifiés par un algorithme d'optimisation d'essaim partiel. De plus, le comportement dynamique du système de pile à combustible intégrant la pile à combustible à membrane échangeuse de protons (PEMFC) et le réservoir de stockage d'hydrogène MH est simulé à l'aide d'un modèle mathématique défini et validé à l'aide d'une base de données provenant des véhicules réels. Une stratégie de gestion thermique avec contrôleur PID est proposée pour réduire la dégradation et prolonger la durée de vie de la PEMFC. Enfin, d'essai est conçu en laboratoire et des expériences sont menées pour valider les modèles et stratégies proposés.

UBFC UNIVERSITÉ BOURGOGNE FRANCHE-COMTÉ

Université Bourgogne Franche-Comté
32, avenue de l'Observatoire
25000 Besançon, France

ACKNOWLEDGEMENT

This work was prepared at the FEMTO-ST laboratory and the FCLAB research federation and was supported by many researchers, collegues, friends and families.

At first, I would like to give the most sincere thanks to Prof. Abdesslem Djerdir , who is my supervisor. I am grateful for his professional guidance and strong support in my research work and the preparation of this dissertation. I would also like to express my deepest appreciation to my co-supervisor Dr. Youcef Ait-Aimrat for his valuable advices and insightful discussion about my work. Moreover, I would like to thank Dr. Abdoul N'Diaye for maintaining laboratory equipment and carrying out experiments with me, which is crucial to this thesis.

Secondly, I would like to thank Prof. HINAJE and Prof. FORGEZ. for accepting to review this dissertation, despite their very busy schedules, and for their helpful comments. I also want to thank Prof. PERREUX, Prof. SARI and Dr. GILLIA for their participation in my defence.

Then, I would like to thank my colleague Dr. Djafar Charbane, who gives me valuable advices and help on the test bench. I also want to thank Dr. Rania Mazzi, Dr. Rabeb and Dr. youcef and Mr. Amine who work in the same office with me during these years, for their enthusiastic help and accompany. I am grateful to the support and help of all my friends I met at UTBM: Dr. Meiling Yue, Ms. Suyao Kong, Dr. Huan Li, Dr, Rui Ma, Dr. Chen liu, Dr. Hanqing Wang, Dr Hailong Wu, Mr Hao Bai and Dr. Bei Li.

The China Scholarship Council (CSC) is thanked for funding me to study and live in France. With the funding, I could concentrate on my research project, and could also travel around Europe to explore a new world.

Last but not least, I would like to thank my husband for supporting and encouraging me to do the research and thank my parents for their understanding and love.

Belfort, 26 May, 2020.

CONTENTS

General Introduction

In last few decades, massive usage of the fossil fuels has lead to many kinds of critical environmental issues, including air pollution, global warming and so on. What's more, our society is facing the rapid growth of global energy demand, which will intensify the emission of greenhouse gases. As reported of U.S. Energy Information Administration (EIA) and the International Energy Outlook 2016 (IEO 2016), world energy-related carbon dioxide (CO_2) emissions will increase from 32.3 billion metric tons in 2012 to 35.6 billion metric tons in 2020 and to 43.2 billion metric tons in 2040 [1]. This predictable of 40% increase in CO_2 emission tremendously pushed us forward in the research and development of renewable energy field as well.

Hydrogen is promoted worldwide as an ideal fuel for its inexhaustibly, cleanliness, convenience and independence from foreign control, which make it as the replacement for gasoline, heating oil, natural gas, and other fuels [2]. At the same time, the fuel cell is one of the most potential clean energy solutions as an energy conversion to transform the chemical energy to electrical energy in both stable and mobile applications. However, in spite of the high specific energy by weight, the hydrogen application meets the extremely challenging in storage and transportation because of its low energy density by volume [3]. According to the U.S. Department of Energy's Freedom Car Program targets, the ultimate targets to enable wide availability for the commercial use across all vehicle platforms are set to be 0.075 kg_{H_2}/kg_{system} of hydrogen gravimetric density and 0.07 kg_{H_2}/L_{system} of volumetric density [4]. Thus, further research is needed to achieve this goal.

Current hydrogen storage methods with relatively high energy density contain compression, liquefaction, absorption and chemical binding. Among these methods, absorbing hydrogen using some specific metal hydride (MH) draw a lot of attention. Such MH materials has been of great interest as kinds of promising carriers for hydrogen storage applications, due to their higher volumetric density when the weight of tank is not a major issue. In addition, the long-term stability with lower pressure and temperature during operation on fuel cell vehicles is also its outstanding advantages.

The practical application of MH hydrogen storage should be analyzed carefully, especially for the on-board integral application coupling with fuel cells. Besides, slow charging and discharging of the MH hydrogen storage units limited by heat transfer is a serious drawback requiring special engineering solutions. In order to improve the performance and maintain the durability of the MH tank, one need to understand:

- How to increase the ratio of the hydrogen mass stored to the weight of the MH tank?
- How to evaluate the state of charging/discharging of the on-board hydrogen storage system using MH tanks?
- What could impede these performances, especially for the degradation phe-

nomenon after long-term operation?

- How does the heat exchange condition among the coupling system of MH hydrogen storage tank and fuel cell operate, and what strategies can help to improve the performance?

The objectives of this thesis are searching for the solutions to tackle with these issues through proposing models and strategies. To be specific, this thesis will focus on the optimized embedded application of the MH hydrogen storage system, including the characteristics evaluation, dynamic modeling and the thermal management. The two main issues we want to solve are the state of charge (SOC) estimation of an embedded MH tank and the effective thermal management of the on-board hydrogen energy system including fuel cell and MH tank.

Above all, the open issues we facing in the research and development of MH hydrogen storage technique are discussed. In order to realize the evaluation of MH hydrogen storage characteristics and the improvement of its efficiency, two major attempts are made. The possibility of online SOC estimation is investigated through numerical study of the reaction mechanism and dynamic response. Then the effective thermal management and control strategy are analyzed. Moreover, experiments are designed for validation separately.

This dissertation is organized into six major chapters, which are planned as follows:

The first chapter provides the state of the arts and related works of this subject. The background and development of FCEHVs, fuel cells and hydrogen storage are introduced. It will be pointed out that electricity generated by PEM fuel cells equipped with MH hydrogen storage tanks has great potential for future power generation. Then, the main issues and challenges of each components in this system will be discussed, especially for automotive application. The objectives and motivations of our research work are therefore to be the characteristics estimation of MH hydrogen storage tanks and energy management of the on-board fuel cell and hydrogen tank coupling system.

In the second chapter, the numerical study of the MH hydrogen storage is carried out based on the databases collected from laboratory experiments and Mobypost project separately. Using the statistical theory, the performance of the main parameters including pressure, temperature, hydrogen flow rate and hydrogen mass are evaluated and modeled.

In the third chapter, combining with the chemical reaction characteristics of hydrogen and MH material, a P-C-T based SOC model is proposed. In addition, a multi-joint classifier is designed for classifying the reaction state during operation. The online SOC estimation method is then presented. It provides an effective online SOC estimation method to detect the remain hydrogen mass in the tank and optimize the operation method.

The fourth chapter discusses the dynamic physical model. Taking the embedded MH hydrogen storage tank as a gray box in the system, the parameters are identified using PSO algorithm. For all the operation conditions with different environmental temperatures, the simulation results of the dynamic model with the optimal parameters show a great agreement with the real operation data. This method provides an universal procedure for modeling the dynamic performance of MH tanks with different kinds of material and

structure.

The work presented in the fifth chapter focus on the development of a thermal management strategy for reducing the degradation of a long-term operating on-board fuel cell system. At first, a mathematical model describing the dynamic behavior of PEM fuel cell and MH tank is simulated and compared with real operation results. It presents the strong dependence of the dynamic response of the MH tank to the thermal condition supplied by the PEM fuel cell. Then, thermal exchange control strategy realizes by fan and circulation water are proposed to maintain the voltage of aged fuel cell. For the long-term operation of the applied integration PEMFC-MHT system, the fuel efficiency and fuel economy could be saved using this strategy.

At last, the test bench and experiments carried out in laboratory are introduced in chapter 6. The experimental results validate the theoretical research of MH hydrogen storage in previous chapters separately. The first experiment supplement the P-C-T based SOC model in discharging process, which provides the basis of online SOC estimation during vehicle operation. The second experiment validates the dynamic model of MH tank using optimized parameters and indicated that the model is avoidable for different hydrogen releasing flow rate. The third experiment focuses on the thermal effects that different value of extra heat are tested, which presented its influence on hydrogen desorption speed.

The manuscript ends with the conclusions and perspectives of the research work, together with the references, appendices of figures and tables.

1

FUEL CELL AND HYDROGEN TECHNOLOGY FOR TRANSPORTATION

1.1/ INTRODUCTION

In recent decades, with the accelerating development of industrialization, our society has become more dependent on fossil fuels. The environment issues caused by over consuming of fossil fuels and the energy crisis with the dwindling reserve of such resource are threatening the world. The harmful greenhouse produced by the fossil fuels such as oil is one of the main reasons leads to the global warming. 450 million tons of greenhouse gas emission could be avoided by 10-20% of reduction in America's oil usage [5]. In order to protect the environment, empower the economy for future and defend our quality of life, the European Union (EU) long-term strategy made an agreement of reducing the greenhouse gases emissions by 40% by 2030 compared to 1990 [6] and the Paris agreement made the total's ambition of cutting the carbon intensity by 15% between 2015 to 2030 [7]. In addition, the fossil fuels requirement for daily consumption is growing, the increasing rate is about 1.2% every year, which is much faster than the speed of discovery and mining. Even worse, the oil might dry among the whole word by the 2050. Thus, concerning the harmful effects of the greenhouse gases emission and the over depletion of fossil fuels, the research and application of alternative clean energy sources present great significance and potential. The alternative fuels like ethanol, compressed nature gas, soy oil, propane, palm oil and hydrogen are considered to replace the oil as fuels. However, all these fuels have to face numerous problems including the production technology, distribution phase, device update, energy supply and transportation. For the current stage, there are three alternative fuel sources, namely, electric vehicles, hydrogen fuel cells, and algae-based fuels, to be the most significant impact on fuel industry.

Automotive transportation is one of the principal symbols of modern civilization for human beings, which play an irreplaceable character of our daily life and social development. A report of U.S Energy Information Administration (EIA) presents that automotive transportation occupies about 55% of world's total energy consumption and 30.9% of CO_2 emission in 2014 [8]. Statistical forecast that three times more cars will occur on the roads in 2050 than today [9], which will further worsening the environmental issues and energy crisis. The vehicles powered by electric and fuel cell have seen a promising future that have huge potential to be the alternatives of the oil powered vehicles.

Electric vehicles (EVs) can reduce the greenhouse gas emissions, which have given rise to huge transform in the electrification of cars. The technology development and practical application of EVs have proliferated during the last couple of years. The application of the electric powertrain have already well developed and achieved great success. The modern high-speed trains show competitive performance over air travel in shorter land journal, including travel time declining and energy consumption saving. About 10% of fuel is saved per kilometer for one passenger [10]. However, EVs on road are still in the minority compared to traditional oil-based vehicles which are being extensively used. The key reason is the low energy density of the applied batteries, which restricts the driving range. More stacked batteries could help for extending the driving time. However, extra weight compounding aggravate the load and decline the distance of a battery-powered car could drive. Meanwhile, the additional production cost, namely, the energy source cost, takes almost one third of the total cost of a vehicle, eventually cut down the fuel economy of the EVs [11]. In general, as part of the solution for future sustainable transportation, EVs still have many challenges need to overcome.

Hydrogen is considered to be a critical and indispensable element of a decarbonized, sustainable energy system that could applied as a kind of cost-effective and non-polluting energy since thirty years before [12]. With significant advantages in zero emissions, high energy density, high reserve and well recyclable, hydrogen energy and fuel cell powered vehicles seem to promise a bright future for transportation reform [13, 14]. On the other side, as another choice for transition to a low-carbon economy, hydrogen and fuel cell technologies also provides similar performance, operation and consumer experience to oil-powered technologies [15]. On the fuel cell vehicles (FCVs), fuel cells are connected in series to generate the required power through the reaction of hydrogen and oxygen. The hydrogen is stored on-board as the power resource. Thus, longer distance travel could be achieved, which is also its more attractive performance. By the year of 2050, 17% of FCVs share in the market is estimated by the international energy agency (IEA) report [16]. However, the fuel cell needs a relatively long starting time and the absorption of the dynamic of current will reduce its lifetime, which make it suitable for constant power demand. Thus, an additional energy storage system is packed up like battery or super capacitor, which improved the development of the fuel cell hybrid electrical vehicles (FCHEVs). Compared to EVs and FCVs, the energy management system on FCEHVs equipped with two power sources or more. As a result, longer driving distance than EVs and faster response to modified load than FCVs are achieved. Nowadays, FCHEVs have been perceived as one of the most promising technologies for future transportation [17].

However, the further commercial promotion and comprehensive application of the FCHEVs still face several challenges. On-board hydrogen storage in a compactively, safety and efficiently way is one of the main issues. The hydrogen storage technologies of how to improve the hydrogen gravimetric and volumetric energy density have been a worldwide subject [18–20]. The thermal management among the components is another essential topic. During operation, the heat generated by fuel cell could be transferred for hydrogen generation reaction [21–25], which help not only save the fuel economy but also improve the dynamic performance [26, 27]. Besides, the durability is also one of the central issues holding back the critical achievement of FCHEVs like the ageing of MH hydrogen storage tank, the degradation of fuel cell, other power source ageing including battery and super capacitor [9, 28, 29]. In addition to the technological innovations in

materials, a well-designed thermal management strategy could help to find the maximum efficiency operation region, reduce the degradation and prognostic the remain useful lifetime [30–32].

In this chapter, state of the arts and related works of the thesis are presented in detail, namely, the introduction of FCEHVs, the fuel cell characters, the on-board hydrogen storage developments. Then the open issues and remaining challenges of the hydrogen storage and application on FCEHVs are discussed. At last, the motivations and objectives of the thesis are explained and the framework of developing an on-board thermal management strategy of the fuel cell system is proposed.

1.2/ FUEL CELL HYBRID ELECTRIC VEHICLES

1.2.1/ STATE OF THE ARTS OF FCHEV

The first success of fuel cell is achieved by Francis Bacon in 1932, an alkaline fuel cell system with porous electrodes is developed. Starting from 1950s, the Apollo space program introduced the fuel cell for energy supply, due to the significant advantages of safety, compact and light over others resources like nuclear, solar and battery [33]. Then the fuel cells obtained generally application on Apollo, Gemini and space shuttles. In 1955, an engineer of General Electric (GE) called Willard Thomas Grubb created an ion-exchange membrane for the reaction of hydrogen and oxygen. Three years later, Leonard Niedrach, another engineer of GE designed a proper method to deposit platinum onto the membrane, which make it possible for transportation application. In 1967, a six-passenger fuel cell vehicle, named Electrovan, is produced in Gemeral Motor, which symbolizing the beginning of fuel cell vehicle era [34].

In recent decades, a number of manufacturers including Daimler, Toyota and so on investing in the development of fuel cell technology for automobile application, which are supported by various government agencies. As mentioned before, General Motors has the longest fuel cell history and developed the first publicly drivable FCHEV in 1998. Since 2007, more than 120 vehicles were delivered to customers and applied for real deriving. The accumulated mileage is over two million miles on road, which make the company to achieve the world's largest FCHEV end user acceptance [34]. In 2011, Daimler delivered a global demonstration of FCHEVs, and invested 36 fuel cell buses, of which the whole operation distance has reached 4.8 million kilometers. Toyota began to sell the FCV Mirai at the end of 2014, and extended its market layout to Europe and US. The Japanese government explicitly indicated the support of the development of fuel cell technology in the 2017 Energy White Paper. As a result, the number of fuel cell passenger cars in Japan is about 2000 till January 2018 and the fuel cell bus is expected to increase to 100 in 2020. Until December 2017, the total sales of fuel cell passenger cars globally reached about 6000, among which Toyota Mirai sold a total of 5300 vehicles, including 2900 in the US, 2100 in Japan, and 200 in Europe, accounting for more than 90% of the total sales of fuel cell passenger vehicles worldwide. As shown in Figure 1.1, through the production optimization, the cost of fuel cell system on Mirai is reduced, and 95% cost reduction is expected by Toyota in 2025 [35].

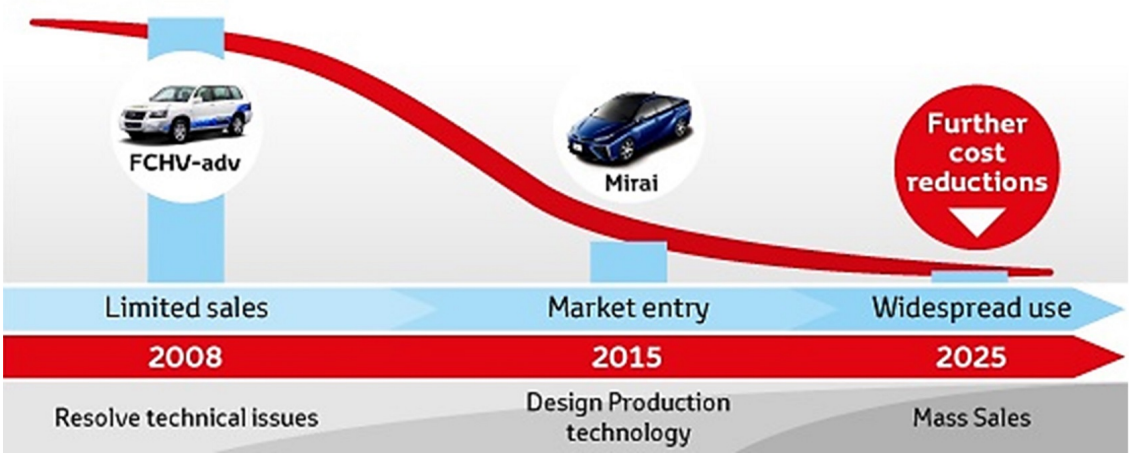

Figure 1.1: Expect of Toyota Mirai: fuel cell technology cost down by 95% [35].

The research and commercial application of hydrogen fuel cells and FCVs are rapidly developing in Japan, the United States, and Europe. The global market for FCHEVs is estimated to reach about 583,360 units by 2030, with Asia Pacific (APAC) countries such as Japan and South Korea dominating the market with 218,651 and 80,440 units respectively [36]. FCHEV markets in Europe and North America are projected to reach 117,000 units and 118,847 units, respectively, by 2030, which is presented in Figure 1.2 [37].

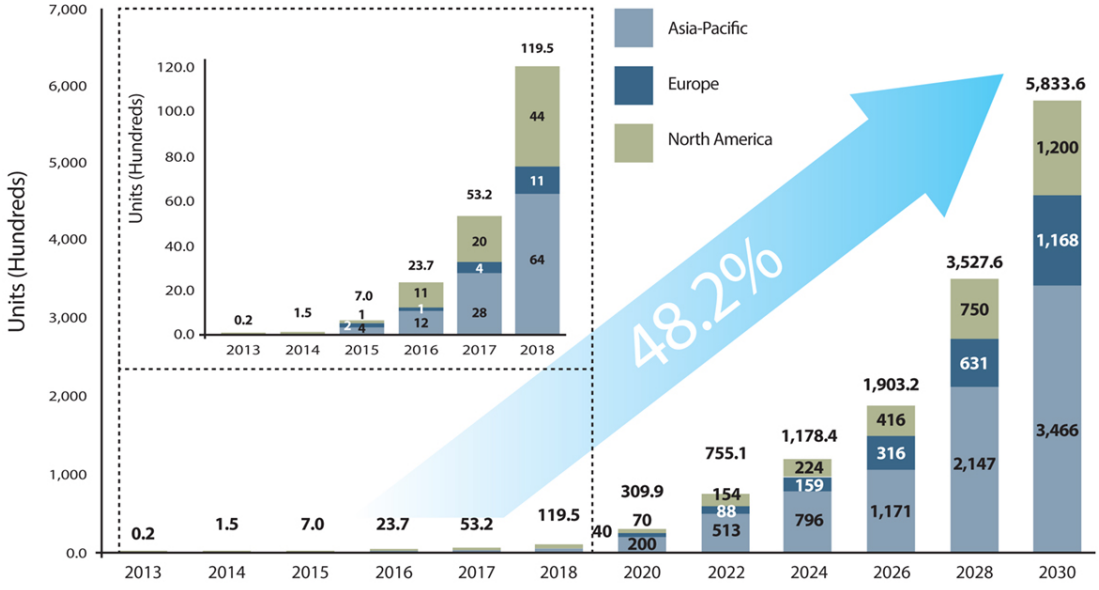

Figure 1.2: Fuel cell passenger car market: Global FCEVs sales by region midline scenario [37].

1.2.2/ STRUCTURE AND COMPONENTS OF FCHEV'S POWERTRAIN

Different from EVs, which store electricity by batteries to power the vehicle, FCHEVs carries hydrogen storage tanks as energy resources. The fuel cell on FCHEVs is applied as an electrochemical device to convert the chemical energy of hydrogen into electrical energy with high energy density. Then, the FCHEVs operates the same way with EVs [38]. For a better performance for dynamic driving load, a peak-power devices such as high-power batteries or super capacitors are embedded on the FCHEVs, which operate together with the fuel cell to supply the power [39]. Thus, under this condition, compared to the EVs, the on-board battery in this power trains can be reduced in size, which help to decline the overall weight of the propulsion system [40]. Meanwhile, the product of reaction in fuel cell is just water, zero-emission target is therefore achieved. Besides, the byproduct heat of the reaction of hydrogen and oxygen could be used as a heating resource for other component, like hydrogen tank or thermal circulation, this help to minimize the energy lost and improve fuel efficiency during operation.

Taking Toyota Mirai fuel cell vehicle as an example. A proton exchange membrane fuel cell (PEMFC) stack with the maximum output power of 144 kW and the volume power density of 3.1 kM/L, is applied as the premier power resource. Then, a high-power battery of 1.6 kW is embedded in parallel as the auxiliary power, for the purpose of response to sudden raised power demand at starting or accelerating, and save energy during regenerative braking. Besides, a high-capacity boost converter is developed between fuel cell and battery to promote the fuel cell output voltage to a maximum value of 650 V. The operation principle of this FCEHV is presented in Figure 1.3. On this vehicle, hydrogen is stored in two high-pressure tanks as the fuel. The nominal working pressure is 70 MPa with a storage density of 5.7 $wt\%$. The tank could be refueled in the hydrogen station within a short time. Oxygen is extracted from air through a air compressor. The fuel cell generates electricity through the chemical reaction between hydrogen fuel on anode layer and oxygen on cathode layer. About 83% of energy in the hydrogen molecule could be convert into electricity by PEMFC, which is more than double energy efficiency of a petrol engine. Electricity produced by the fuel cell is delivered to an electric motor to drive the vehicle. Regenerated energy is stored in a secondary battery that supplements power from the fuel cell by providing auxiliary power to the electric motor [35]. Some other vehicles enterprise also interested in adopt this kind of parallel configuration made produced the commercial FCHEVs like Honda's Clarity fuel cell vehicle, Hyundai's NEXO fuel cell vehicle, etc. Different to Toyota Mirai, the lithium-ion battery is chosen on Honda Clarity and Hyundai NEXO.

Modifying the control strategy of energy distribution, adjusting the power sources arrangement, or selecting other energy storage device, other configurations of powertrain structure also exist in research lab and literature [33, 41–44]. Commonly used powertrain structure are presented in Figure 1.4. Figure 1.4(a) show a completely parallel FCHEV power train structure, on which fuel cell system and batteries connected in parallel and provide power separately. This kind of vehicle could operation in different mode: fuel cell alone mode, battery alone mode or combined mode. Thanks to the relatively independent working mode, simpler and complex propulsion devices are capable for the same performance with series configuration. Well designed energy management strategy is necessary for variation load demand due to the different character of fuel cell and battery.

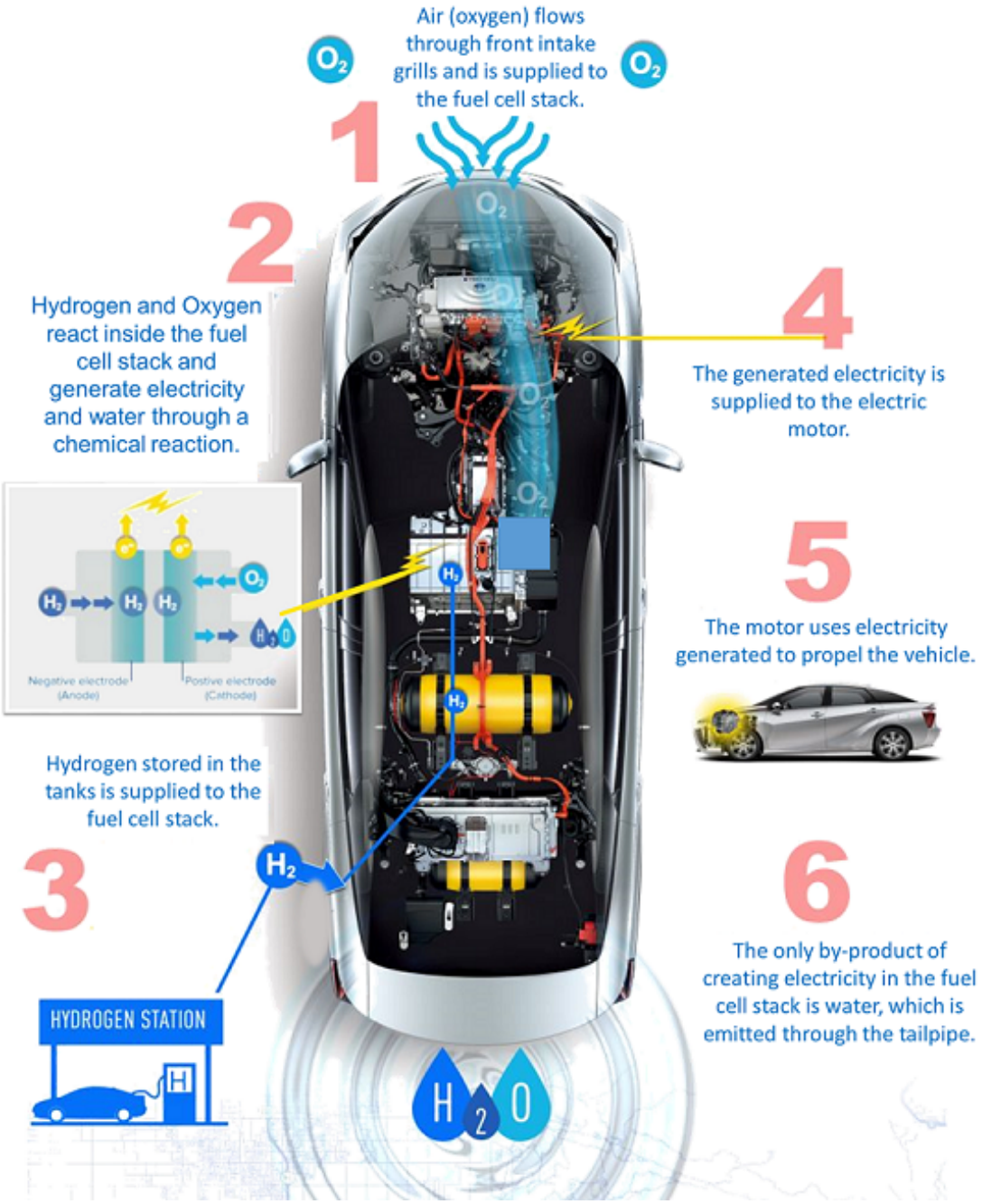

Figure 1.3: Principle of Toyota Mirai fuel cell vehicle [35].

Besides, the regenerative braking mode only happens alone with the battery mode and combined mode. In Figure 1.4(b), fuel cell system is connected to the battery instead of accessing the load, indicating that the fuel cell system is applied as an extra power for battery and a range extender for vehicle. Through the same electric motor and internal combustion engines with EVs, the short mileage defect of EVs could be remedied and better performance could be achieved. The powertrain structure discussed above is shown as Figure 1.4(a), a series-parallel configuration that the fuel cell is the principle power source and the battery is used as a secondary source. The advantageous feature

of both parallel structure and series structure can therefore be possessed. Nevertheless, a relatively more complicated control and energy management strategy is required and the manufacturing cost is raised. In spite of this, the commercial promoted vehicles prefer to adopt this kind of system, for the reasons that a better performance help to lead the market share and the technology is believed to be able to improved.

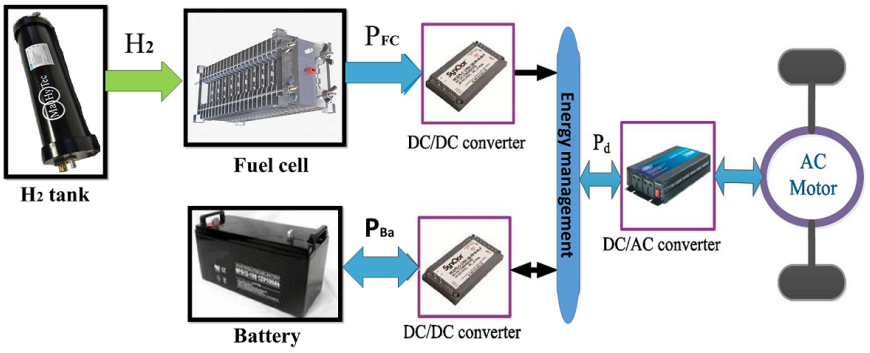

(a)

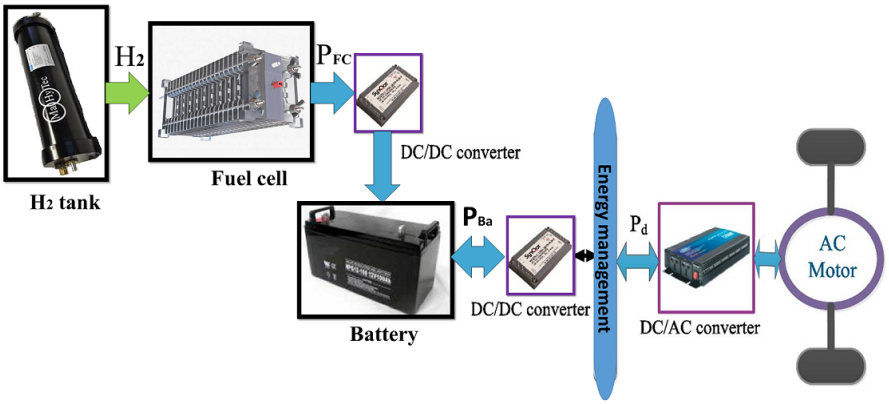

(b)

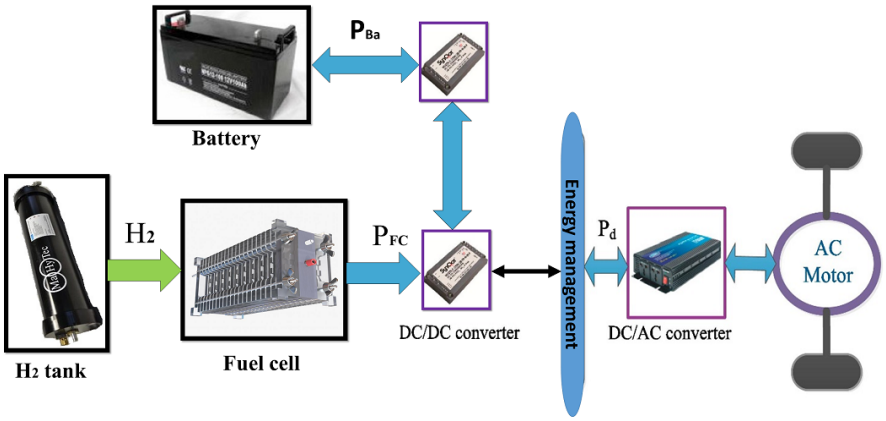

(c)

Figure 1.4: Powertrain structure of FCHEVs.

1.3/ PROTON EXCHANGE MEMBRANE FUEL CELL PROPULSION

1.3.1/ GENERAL DESCRIPTION OF PEMFC

1.3.1.1/ FUEL CELL TYPES

As one of the most attractive and potential energy generation device in recent years, fuel cell draw great attentions of research and application on a global scale. Fuel cells are energy conversion device that the chemical energy stored in fuel, usually hydrogen, and oxidant from air or pure oxygen are converted into electricity through the electrolyte. The type of electrolyte dominates the chemical reaction condition inside the fuel cell, including the operation temperature, reaction speed and dynamic performance. The main applied fuel cell types categorized by electrolyte types include Proton Exchange Membrane Fuel Cell (PEMFC), Alkaline Fuel Cell (AFC), Phosphoric Acid Fuel cell (PAFC), Molten Carbonate Fuel Cell (MCFC), Solid Oxide Fuel Cell (SOFC), Direct Methanol Fuel cell (DMFC), etc [45]. Table 1.1 presents the comparison of the main features of these types of fuel cells [46–49].

The PEM Fuel cell is widely applied for automobile transportation for its ability to develop high power density under relatively low operating temperature and low pressure [50]. In the PEMFC, a proton exchange membrane is installed for conduction of protons, generally applied materials is Nafion, and platinum is widely used as the catalyst for reaction. AFC is one of the most developed fuel cell, which was the first practical applied fuel cell and has been applied in Apollo space program for both electrical and drinking water supply [51]. It operates at a relatively low temperature similar to PEMFC while the starting time is shorter. During reaction, the negative ions is transferred from anode to cathode via electrolyte, which is the aqueous solution of potassium hydroxide, meanwhile, producing water. High efficiency can be achieved of $60 - 70\%$. However, the corrosive electrolyte decline the life span [52].

PAFC is generally applied in stationary application, in which the used phosphoric acid is non-conductive liquid, therefore the electricity is produced through an external electrical circuit that positive hydrogen ions is delivered from anode to cathode [53].

The electrolyte applied in MCFC is composed of carbonate salts suspended in a porous ceramic matrix and chemically inert solid electrolyte of alumina beta. Electricity is produced by electrons migration from the cathode to anode, along with the reaction of hydrogen and carbonate ions generating water and carbon dioxide at the same time [54].

SOFC is also suitable for stationary application since the operating temperature is extremely high. Rather than liquid electrolyte, the electrolyte is combined by a solid ceramic inorganic oxide [55].

DMFC is developed on PEMFC, in which the hydrogen fuel of reaction is replace by methanol. As a liquid form fuel, methanol is more stable than hydrogen, which is easier for storage and transportation. However, the fuel efficiency is not as high as other type of fuel cells [56].

Table 1.1: Fuel cells comparison

FC	Electrolyte	Charge Carrier	Catalyst	Operating Temperature	Electrochemical Reactions
PEMFC	Nafion exchange membranes	H^+	Platinum	$290K - 350K$	Anode: $2H_2 \rightarrow 4H^+ + 4e^-$; Cathode: $O_2 + 4H^+ + 4e^- \rightarrow 2H_2O$
AFC	Potassium hydroxide	OH^-	Platinum	$340K - 500K$	Anode: $2H_2 + 4OH^- \rightarrow 4H_2O + 4e^-$; Cathode: $O_2 + 4H_2O + 4e^- \rightarrow 4OH^-$
PAFC	Liquid phosphorus	H^+	Platinum	$478K$	Anode: $2H_2 \rightarrow 4H^+ + 4e^-$; Cathode:$O_2 + 4H^+ + 4e^- \rightarrow 2H_2O$
MCFC	Liquid molten carbonate	CO_3^{2-}	Nikel	$820K$	Anode: $CO_3^{2-} + H_2 \rightarrow CO_2 + H_2O + 2e^-$; Cathode:$CO_2 + \frac{1}{2}O_2 + 2e^- \rightarrow CO_3^{2-}$
SOFC	Ceramic	O^{2-}	Perovskites	$870K - 1270K$	Anode: $2H_2 + 4O^{2-} \rightarrow 2H_2O + 4e^-$; Cathode: $O_2 + 4e^- \rightarrow 4O^{2-}$
DMFC	Proton exchange membranes	H^+	Platinum	$300K$	Anode: $CH_3OH + H_2O \rightarrow CO_2 + 6H^+ + 6e^-$; Cathode:$\frac{3}{2}O_2 + 6H^+6e^- \rightarrow 3H_2O$

1.3.1.2/ STRUCTURE AND REACTION OF PEMFC

As shown in Figure 1.5, a PEMFC stack is consisted of several single fuel cells connected in series for the purpose of meeting the requirement of power load. One single fuel cell is combined by eight cell layers, including cathode gas supply channel layer, cathode gas diffusion layer, cathode catalyst layer, proton exchange membrane layer, anode catalyst layer, anode gas diffusion layer and anode gas supply channel layer. Besides, a cathode cooling channel layer is installed aside of cathode gas supply channel layer for thermal control for reaction [57, 58].

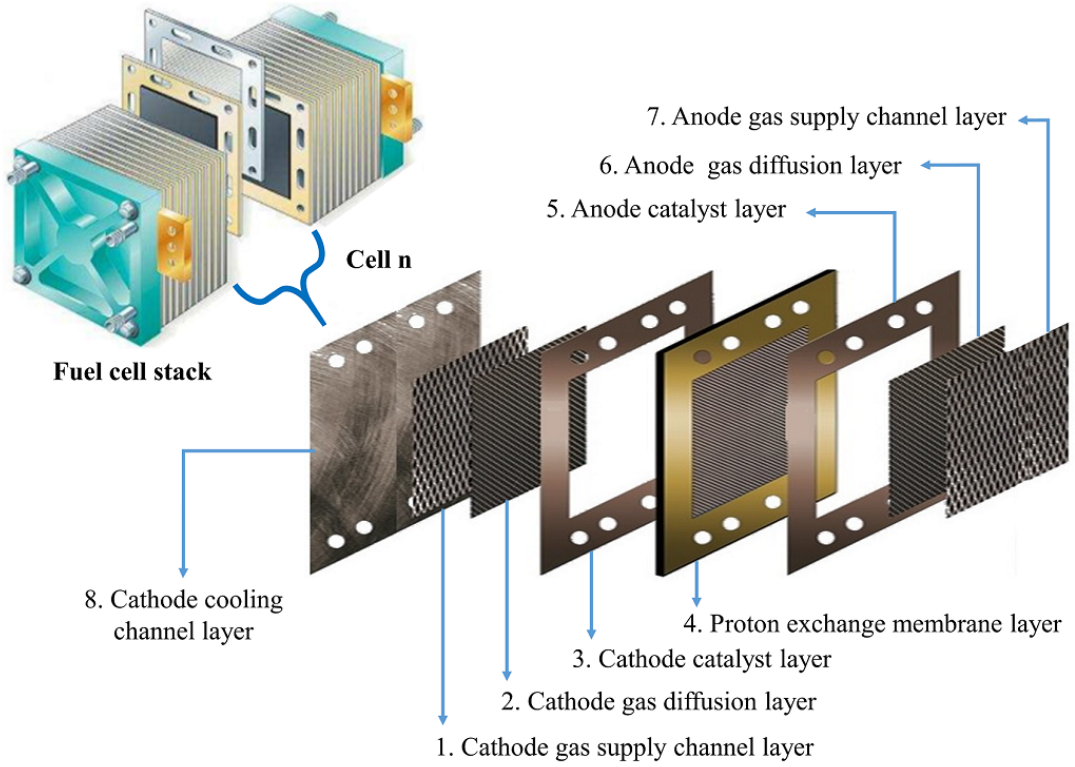

Figure 1.5: The structure and components of fuel cell stack and single fuel cell.

A typical operation principle of a single cell of a PEMFC is presented in Figure 1.6 [59]. During the reaction, the hydrogen is fed to the anode side and the air or pure oxygen is supplied to the cathode side. Then the hydrogen and oxygen are diffused through the gas diffusion layer to the catalyst layer on each side respectively. At anode catalyst layer, under the effect of platinum catalyst, the hydrogen molecules are disassociated to hydrogen ions and electrons. These hydrogen ions, also called proton, pass through the humidified polymer electrolyte, namely, the proton exchange membrane, migrating from the anode side to the cathode side. Meanwhile, the electrons flow through the external circuit from anode to cathode, the electrical current is therefore generated. At the cathode catalyst layer, the delivered hydrogen ions and electrons are combined with the local oxygen molecules and product water and heat.

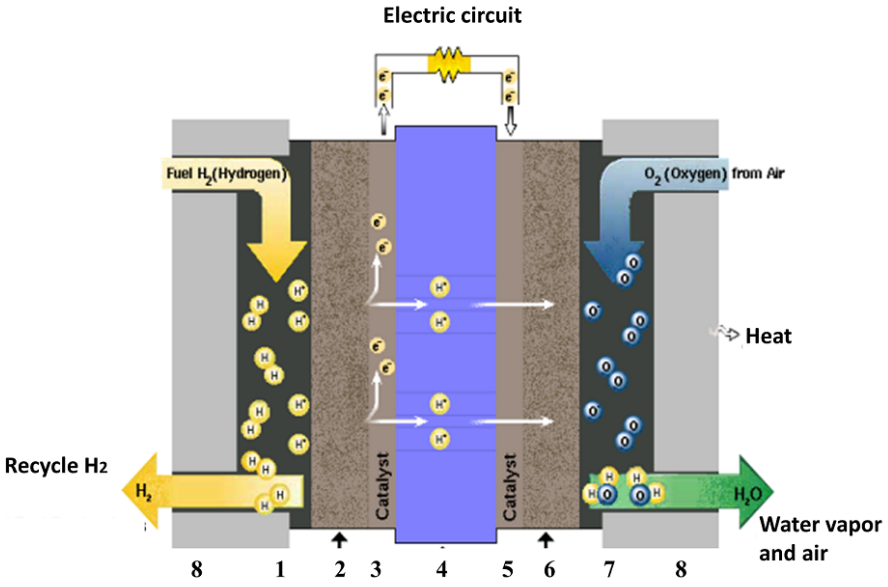

Figure 1.6: Operation principle of a single fuel cell.

1.3.2/ Dynamic characters and polarization curves

Dynamic characters and performances are obviously significant for fuel cell analysis and applications. The current studies mainly focus on two aspects that numerical simulation and experimental study, on which a considerable amount of literature has been published [60].

The numerical simulation study is mainly focuses on model design and simulation. Fifteen years before, Chen et al. had developed an unsteady mathematical model of PEMFC, and proved that the dynamic performance of the cell was related to the mass transport of water in the membrane [61]. A simplified model which can well characterize the transient behavior of the output voltage and temperature of the PEMFC stack in the case of the current step change is then characterized by a simplified model proposed by Kim et al. [62]. The effect of heat transfer on the fuel cell dynamic performance is introduced by a non-isothermal transient model [63]. Raga et al. proposed a black-box model that can capture the dynamic response process of the fuel cell only need to obtain the relationship between step current and time, and the fitting error did not exceed 4% [64]. The stack temperature significantly affected the dynamic characteristics of fuel cells, as well as the hydrogen purge on actual hydrogen consumption [65, 66].

In terms of experimental research, large amount of test had been done in laboratories. It is reported that transient voltage behavior of the individual cell varied depending on its location in the stack. Specifically, the cell close to the reaction gas inlet had better dynamic performance than that of the last one [67]. When the load suddenly rose or dropped, the voltage of the PEMFC stack would exhibit a significant undershoot or overshoot [68]. They explained that these phenomenon in the transient response process were closely associated with the mass transfer of water and gas. By measuring the local current density and high-frequency resistance, humidification was found to be a very important factor

influencing the transient behavior of the current [69]. An air-cooled PEMFC stack is tested with the dead-end anode [70]. They confirmed that purge can cause voltage fluctuations, and this effect was more significant at high current densities.

Polarization curve presents the typical static characteristic of fuel cell, which is a plot of cell voltage versus current to determine voltage-current relationship of fuel cell. Figure 1.7 present a typical single cell polarization curve operating at $100^{circ}C$ and normal air pressure [71]. The curve is characterized by three important regions: activation polarization, ohmic polarization, and concentration polarization [72].

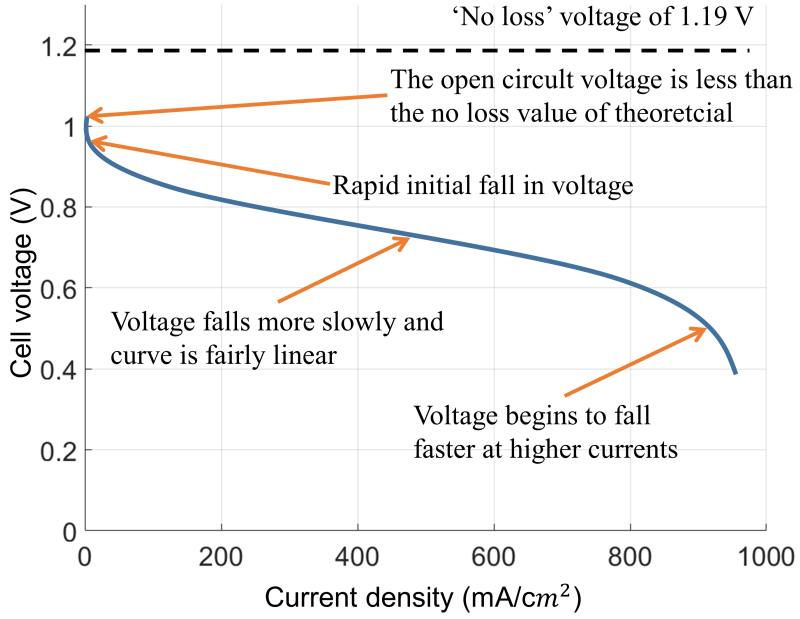

Figure 1.7: Typical polarization of PEMFC [73].

The initial part of polarization curve (activation polarization) indicates the nature of the reactions. The reversible open circuit voltage is calculated form the basic Nernst equation with an extra term to take into account the effect of temperature and pressure. The Nernst reversible voltage equation is therefore given by [74]:

$$Enernst = 1.229 - 8.5 * 10^{-3}(T - 298.15) + 4.3085 * 10^{-5} * T(ln[P_{H_2} + 0.5P_{O_2}]) \quad (1.1)$$

where P_{H_2} and P_{O_2} are the partial pressures of hydrogen and oxygen respectively and T is the cell temperature.

The overall activation potential (V_{act}) represents the slowness of the reactions that takes place on the surface of the electrode. The overall activation potential can be written as [74]:

$$V_{act} = \xi_1 + \xi_2 T + \xi_3 T * ln(C_{O_2}) + \xi_4 T * ln(i_{cell}) \quad (1.2)$$

where $\xi(1...4)$ represents the semi-empirical parametric coefficients and C_{O_2} is the con-

centration of oxygen at the catalytic interface of the cathode ($mol * cm^{-3}$).

The central portion of ohmic polarization reflects the ohmic losses (V_{ohmic}) caused by the membrane, electrical and contact resistance. This voltage drop is proportional to current density and it is linear. The ohmic loss in the fuel cell can be mathematically represented as [74]:

$$V_{ohmic} = i * (R_m + R_c) \tag{1.3}$$

where R_m and R_c denote the electronic, and the ionic resistances($\Omega * cm^{-2}$) respectively.

Depending on the amount of current drawn from the fuel cell along with other physical parameters, the output voltage of the fuel cell reduces. This loss is accounted as mass transport or concentration loss and can be determined by [74]:

$$V_{conc} = -b * ln(1 - \frac{J}{J_{max}}) \tag{1.4}$$

where b is a parametric coefficient (V), which depends on the cell and its operation states. J and J_{max} represents the actual and maximum current density of the cell (A/cm^2).

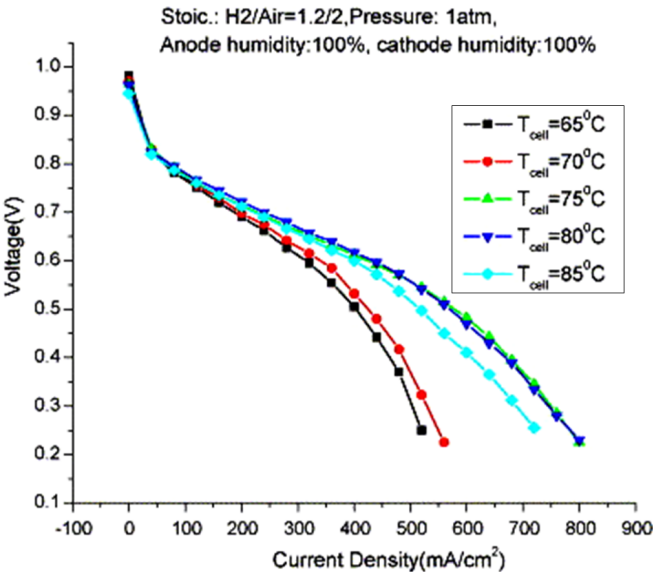

Figure 1.8: The effects of temperature on fuel cell performance [75].

The relative humidity and operating temperature of fuel cell essentially effect on the polarization curves [76]. Figure 1.8 shown the influence of operation temperature on fuel cell performance, which indicates that suitable choice of temperature is quite important for achieving better result, both too high or too low temperature could lead to extra voltage losses. A proper humidity level should be held in the fuel cell. Figure 1.9 illustrates the effects on the performance of a fuel cell with variation in the relative humidity. In this figure, the polarization curve with different relative humidity on the cathode side (CRH) is illustrated. According to the figure, the best performance occurs at about 70%. Pressure

of the reactant gas has significant effects on fuel cell performance as well, as shown in Figure 1.10, when the pressure is varied from 1 atm to 4 atm, the fuel cell performance is improved [75].

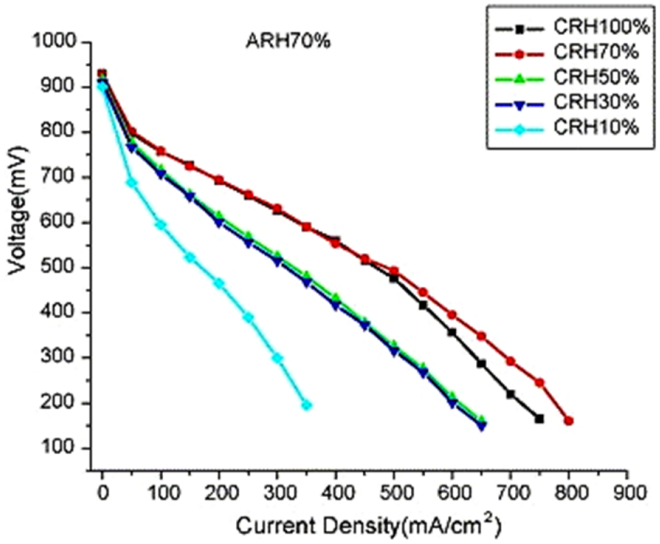

Figure 1.9: The effects of gas humidity on fuel cell performance [75].

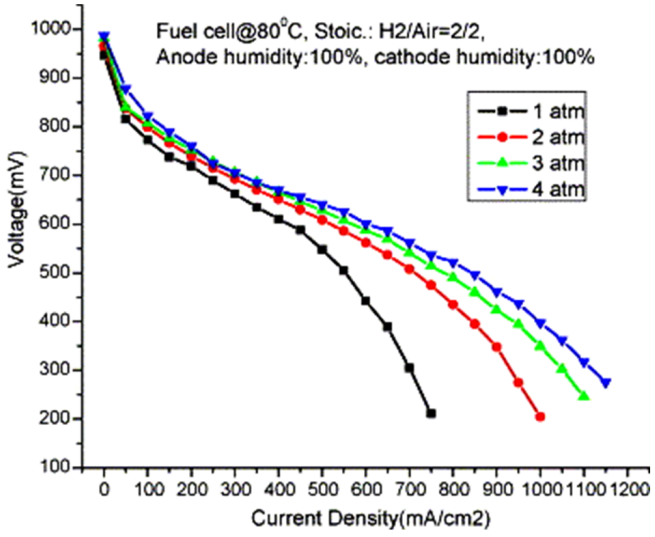

Figure 1.10: The effects of air pressure on fuel cell performance [75].

1.3.3/ DEGRADATION MECHANISM AND EFFECTS

Along with long-term operation, each component in fuel cell avoidably degraded, thus causing the PEMFC degradation or failure. The degradation mechanisms on each component are listed as follows:

- Membrane:

The membrane play an important role in fuel cell because it not only allows the protons transport from the anode to the cathode thanks to its hydrophilic and hydrophobic domains, but also acts as a separation between the fuel and the air. Thus, the membrane must have an excellent proton conductivity, a thermal and chemical stability, a good mechanical resistance, flexibility, a low permeability to gases and a low water drag. Three impacts including chemical degradation, mechanical degradation and shorting generally combine the degradation of membrane. The chemical degradation attacks the polymer by radical species directly, which will lead to the decomposition of the membrane. The membrane might fracked due to cycled constrains or fatigue imposed by charging temperature or humidity. An over-compression of the cell or topographical irregularities of the neighboring components could lead to local over-compression and creep, and then the shorting is caused. In addition, the membrane also suffers from thermal degradation characterized by the decrease of proton conductivity at high temperatures [77, 78].

- Electrodes:

  The electrodes are composed of two layers: a catalyst layer and a carbon support layer. A conventional catalyst layer is made with platinum (Pt) nano particles and supported by a surface of black carbon in close contact with a controlled quantity of ionomer (membrane material). The carbon support allows the nano particles to have a high dispersion (2-3 nm) and provides a porous structure electronically conductive. Two main phenomena are responsible of the loss of performance with the electrodes: the catalyst layer degradation and the carbon support degradation. Together these phenomena lead to a loss of active area of the electrode and its consequent loss of electrochemical activity [79].

- Gas diffusion layers (GDL):

  The reactant needs to diffuse from the flow fields to the active sites, where the GDL plays an essential role thanks to its porous nature. The generated vapor water mixed with the reactants and liquid water are also evacuated through GDL, which facilitated the water management in the catalyst layer and in the membrane. The degradation of GDLs is coupled together with membrane-electrodes due to its electrically conductive ability. When the GFLs are ageing, loss of hydrophobicity and changing of the carbon surface leads to the abnormal behavior of water. Besides, the loss of porosity will change the electrical and thermal resistances. Even the structure of GDL is modified due to the serious carbon corrosion and mechanical constraints after long time operation [79].

- Bipolar plates:

  The bipolar plates are the skeleton of the stack, which installed between two single fuel cells in order to isolate the individual cells. They also used for conducting the current between the single fuel cells and providing flow fields for incoming reactants and outgoing products. Besides, the water and thermal managements are work on the bipolar plates. Along with time, the raised surface resistive on the plates well lead to a higher ohmic resistance. In addition, operational impacts such as thermal cycles, bed temperature distributions or non-uniform currents might rapidly accentuate fractures or deformation of the plates. Moreover, the corrosion of bipolar plates

produced multivalent cations, which seriously affect the durability of the membrane and the catalyst layers [79].

- Sealing gaskets:

  The assembly of the membrane and electrodes includes sealing components to prevent not only the mix of hydrogen and air but also the leak out of the stack. All the components should be perfectly aligned to maintain the appropriate closing pressure. This is important to reduce the contact resistances and to avoid an over-compression of the GDLs [77, 78].

Some constant load experiments have been done in laboratories. For example, a continually test lasting more than 1500 hours is did in FClab in France, the fuel cell stack is operated under a constant load of 60 A which corresponds to the nominal current given by the manufacturer [80]. Figure 1.11 shown the static response by the modification of the polarization curve throughout the life of the PEMFC.

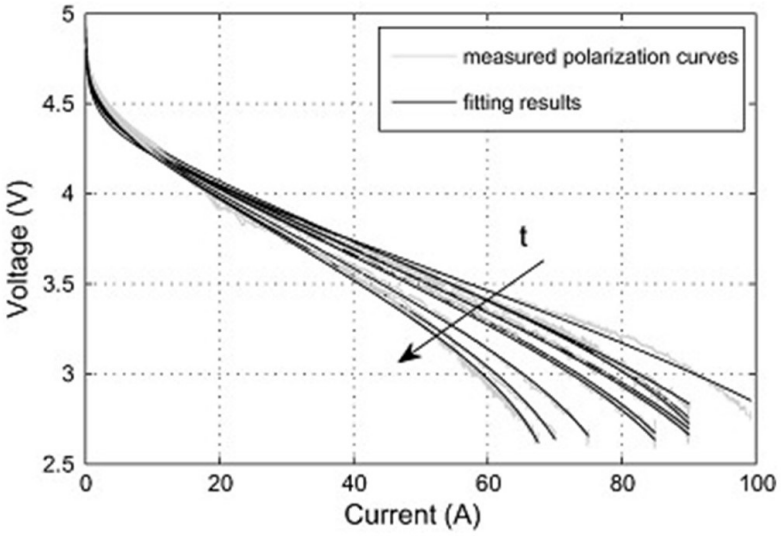

Figure 1.11: Polarization curves during ageing [80].

It is also generally acknowledged that the performance of a fuel cell is impacted by the dynamic load cycle much more strongly than by the constant load condition [81, 82]. For the reason that under dynamic driving cycle, the variety of operation condition was much more dramatically compared to the steady condition than under constant load conditions. This may result to the oxidant starvation, local “hotspots” and physical degradation, so the performance of fuel cell would be much seriously degraded [83].

During operation, the performances of PEMFC might degraded for many reasons impacted by the fuel cell stack itself or by the auxiliaries. One of the constraints is the decrease of the fuel cell voltage in case of faulty operation of the stack. As an example, when the low temperature PEMFC stack does not operate with pure hydrogen, a poisoning risk by pollutants, especially carbon monoxide (CO) can occur. Poisoning leads to a

blocking of the active platinum catalyst areas and leads to a decrease of the global electric voltage. A same tendency can occur during the ageing process of a fuel cell stack. Figure 1.12 illustrates the modification of the polarization curve due to CO poisoning or ageing phenomena [84].

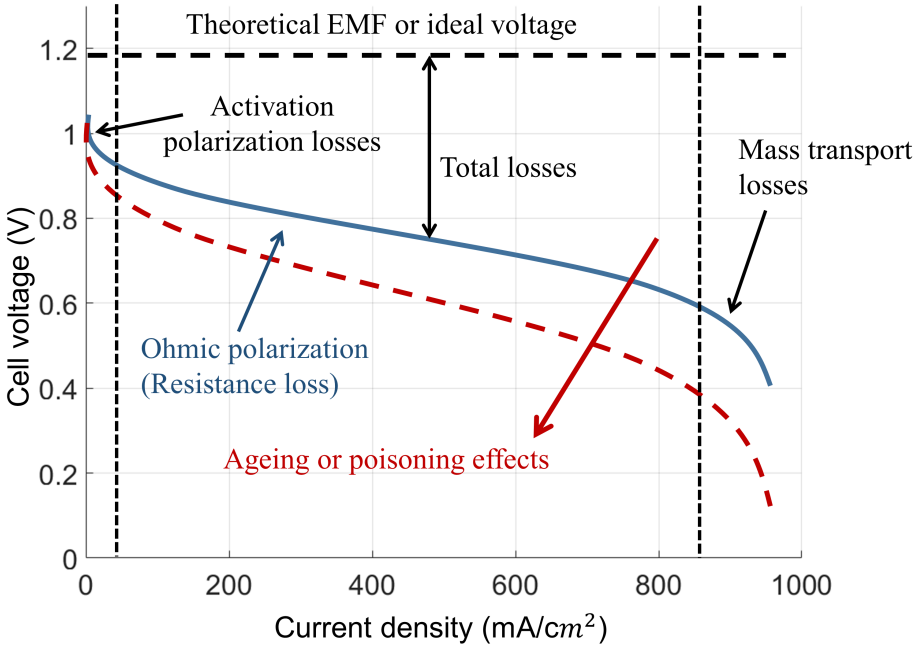

Figure 1.12: Modification of the fuel cell polarization curve owing to the influence of ageing or CO poisoning [84].

Moreover, in a fuel cell stack operation, some of the cells can suffer from starvation: the cells are not fed with a sufficient amount of reactants (hydrogen, air). Then the voltage of the cells will drop down to a lower level that can be critical to the stack working and lifetime. In the case of real insufficient fuel feeding, the starved cells might drop to negative values due to electrolysis current [85]. Many factors like a sudden load current demand can cause starvation in a fuel cell. Among those operating problems, some severe stack degradation could leads to irreversible damage or drastic reduction of the lifetime operation.

1.3.4/ Advantages and challenges of PEMFC

Compared to other types of fuel cells discussed above, the PEMFC has significant advantages in automobile application, namely, high power density, low operating temperature and pressure, faster start-up, etc, [86]. Specifically, the structure and components allow a better performance. For one thing, a simple mechanical design using stable materials of construction make the fuel cell stack more compact and sturdy, which is of great importance for portable application. The applied electrolyte is in solid and dry form with no corrosive, the corrosion problems are minimized and the safety is raised. Besides, the electrolyte is also tolerant of carbon dioxide, that help to reduce the cost that air can be

used as oxidant directly without extra purification [87]. For another thing, low temperature and pressure operating condition simplifies the operation process and improves the performance, which reduced start-up time and response time to instantaneous loads as well.

Nevertheless, challenges exist for widely commercialization of PEMFC to overcome its obvious drawbacks. For the fuel cell itself, the gas involved in the reaction need to be humidification, which not only increases the complexity of system, but also effects the performance of proton exchange membrane and accelerating the degradation [88, 89]. The cost of platinum catalyst and membrane is one of the main impacts that blocking the process of commercialization. Another challenge for automobile application is the development of control and management strategy for on-board PEMFC and auxiliaries, which is of great help for optimizing the operation condition and performance. Besides, the durability of fuel cell system is not as well as internal combustion engines, reducing the degradation rate is necessary for practical application, especially in real world environments. Finally yet importantly, the on-board hydrogen storage is the key issue for PEMFC vehicles promotion. Without the safety, effective and enough capacity of on-board hydrogen storing, PEMFC, or almost all types of fuel cell are unable to function [9].

1.4/ METAL HYDRIDE BASED HYDROGEN STORAGE

1.4.1/ HYDROGEN STORAGE TECHNOLOGIES

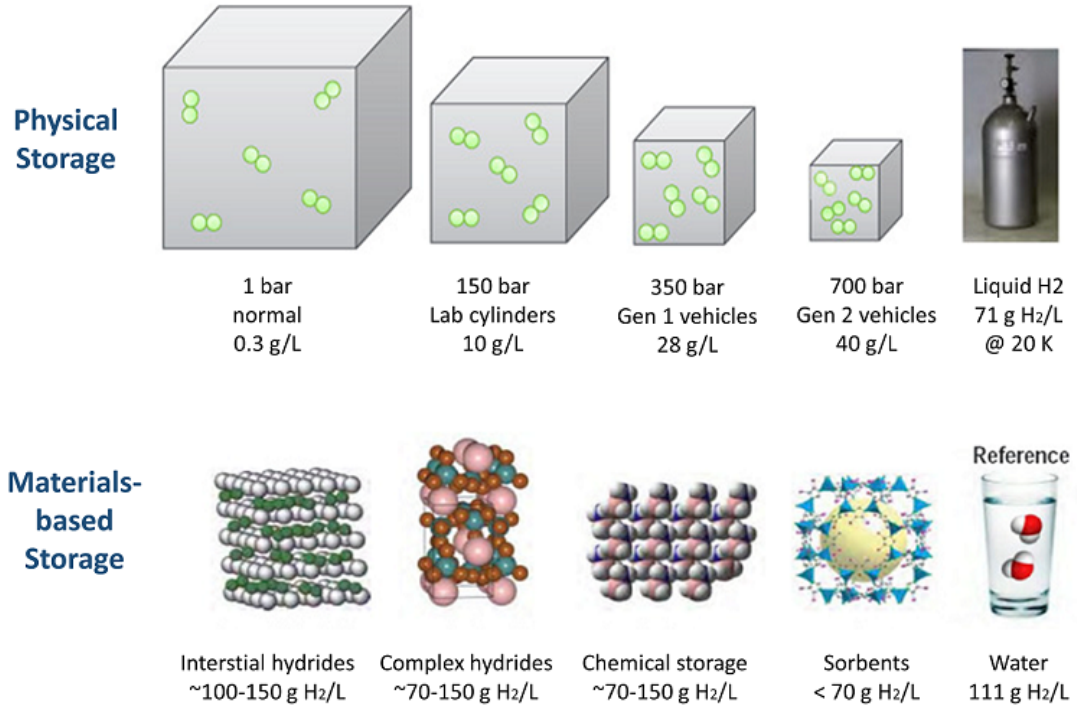

Figure 1.13: Compressed hydrogen vs. materials-based hydrogen storage [90].

The key issue faced by hydrogen storage is that the energy density by volume of hydrogen is extremely low, which is only 40.6 J/m^3 at atmosphere temperature and pressure [91]. Compared to fossil fuels, the energy density by volume of 9.9 MJ/m^3, a huge storage vessels will be required for hydrogen storage [92]. Obviously, it is unrealistic. The 2020 targets of hydrogen storage set by the US DOE are: gravimetric capacity of 5.5 $wt.\%$ and volumetric capacity of 40 g/L at an operating temperature of $50°C$ to $70°C$ under a maximum delivery pressure of 12 bar [93].

Generally, hydrogen storage method are presented in Figure 1.13, which can be divided into two main groups of physical storage and materials-based storage. Physical storage means change the physical form of hydrogen, including compressed gas form, cold or cry compressed form, and liquid form [94]. Material-based storage is storing the hydrogen in variety of materials through chemical reaction or physisorption between hydrogen and storage material.

1.4.1.1/ HIGH PRESSURE STORAGE

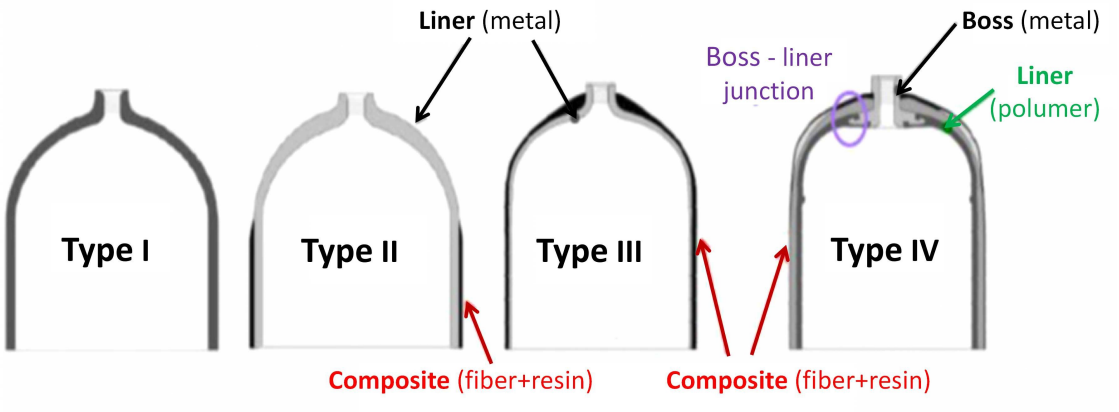

Figure 1.14: Four types of hydrogen compressed tank [95].

The technology of storage gas in a metallic pressure tank is developed since the end of $19th$ century for CO_2 storage. Using this high pressure tank to storage hydrogen was firstly occurred in 1880 for military, that a wrought iron tank stores hydrogen at 12 MPa [2]. Currently, four types of pressure tanks are developed for hydrogen storage, as presented in Figure 1.14 [95], that:

- Type I: Fully metallic pressure tanks, widely applied for industrial with pressure of 20 to 30 MPa, which is the most conventional and least expensive, however, is the heaviest.
- Type II: Steel pressure tank with a glass fiber composite over-wrap, is able to bear the highest pressure tolerance than other types.
- Type III: Full composite wrap with metal liner, is mainly carried by the composite structure while metal liner is applied for sealing purpose.

- Type IV: Fully composite, this type of tank is composed by polyethylene and carbon fiber so that the weight is the lightest.

Among these type of tanks, the steel tanks are generally used for stationary application for the purpose of reducing the cost, since the weight is not a problem. For automobile application, high pressure hydrogen storage tanks are widely used that $10,000psi(70MPa)$ tanks have been commercially promoted for the promising of quick refueling [96]. However, the energy content of high pressure tanks is still significantly less than that of the same volume of gasoline, just like presented in Figure 1.14, the volume of the high pressure tank to store 6 kg of compressed hydrogen is about 150 L, in which the pressure is already high as 700 bar. Besides, under high pressure and high temperature conditions, the tank might crack due to the hydrogen embrittlement, the safety and durability issues raise big challenges for high pressure hydrogen storage theologies [97].

1.4.1.2/ CRYGENIC STORAGE

Cryogenic vessels are commonly used for the storage and transportation of industrial and medical gases, in which the gases are liquefied. Since the energy density by volume of hydrogen is drastically raised from gaseous form to liquid form, making the cryogenic storage an attractive medium. Hydrogen can be liquefied at $-253°C$ at ambient pressure. Under this situation, cryogenic tank is able to storage 0.07 kg/L of liquid hydrogen, higher than that about 0.03 kg/L of compressed hydrogen stored in high pressure tank. However, owing to the low boiling point of liquid hydrogen, the liquefaction process is intensive energy and time consuming, and the energy content lost estimated as 40% in contrast to energy lost for compressed hydrogen, about 10% [98, 99]. For safety concerning, an extra protection vacuum jacket is covered outside of the tank [100], it also essential to mitigate heat leakage.

As a result, the practical application of cryogenic storage is quite limited, which is often used for large scale storage and delivery, for the reason that the cost of hydrogen is not an important issue and the hydrogen is consumed in a relatively short time, such as truck delivery and intercontinental hydrogen shipping, as shown in Figure 1.15.

Figure 1.15: Cryogenic trailer and pilot liquefied hydrogen carrier of Kawasaki [101].

1.4.1.3/ HYDRIDE STORAGE

Hydride storage is material-based storage that hydrogen is physical or chemical absorbed reversibly by solid compounds under certain temperature and pressure conditions. The physical sorption happens between hydrogen and materials that hydrogen molecular is absorbed on the surfaces by van der waal interactions. Available materials include some carbon-based materials like carbon nanotubes, fibers, fullerences metal organic frameworks (MOFs), covalent organic frameworks (COFs), etc. A recently discovery of microporosity (PIMs) is attractive as well. The reversibility of physical sorption is very strong that hardly any hydrogen loss during absorption and desorption. The fast kinetics make the quick refueling possible to achieve. The capacity problem is the critical drawback of physical storage that high capacity could only be obtained under extremely low temperature [94, 102–105].

During chemical sorption, chemical reaction occurs between hydrogen and material that hydrogen molecules are split into atoms and integrated with the storage material then generates hydride. Practically, except the inert gas elements, almost all elements can combine with hydrogen and form hydrides [106]. However, most of them can not be put into practical usage due to the low storage capacity and reversibility. Some kind of metals have been attractive great attentions as the more promising materials for hydrogen chemical sorption, the main reasons containing the relatively low cost, low weight and low operating temperature and pressure. The first hydrogen absorption phenomenon was discovered in palladium, nowadays, some other metal, either pure or alloy are found, that have the capability to absorb hydrogen under moderate temperature. For example, with a catalyst, the theoretical hydrogen productivity of sodium boro hydride ($NaBH_4$) reaches to $10.8wt\%$. Several prototypes of complex hydrides vessels mostly with $NaAlH_4$ and $Mg(NH_2)_2 - LiH$ have been developed and tested with confirmed high energy densities [107]. The common used low temperature hydrides for hydrogen storage can be grouped based on the stoichiometries as AB_5–type (e.g. $LaNi_5$), AB_2–type (e.g. $Ti - Zr$ alloys), A_2B–type (e.g. Sb_2Ti, Sn_2Co) and AB–type (e.g. $Ti - Fe$ alloys), where A represents elements with high affinity for hydrogen typically rare-earth or alkaline earth metal (e.g., Ca, Ti, Y, Zr, Hf, La, Ce, $etc.$) and B represents elements with low affinity for hydrogen typically a transition metal that forms only unstable hydrides (e.g., Cr, Mn, Fe, Co, Ni) [102, 103, 107, 108].

1.4.2/ ADVANTAGES AND CHALLENGES OF HYDROGEN STORAGE

Recently, MH hydrogen storage has been considered as both an economically viable option and a long-term solution for storing hydrogen. Comparing to compressed hydrogen and liquid hydrogen, the energy density of MH is higher, the hydrogen storage density of magnesium hydride ($6.5Hatoms/cm^3$) is way higher than hydrogen gas ($0.99Hatoms/cm^3$) or liquid hydrogen ($4.2Hatoms/cm^3$), so that a complex hydrogen storage tank is possible for automobile application. As shown in Figure 1.16, a medium size vehicle powered by fuel cell needs 4 kg of hydrogen to drive a distance of 400 km, the volumetric scale for storing 4 kg of hydrogen in different way are compared to the vehicle visually separately. Obviously, the volumetric densities of chemical hydrides are much higher than that of compressed hydrogen and liquid hydrogen, the examples of MH materials are Mg_2NiH_4

and $LaNi_5H_6$.

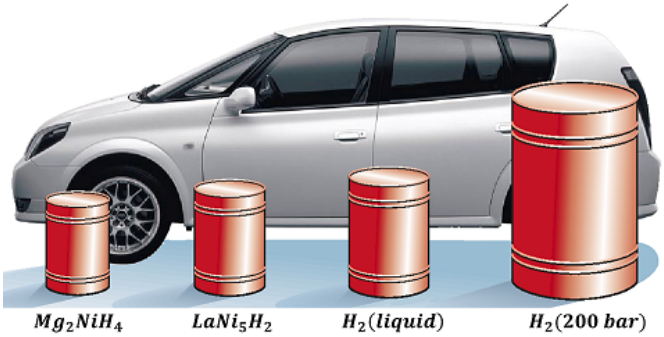

Figure 1.16: Volume of 4 kg of hydrogen compacted in different ways, with size relative to the size of a car [109].

Besides, the physisorption processes are cycling stability and fast kinetics, which contributes to the long-term usage for automobile application. As a solid storage medium, the vessels are generally special designed and barely no more empty space inside. The hydrogen purity is therefore guaranteed. Moreover, the hydrogen absorption and disorption process are both carried out under relatively low temperature and pressure. Even through extra heat is generated or should be provided, a slight change in pressure and temperature happened during the reaction. The potential of hydrogen leakage is quite small since the hydrogen is stored in atom form in a stable hydride material instead of the hydrogen molecular form which is flammable. Thus, the MH hydrogen storage method is quite safe, even for dynamic transportation missions.

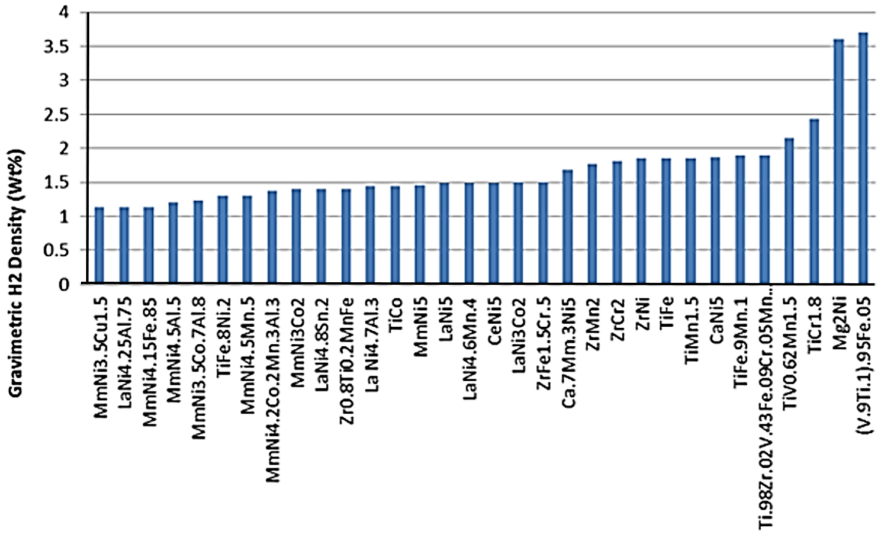

Figure 1.17: Metal hydrides versus hydrogen capacity [110].

The challenges still exists in many impacts for MH hydrogen storage. For the material itself, low gravimetric storage capacity is still a key limitation. Numerous compounds known for their absorption properties are listed in the hydride database US Department

of Energy (DOE) Hydrogen Storage Materials Database [110]. Interstitial hydride by their nature are composed of high atomic number transition metals, and therefore contain a low mass fraction of hydrogen. As shown in Figure 1.17, most of the known compounds have a reversible storage capacity less than 3 $wt\%$ of hydrogen [2]. Besides, high density leads to a comparatively heavy MH tank. It might not be a serious issue for stationary application, but novel light materials could of significant help in solving the problem of on-board hydrogen storage.

Nowadays, many research have done in MH material area. MgH_2 is the very attractive for its low raw material cost and high gravimetric capacity of 7.6 $wt\%$, which was proposed 40 years ago for hydrogen storage [111]. Some new techniques are proposed to overcome kinetics and thermodynamic limitations of hydrides and improve the the gravimetric capacity [112]. To reduce the heat of hydride formation and releasing hydrogen at lower temperature, new chemical species that reacts with the metal are introduced to forming an intermediate compound [113–115]. Cation substitution to form dual-cation hydride is generally used as a technique to modify thermodynamic properties [116, 117]. The reduction of the particle size of the hydride into nano scale allows to reduce the crystallite size and increase the surface area of the hydride. These changes are associated to an increase of surface energy of the metal hydride phases and a reduction of diffusion lengths, which improve the decomposition rate [99].

Another challenge is the thermal management of the reaction. Focusing on the heat transfer and management of reaction when hydrogen is absorbed or released is of great significant. For all these single gaseous or thermal applications, the corresponding coupled effect has to be considered as the hydrogen storage/release and the heat removal/supply occur simultaneously.

The dynamic performance is important in the design and application of hydrogen storage. The numerical analyses of its performance in order to quantitatively analyze the characteristics in detail are of great significant [118]. Many different kind of mathematical models are designed to simulate the reaction kinetics, equilibrium conditions, heat and mass transfer inside the tank during absorption and desorption process [119–124]. A.Jemni et al presented two-dimensional numerical model to emphasize the effect of the shape, pressure and cooling system more than 20 years before [125], which is widely applied in the later research in this area. A three-dimensional model figured out the parameters could be optimized to get an optimal storage are load pressure, the permeability and the thermal conductivity of the hydride [126, 127]. Dhaou et al. [128] presented the pressure-composition-isotherm (P-C-T) curves for three temperatures for both absorption and desorption process. They also proposed an analytic expression of the equilibrium pressure by polynomial interpolation based on experimental data. As a determining factor of the direction of the reaction, equilibrium pressure shows a great dependent on the temperature and hydrogen concentration. Based on the analyses of equilibrium pressure, the effect of operating parameters including hydrogen flow input and output of the tank, temperature of the cooling fluid, volume of metal in the tank have also been deeply discussed [129, 130]. The mass and heat transfer during operating process are simulated to analysis the effects of these parameters to the efficiency of the reaction and supply capacity of the hydrogen storage system [131, 132].

1.4.3/ REACTION OF METAL HYDROGENATION

Most metals or alloys can react with hydrogen to form new components. The formation of a MH is an exothermic process associated with heat release. With the supply of a sufficient amount of heat, hydrogen can also be liberated from metal hydrides [133]. The reversible MH can undergo a reversible equilibrium reaction as follows:

$$M + \frac{x}{2}H_2 \rightleftarrows MH_x + Q \tag{1.5}$$

where M represents the metal or alloy; MH_x is metal hydride and Q is the generated of required heat. Another possibility for hydride reaction is electrochemical splitting of water that alkaline ions are generated besides water. The reaction can be present as:

$$M + \frac{x}{2}H_2O + \frac{x}{2}e^- \rightleftarrows MH_x + \frac{x}{2}OH^- + Q \tag{1.6}$$

Except for single metal, large amount of inter-metallic hydrides contain at least two metals in addition to hydrogen that the general formula $A_mB_nH_x$. In this kind of hydrides, metal A has a strong affinity for hydrogen and forms a stable binary hydride while metal B does not interact with hydrogen, such as $LaNi_5$, $TiNi$, Mg_2Ni, etc.

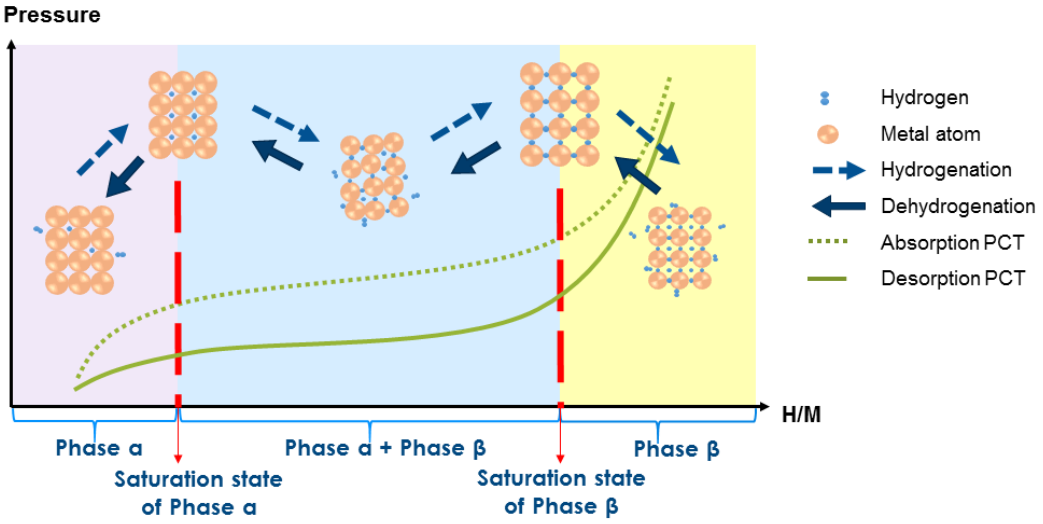

Figure 1.18: Diagram of MH formation process and P-C-T curves.

By removing or providing the heat, the reaction will alternate in one direction or the other (reversible) and the hydrogen will be absorbed into the hydrogen tank, or be desorbed and realized from the tank [134]. The hydride formation is exothermic and consequently the reverse reaction is endothermic. The variation of pressure and temperature in the tank could be generally inferred form P-C-T isotherms, which show how the equilibrium hydrogen pressure depending on the amount of hydrogen absorbed from the solid phase at different constant temperatures. Figure 1.18 shows the trend of P-C-T curves and the atomic structure schematic of the MH formation process during absorption and desorp-

tion, which could be separated into three stages.

These three stages of a MH or compound inter-metallic process could be described by a direct combination of the compound and hydrogen, according to the following steps [135]:

- Adsorption of the hydrogen molecule on the surface of the compound (physisorption).
- Dissociation of the hydrogen molecule in two atoms at the surface of the compound (chemisorption).
- Penetration of hydrogen atoms into the solid structure and formation of the solution.

During the whole process, the phase α corresponds that when the hydrogen concentration in the tank is low, the hydrogen atoms are in single-phase solid solution, which corresponds to the insertion of the hydrogen atoms in the crystal lattice. At this stage, the pressure increases rapidly until a critical value of concentration is reached. After the saturation state of phase α, the state in the tank turns into the mix phase of phase α and phase β. During this phase, the hydrogen is absorbed by the inter-metallic compound. After the hydride is completely formed, the state is phase β. During this phase, the hydrogen pressure rises steeply with the increased hydrogen concentration since no more hydrogen could be absorbed.

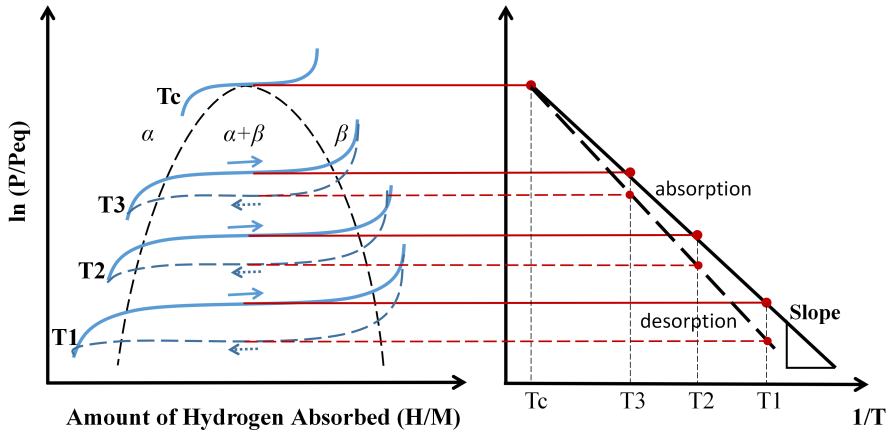

Figure 1.19: Schematic P-C-T curves at different temperature ($T1 < T2 < T3 < Tc$) and the Van't Hoff plot [136].

As can be seen in Figure 1.19, during the period of the mix phase of phase α and phase β, the isotherms show a flat plateau. The length of this plateau reveals the amount of stored hydrogen. Accompanying the increase of temperature, the pressure of its plateau increases linearly until the critical point T_c, above which the phase transition of phase α to phase β take place continuously [134]. Figure 1.19 also presented a Van't Hoff plot on the right side, which is an appropriate way to estimate the pressure-temperature stability of hydrides, for the purpose of reporting the value of $ln(P)$ as a function of $1/T$ as follow equation:

$$ln(\frac{P_{eq}}{P_0}) = \frac{\Delta H}{RT} - \frac{\Delta S}{R} \tag{1.7}$$

where P_{eq} is the equilibrium pressure and R is the gas constant. ΔH and ΔS are respectively the entropy and enthalpy of the formation of the hydride in phase β. The slope of the line is equal to the dehydrogenation entropy divided by the gas constant, namely, $\Delta H/R$, and the intercept is equal to the enthalpy of formation divided by the gas constant that $\Delta S/R$.

1.4.4/ SORPTION MEASUREMENT OF THE MH HYDROGEN STORAGE TANK

The need to accurately characterize the hydrogen storage properties of a variety of materials, including the thermodynamic and kinetic information, is of great importance for applications, including solid state hydrogen storage, electrochemical and thermal energy storage, and hydrogen gas compression and purification. Several methods are proposed for sorption measurement of a MH hydrogen storage [137] that:

- Gravimetric method:

  In gravimetric method, the hydrogen uptake is measured by monitoring the mass of the sample by the micro balance following a step change in the hydrogen pressure [138]. Thermodynamic properties such as entropy and enthalpy of the reaction can be calculated by measuring the hydrogen sorption isotherm at different temperatures. There are two types of gravimetric instruments: single-sided balance and double-sided balance. A single-sided balance with a magnetic couple does not have a tare, so the calculation is simpler as it does not involve the correction in tare side. However, the double-sided balance with a tare tends to have a better accuracy in the mass change measurement. The schematic chart of a double-sided gravimetric instrument is shown in Figure 1.20 [137].

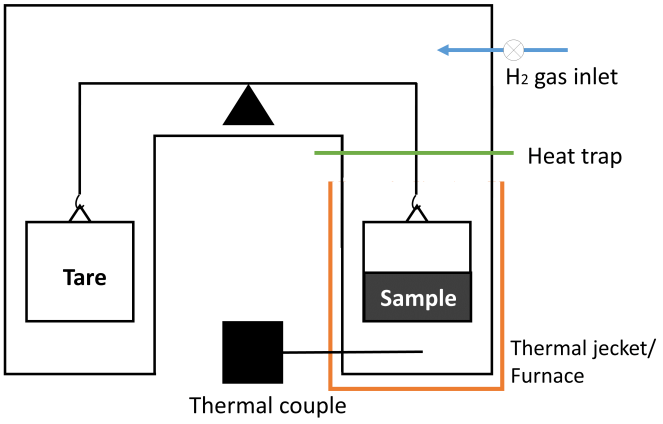

Figure 1.20: A schematic diagram of a simplified two side thermal gravimetric instrument [137].

In this method, the mass change of sample can be measured directly and continuously, this provides a better monitoring on the equilibrium of the reaction and also the gas uptake kinetics. In addition, the accuracy of density measurement here will be less stringent than that in volumetric methods. The main drawback of the gravimetric method is that the gas must be purified. Where there is a mixture of gases, the composition cannot be determined from the mass alone.

- Volumetry method:

  The sorption measurement of volumetry method is based on the Sievert technique, which is the most popular technique to determine the hydrogen storage capacity of hydrogen storage materials since it is cost-effective, easy to set up, simple, physically robust and reasonably reliable.

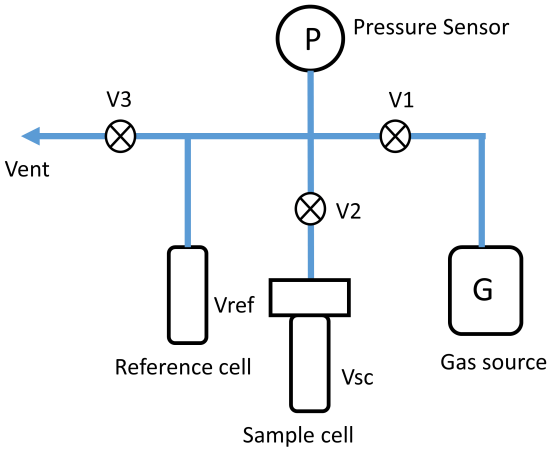

Figure 1.21: Schematic for a simplified Sieverts apparatus [139].

Figure 1.21 shows a generic Sieverts apparatus that the device can be used to measure the hydrogen uptake of a sample in the sample cell with a volume V_{SC}, the starting hydrogen pressure in reference cell with a volume V_{ref} will change when the valve V_2 is opened [139]. The technique entails injection of a known quantity gas from a well calibrated reference volume into a known cell volume containing the sample. The quantity of gas adsorbed/absorbed by the sample is calculated from the difference between the expected and measured gas pressure of the system. Repeated applications of this pressure step at successively higher (for absorption) or lower (for desorption) pressures builds a map of hydrogen uptake as a function of pressure for a constant temperature. The resultant P-C-T isotherm can be repeated at different temperatures and used to determine the entropy and enthalpy of the reaction [140].

- Secondary ion mass spectrometry:

  The secondary ion mass spectrometry (SIMS) is a technique for qualitative/quantitative surface/subsurface characterization. In SIMS, the secondary ions produced by the ion bombardment on a sample surface will be analyzed to reveal the chemical compositions and structural information of the sample. SIMS is a very sensitive technique, which can detect most elements down topper level, and

the lateral and depth resolutions range from tens to hundreds micron and a few nanometers to microns respectively [141].

SIMS is a powerful tool for hydrogenation species characterization.This direct-detecting, sensitive and rapid technique is able to quantitatively acquire localized hydrogen content across the sample surface and depth. It finds particular applications on the hydrogen analysis of thin films, and for the investigations that require rapid analyses of hydrogen depth profile and distribution in a material. However SIMS is not suitable for analyzing porous samples and materials that would degas easily under vacuum. In addition, SIMS does not provide thermal dynamic information such as entropy and enthalpy of hydrogenation,thus it is hard to compare the SIMS result with those results obtained from other methods. The expensiveness of instrument also makes SIMS not readily available.

- Thermal desorption spectroscopy:

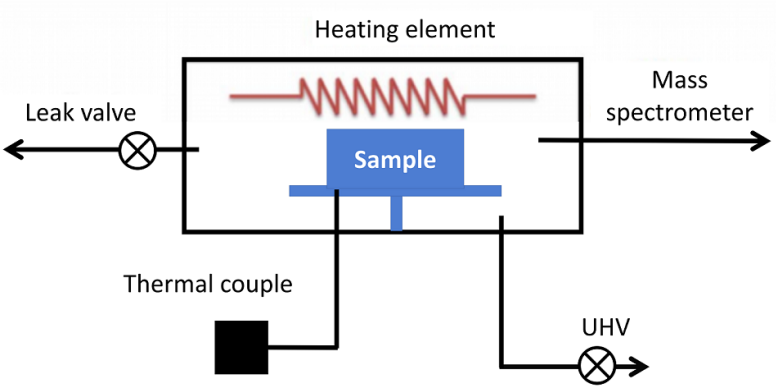

Figure 1.22: A schematic chart of thermal desorption spectroscopy equipped with mass spectrometer [137].

Thermal desorption spectroscopy (TDS) is a simple, non-isothermic, physically non-destructive technique to study the surface kinetic of adsorbates by measuring the gas desorption rate in vacuum/desired gas environments with controlled temperature ramping rate. TDS was originally used in the study of hydrogen concentration in the material and the assessment of interactions between the trapping sites with hydrogen atoms. It can also be used to identify the thermodynamic and kinetic properties of hydrogen storage alloys. There are four major parts in a TDS, namely, sample chamber, vacuum system, heating element and the detector. Mass spectrometer (MS) is frequently employed in TDS for better detection limit. Figure 1.22 shows a schematic chart of TDS with MS.

TDS has superior detection limit and only a small amount of sample is needed in a short experimental duration. Quantitative analysis is possible when a proper standard is provided. However, the TDS is only used to investigate the gas desorption process, and TDS-MS is not suitable for samples with high hydrogen diffusion since UHV is needed. In addition, it is difficult to distinguish the hydrogen signal from different trapping sites if the hydrogen desorption temperatures of these sites are

similar. The case could be more complex when studying quasi-crystalline and amorphous materials, as they are likely to experience major changes in micro structure during the heating process. The interpretation of TDS spectra could be complicated and require mathematical models to extract meaningful results.

- Neutron scattering:

  Neutron scattering is very similar to X-ray diffraction, but owning to the intrinsic properties of neutron, the study of light atoms in the lattice becomes possible. Neutron is an uncharged particle existing in atomic nuclei except for hydrogen atoms. It has a wave-length typically of 1-10 $\mathring{A}$, and can be generated through nuclear fission or spoliation. Neutron reacts with the nuclei of atoms and this makes hydrogen visible to neutron [137].

  Neutron scattering can be applied on varies types of materials like porous material and MHs for investigating the hydrogen diffusion and the structure of hydride in the materials. The high sensitivity and capability for in-situ experiment make neutron techniques a very powerful tool for the characterization of hydride. Nevertheless the beam flux is relatively small when compared with that in synchronous, larger sample size is required since neutrons react with matter weakly. Moreover, the beam source is not readily accessible for some researchers [137].

- Electrochemical characterizations:

  The hydrogen can be used as fuel to generate energy by gas combustion, but it can also act as a charge carrier in battery systems to generate electricity. A very successful example is the nickel MH ($N_i - MH$) battery, which utilizes a hydrogen storage alloy as its negative electrode. In this case, the electrochemical performance of a $N_i - MH$ battery is directly related to the hydrogen storage capacity and microstructural features of the hydrogen storage alloy in the negative electrode. Several electrochemical techniques have been reported to characterize the electrochemical properties of the negative electrode.These techniques mainly focus on the effects of hydrogen diffusion in bulk electrode and charge transfer at electrode-electrolyte interface [137].

  Electrochemical methods are cost-effective, rapid, accurate and readily available. Unlike other techniques for hydrogen material characterization which usually require precise pressure and temperature controls, the electrochemical method has less stringent requirements. However, the compositions of the electrolyte, including the impurities and dissolved gases, play a critical role in the reproducibility of the evaluation. Likewise, the result acquired by electrochemical method is not simply dependent on the intrinsic hydrogen storage properties of the sample, it might also be affected by other factors such as cell volume, size of particle and additives and the surface conditions of the positive and negative electrodes. Metals with high corrosion susceptibility or surface passivity are obviously not suitable for electrochemical characterization.

It can be seen from the above information that each technique has its own merits and limitations. Thus the choice of a particular hydrogen characterization technique depends on the nature of the material to be examined; the amount of hydrogen to be detected and

the accuracy required; the data or properties sought; and of course, the accessibility of such facility.

1.4.5/ DEGRADATION MECHANISM AND EFFECTION

The high quality of repeated hydrogen absorption and desorption process is required in practical applications of hydrogen storage. Therefore, understanding the degradation mechanisms of the hydrogen storage ability is the up most task for improving the cycling stability of the storage materials. Tanking $LaNi-$ based MH materials as examples, it is found that the degradation of the alloys can be divided into extrinsic and intrinsic process [142]. The extrinsic process including poisoning caused by the low purity of hydrogen gas, which could be minimized by reducing the impurities in the charged hydrogen gas. Hydrogen storage capacity can also be lost during extended cycling in pure hydrogen due to the intrinsic process dictated by thermodynamics of metal to hydrogen interactions [143]. The possible capacity degradation mechanisms of the reversible hydrogen storage reaction is caused by disproportion and disordering of the inter metallic alloy to form a stable binary hydride.

As example [144], in the case of $LaNi_5$, the reversible hydrogen absorption and desorption reaction in the hydrogen storage tank is:

$$LaNi_5 + 3H_2 \leftrightarrows LaNi_5H_6 \tag{1.8}$$

Another reaction between $LaNi_5$ and hydrogen can be expressed as:

$$LaNi_5 + H_2 \rightarrow LaH_2 + 5Ni \tag{1.9}$$

Reaction in Eq. 1.8 is less thermal dynamically favourable comparing to the irreversible at the same operation conditions disproportion process in Eq. 1.9. Moreover, some intermediate processes take place along with the reaction in Eq. 1.8 and Eq. 1.9, such as amorphisation, formation of lattice defects and H-trapping sites, and all these process reduce the hydrogen storage capacity of the MH.

M. Grollet al presented an experimental studies of degradation effects along with cycling that up to 90,000 thermal cycles have been tested [145]. The reversible hydrogen capacities calculated as a function of cycle numbers were determined for several AB_5-type and AB_2-type alloys. Various investigations such as pressure-composition-isotherms (P-C-T), TDS, XRD, magnetization, laser granulometry, SEM/EDS were performed in order to determine the degradation and regeneration mechanisms involved.

Figure 1.23 presents the degradation phenomena of P-C-T curves variation along with cycle [143]. Compared to initial hydrogenation reaction, the plateau pressure decreased after numbers of absorping and desorption cycles. After 2000 cycles, the plateau pressure of the absorption P-C-T curve drops drastically from 0.6 MPa to 0.2 MPa.

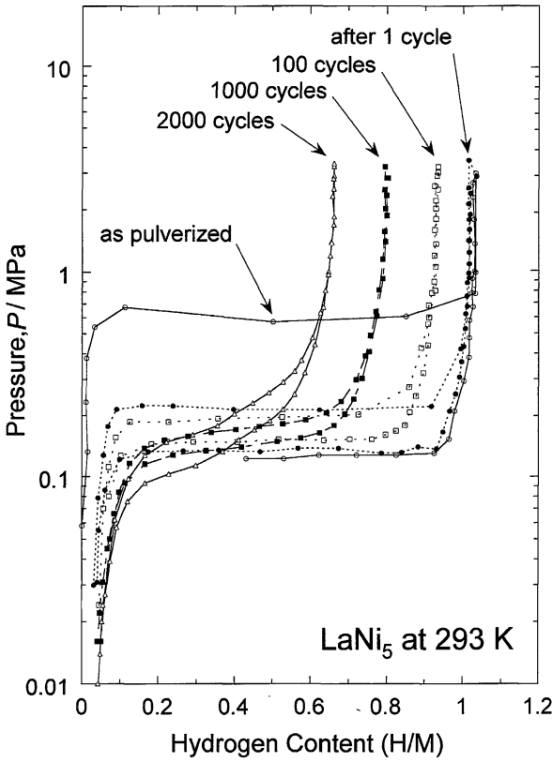

Figure 1.23: P-C-T curves for $LaNi_5$ in a pulverized state and after cycling treatments [143].

Figure 1.23 also shows that the hydrogen storage capacity of the decayed during the cycling. Some other researchers have reported similar effect in other AB_5 alloys like $LaAl_5$, $LaSn_5$, $MmNi_5$ and so on. This effect is stronger at higher temperatures and pressures. However, the original capacity of the materials could be recovered by heating to about $500°C$ in vacuum, which can lead to the decomposition of binary hydrides and recombination of inter metalloid [146]. In spite of no disproportion happened, the prolonged hydrogen absorption and desorption cycling can impair hydrogen storage properties as well. Indeed, a 20% reduction in hydrogen storage capacity accompanied by hysteresis increasing was observed for vanadium hydride during 1000 absorption and desorption cycles performed between $24°C$ and $135°C$ [144]. The most probable reason for that was assumed to be sintering effects accompanied by grain growth and strain relaxation. In chemically related $V-Ti-FeBCC$ alloys a 40% total decrease of the hydrogen storage capacity was observed after 400 cycles at 10 bar hydrogen and $20°C-600°C$. The cycling was accompanied by a $BCC-BCT$ transition and by the formation of amorphous phase in the MH matrix [147]. Structural analysis shows that with hydrogen absorption and desorption cycling, part of the $LaNi_5$ lattice structure is damaged because of the strains in the alloys and the mislocation of metal atoms in the lattice, leading to the degradation in the hydrogen storage property [148].

During the last decade the degradation issues for the MH compression materials were studied by Golben and DaCosta [149], Bowman et al. [150], Laurencelle et al. [151], Liet al. [152]. It was shown that disproportion resistance of AB_5–type intermetallics increases with the raise of the binding energy between the metal atoms, and with introduction of the

additives strengthening this interaction (e.g., tinsubstituted $LaNi_{5-x}Sn_x$), which results in the improvement of the cycle stability [153].

1.5/ OPEN ISSUES AND REMAINING CHALLENGES

1.5.1/ STATE OF CHARGE ESTIMATION OF THE HYDROGEN STORAGE SYSTEM

Among all the well known green alternatives energies, hydrogen is outstanding for transportation and application thanks to its abundance and diverse production sources. Therefore, Hydrogen Economy (HE) is highly valued and considerably funded by governments, in which hydrogen production, storage, delivery, and utilization are the key parts [154]. Comparing with high pressure gaseous and low temperature liquid state hydrogen storage, solid state hydrogen storage is favored because of safety consideration and high energy density. However, applying and mentoring hydrogen in an efficient and safe way is one of the remaining challenges.

As mentioned above, several methods are proposed to characterize the hydrogen storage properties including gravimetric method, volumetry method, secondary ion mass spectrometry, TDS, neutron scattering, and electrochemical characterizations. In these methods, parameters like heat of formation or decomposition of the hydride, maximum hydrogen storage capacity, hydrogen absorption and desorption kinetics and cycle durability are considered to be the symbols to evaluate the performance of the MH hydrogen storage materials. It is critical and difficult to select a proper method for determining the thermodynamic and kinetic properties of a variety of materials in different forms, because the estimation errors can be exaggerated when inappropriate apparatus and assumptions are employed. For example, the sieverts apparatus may not be an ideal tool for characterizing the hydrogen storage properties of porous material such as MOFs, since it is difficult to define the sample density as well as the volume of the measuring system. On the other hand, electrochemical techniques are not suitable for sample with high corrosion susceptibility since the result can be significantly affected by corrosion product formed on the sample surface [137].

Mathematical modeling is also an effective way to simulate the state of the MH reactor during absorption and desorption process and determine the relationship between different effective factors like transport properties, equilibrium conditions and reaction kinetics [155]. Many hydride tank models used to describe the process of absorption and desorption have been proposed [119, 120]. However, numerous complex elements like heat transfer, MH density are needed to be taken into consideration in these models.

In addition of the evaluation of the hydrogen storage properties and performances of each MH material, the state of charge (SOC) estimation of an embedded MH hydrogen storage tank is of paramount importance in practical application. For the reason that estimating SOC with high accuracy not only provides the information of remaining useful energy, but also evaluates the reliability of a MH hydrogen storage tank. Moreover, an accurate and efficient SOC estimation gives the idea of charging/discharging strategies, which have a significant impact on thermal management of the reaction process, since the condition of the current MH tank might under different capacities due to ageing, operation temperature

and manufacture difference. Therefore, the development of the SOC estimation is an interesting and unignorable research orientation in MH hydrogen storage application.

1.5.2/ EFFICIENCY AND THERMAL MANAGEMENT OF THE HYDROGEN STORAGE PROCESS

The MH material is normally formed as a tank for the industrial application like hydrogen storage, heat pump, thermal compression, gas separation, *etc*. The performance of a MH tank is generally affected by its material, configuration and management, which deserve careful analyses. Given the complicated nature of the hydride formation and decomposition processes, a series of technical issues are involved in the design of MH tanks, such as primary configuration, thermal management, hydrogen transfer and mechanistic strength. These issues should be well addressed to fulfil the requirement of specific applications [156].

The design of the practical MH hydrogen storage tank should respect to the different physical properties, namely, thermodynamics, kinetics, mass and energy transport, and all these need to be in a great agreement with the experimental conditions. Mathematical modelling is a useful tool to identify and predict the state of the MH during absorption and desorption as well as to determine the relationship between different effective factors with the aim of finding the best performance of the MH hydrogen storage system [155]. In recent years, many attempts have been made to identify the relationship between different operating and design variables for the resultant performance. Important challenges are the hydrogen pressure and mass flow, thermal condition and energy transportation among the system, which affect the dynamic kinetics and mass transport of the reaction.

For the automobile application, a MH hydrogen storage system is generally connected with a fuel cell stack, and normally they are thermally integrated tightly through a common water circulation loop. Low hydrogen discharge rate from MH is a common challenge for this type of energy system. Researchers proposed several solutions containing the utilization of the heat generated by fuel cell with a fan matrix or heat pipes and applying an additional heater to warm the circulation water [157]. For the purpose of releasing constant hydrogen flow under the request of fuel cell operation, the thermal management system should be carefully designed to deliver relatively uniform temperature distribution.

1.6/ CONCLUSION

This chapter is focus on the state of the arts and related works of the thesis: The FCEHVs are firstly introduced with the information of its development and structure. The typical commercial FCHEVs are presented in detail. Then, the fuel cell characters is introduced, namely, the structure and reaction of PEMFC, the dynamic characters during operation, the polarization curves, the degradation mechanism. The advantages and challenges of PEMFC is also discussed. Moreover, the on-board hydrogen storage developments are discussed. Three kind of hydrogen storage technologies are presented including high pressure storage, cryogenic storage and hydride storage. After analyzing the challenges of hydrogen storage, the MH hydrogen storage method is presented with its reaction,

sorption measurement and degradation mechanism. In addition, the open issues of the hydrogen storage and application on FCEHVs are discussed. The remain challenges can be summarized as follows:

- How to estimate the SOC of an on-board MH hydrogen storage system?
- Which kind of model can be used to describe the dynamic response of a hydrogen storage system in an efficient and systematic way?
- How to design a thermal management strategy to control the desorption reaction and improve the efficiency of a fuel cell system?

In the following chapters, the analysis and solutions to the above problems will be discussed and explained in detail.

2

NUMERICAL BASED MODELING OF MH TANK

2.1/ INTRODUCTION

Fully understanding of the dynamic performance is the basis for designing and applying the metal hydride (MH) hydrogen storage tank in practical. Associated researches mainly focus on three regions, namely, the characteristic test of MH material to analysis the storage capacity and cycling stability [108], the dynamic response analyses of a MH hydrogen storage tank through designing the mathematical model [119], the numerical analyse of the performance to quantitatively analyses the characteristics in detail [118].

The objective of this chapter is to propose the statistical model for describing the dynamic response based on the database created from real driving cycle and then to evaluate the effects of main parameters on hydrogen supply capacity of an on-board MH hydrogen tank. In this chapter, the applied databases in the research are introduced firstly, which are recorded from laboratory experiment and during the Mobypost European project respectively. The constitution and operation condition are also demonstrated in Section 2.2. In Section 2.3.1 and Section 2.3.2, the statistical models of the performance of the on-board hydrogen storage system in both charging and discharging process are presented. For the detailed results and discussions, Section 2.3.3 focus on the analysis of the coefficients of the statistical models by comparing the database and model results. In addition, the meaning and relation of the coefficients are discussed.

2.2/ ANALYSIS OF THE APPLIED DATABASES

2.2.1/ LABORATORY EXPERIMENTAL DATABASE

The test bench in laboratory is used to detect the features of the applied MH hydrogen storage tank on the operation vehicle. The validation databases from these laboratory experiments are collected in the similar way of D. Chabane did for both charging and discharging process [158]. The database includes the temperature on the surface of the tank, the pressure at the inlet of the tank, the hydrogen flow rate and the amount of hydrogen absorbed or desorbed.

In the process of absorption, the initial conditions were set as the ambient temperature and empty tank. In order to avoid high kinetics and to limit hydride temperature variations, the flow rate is deliberately kept at a low speed of 0.6 kg/h when filling the tank. A specific amount of hydrogen mass is also controlled, and a pause of 30 s is observed during the process after each packet of 0.5 g.

The hydrogen mass flow filling into the tank was controlled via the software interface during the test. A threshold of temperature is defined to control the process that hydrogen filling will be stopped when the temperature reached the threshold. During the process of hydrogenation, by imposing the hydrogen mass flow rate, the hydride undergoes a volume expansion, then it changes to another state. At the same time, the exothermic absorption process causes the temperature in the tank to increase. It could lead to the pressure increases based on the ideal gas equation of state, since the volume of the tank is relatively stable. After convection and heat transfer with the circumstance water and atmosphere, the system will naturally return to the ambient temperature and the pressure will decrease as well. This process of charge will be repeated several times until the tank is fully charged. During this entire process, the data of temperature, mass of hydrogen absorbed, pressure were recorded. As part of P-C-T curves, data related to pressure and hydrogen mass at certain temperature are saved at the same time.

Figure 2.1 to Figure 2.2 show part of the principle of the method used to characterize the MH based on the thermal variation control. By using this process, the experimental data points of each P-C-T curve for this MH hydrogen storage tank were obtained. As we can see, the hydrogen absorption process is characterized by three phases which are depending on the temperature and pressure in the tank. The amount of hydrogen that absorbed by the MH hydrogen storage tank is shown in Figure 2.2. For this tank, the hydrogen quantity absorbed is about 180 g. Figure 2.3 shows the pressure variations in the tank during the process, which are limited by the threshold of temperature. The detailed information of the relationship between temperature and pressure are presented in Figure 2.4. Obviously, the variation cycle of temperature and pressure are synchronous that they influence each other.

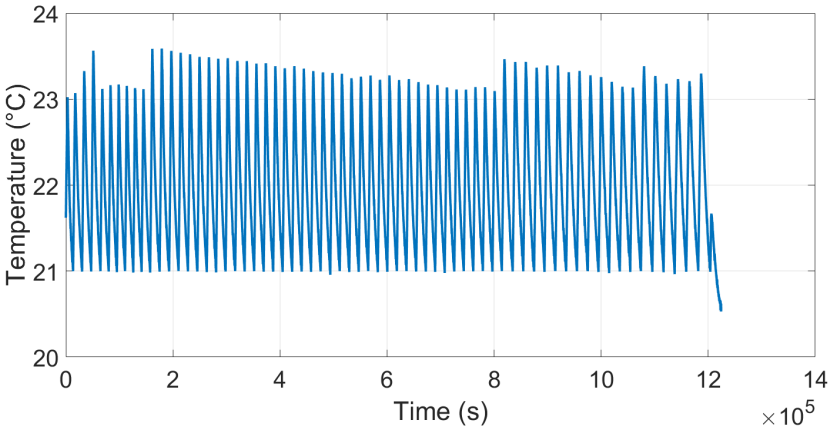

Figure 2.1: Temperature variation during absorption process in laboratory experiment.

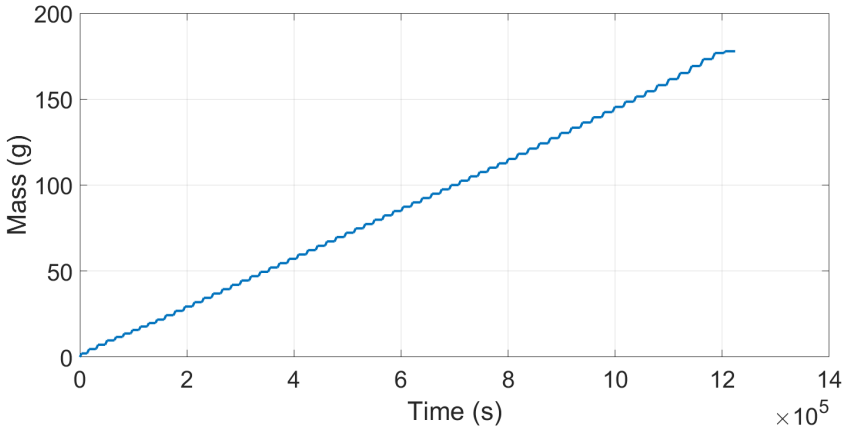

Figure 2.2: Hydrogen mass variation during absorption process in laboratory experiment.

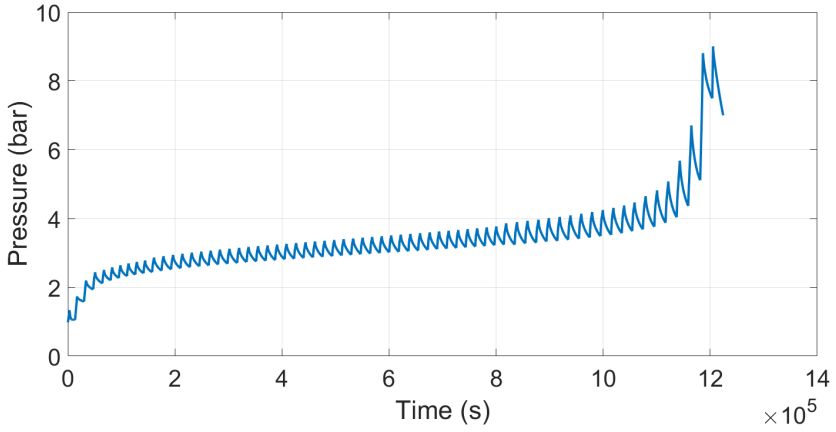

Figure 2.3: Pressure variation during absorption process in laboratory experiment.

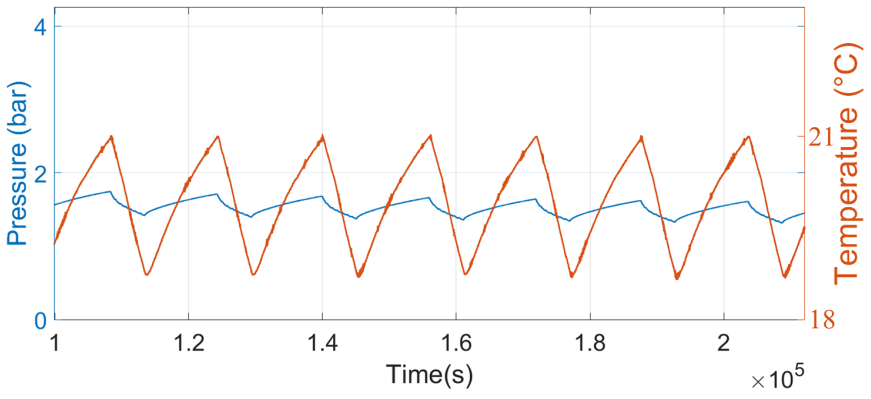

Figure 2.4: Temperature and pressure variation during absorption process in laboratory experiment.

For the experimental result, three stages of the MH behavior depending on hydrogen concentration were fully analyzed. At first stage, most of hydrogen is in gaseous form and the pressure in the tank increased quickly until a critical value. For the second stage, the hydrogen is absorbed by the inter-metallic compound and turned from gaseous form to hydride form. During this stage, the pressure grows slowly with the stable increased of the hydrogen concentration. The end of this stage is determined by the hydrogen storage capability of the MH material. For the last stage, the hydride is completely formed so the hydrogen been charged into the tank maintains in gaseous form, which leads to the pressure rises steeply.

Figure 2.5 to Figure 2.7 presents an example of the discharging test in laboratory experiment. Similar to absorption process, the discharging process is controlled by software that the temperature threshold is set and the hydrogen flow is defined. The database will be used for characteristic analysis of the MH hydrogen storage, which will be presented below.

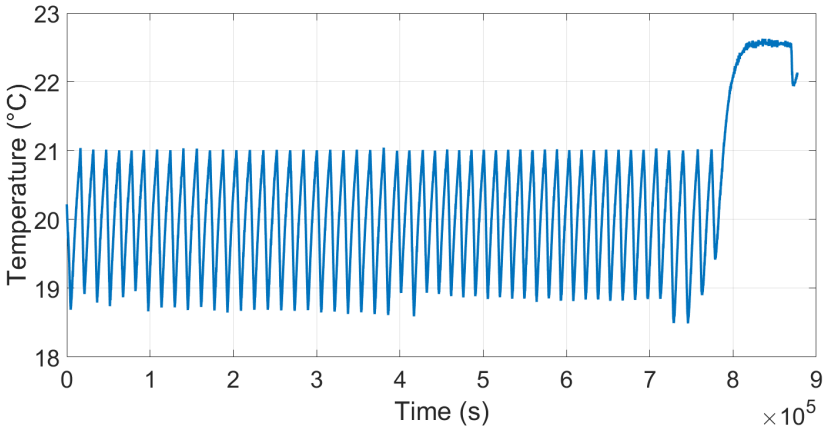

Figure 2.5: Temperature variation during desorption process in laboratory experiment.

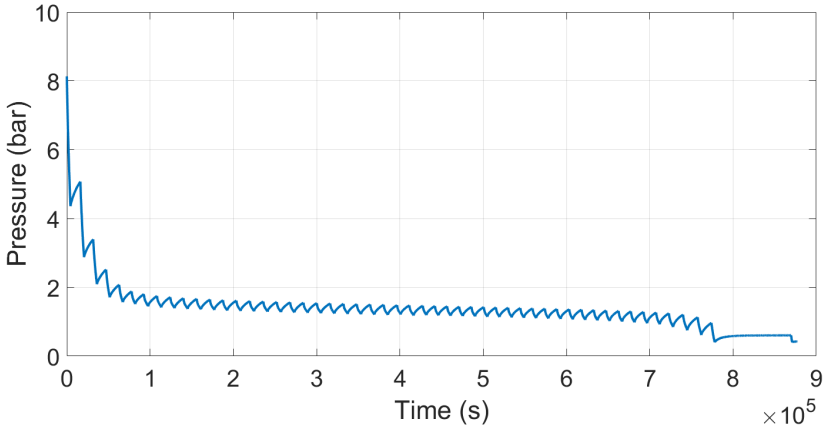

Figure 2.6: Pressure variation during desorption process in laboratory experiment.

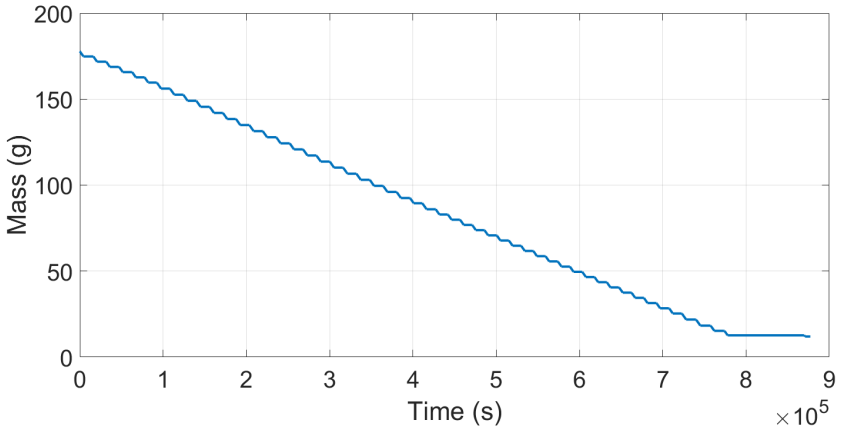

Figure 2.7: Hydrogen mass variation during desorption process in laboratory experiment.

2.2.2/ DATABASE FROM MOBYPOST PROJECT

The real operation database applied in this thesis is collected from Mobypost European project. This project is aiming to develop a new sustainable mobility concept and meet the challenge of developing a whole system combining a carbon neutral vehicle with a novel technology based on a solar hydrogen fuel cell system [159].

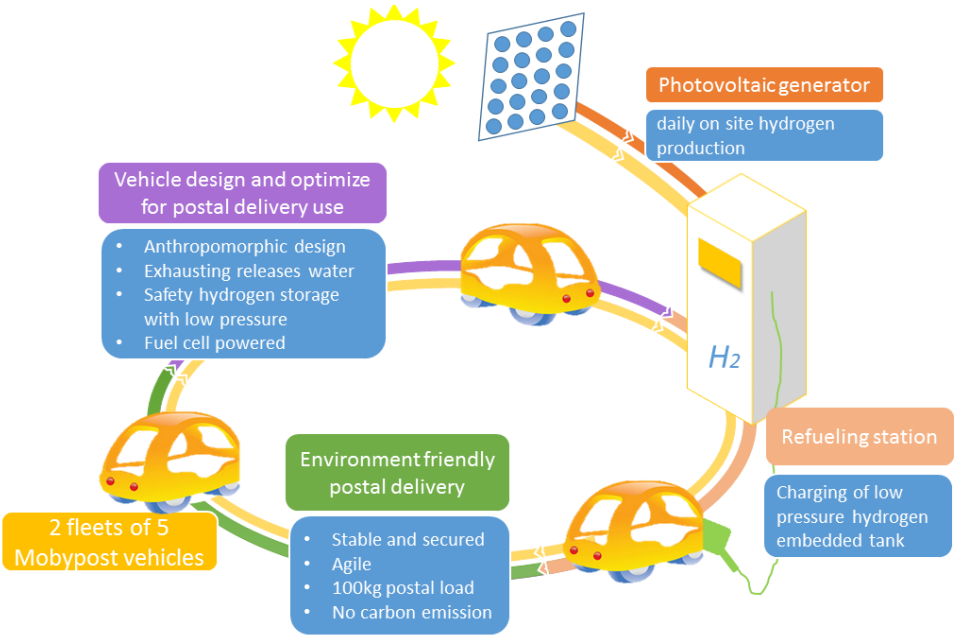

Figure 2.8: Concept of Mobypost European project.

Figure 2.8 shows the concept of the Mobypost European project which is divided into four parts. The first part is infrastructure part, which aims at designing and building a hydrogen production and distribution station. Photovoltaic generator is used to meet the mission of daily on site hydrogen production. The second part is about the designing and

optimizing of the fuel cell hybrid electrical vehicles. According to the demands of postal delivery services, the hybrid electric vehicles are produced with batteries and fuel cell system including a low pressure MH hydrogen storage tank. After the design and built of the infrastructure in part one and hybrid vehicles in part two, practical applications are necessary for testing and optimizing the system, which is achieved in the next two parts. Part three focus on the hydrogen tank charging process. The MH tanks on vehicles are charged at the refueling station with low pressure hydrogen supply. In part four, the vehicles are used by postmen for the delivery mission and their characteristics are tested during operation. Then the experimental results could be used to optimize the vehicles.

For one step of this project, ten FCEHVs powered of hydrogen fuel cells were designed and tested. The vehicles are powered by PEMFC stacks that recharges the batteries. Two MH hydrogen storage tanks work in parallel. They are charged at refueling station and discharged under the request of fuel cell during vehicle operation. As shown in Figure 2.9, the supervisors of the Post put the MobyPost vehicles in refueling station for charging the hydrogen storage tanks. The initial conditions were set as the ambient temperature and pressure. The pressure of the refueling station provided is set as 10 bar, the differential pressure between refueling station and tank help to move the gaseous hydrogen into the tank. The hydrogen flow altered also due to the vibration of the differential pressure. The value of pressure and flow are measured and recorded by the sensors located at the tank outlet. Temperature control system works together during the process, to remove the heat of the hydrogenation reaction inside the tanks through the circulation water. Temperature sensors record the variation during the charging process, the flow of water is also being recorded. The charging process is stopped when the value of hydrogen flow is lower than 5 NL/min and this phenomenon continues more than 3 min, which considered as the result of zero differential pressure. This refueling process of hydrogen will take around 2 to 3 hours.

Figure 2.9: Vehicles MobyPost charging at the hydrogen refuelling station.

During the hydrogen tanks charging time, the postmen will arrive and start to prepare the postal delivery. Each postman will integrate all mail inside the vehicles, and they will deliver the mail with these FCHEVs. Ten vehicles quadric cycles can carry up to 1000 kg of postal mails. The vehicle will use the quantity of hydrogen necessary to ensure the

experimentation and to have the same energy in the battery at the beginning. Figure 2.10 described how the mails are placed inside the vehicle and how the vehicles operation during experimentation. The operation of MobyPost vehicle will take around 4 to 5 hours. These vehicles will come back to the garage and get ready for next round. During the vehicles operating, hydrogen was desorbed from the MH material and delivered from the tanks to fuel cell. The hydrogen flow is under the request of the reaction in fuel cell. Large amount of hydrogen gushed to purge the air inside the fuel cell regularly for safety concerns, and extra hydrogen is sent to the atmosphere. Fan works together with the water circulation as the heat exchange system.

Figure 2.10: Mobypost vehicle with postal delivery mails and vehicle during the experimentation.

Table 2.1: Mobypost project database profile

Vehicle	cycles (n)	H2 charging time (h)	Discharging time (h)
1	8	14.81	17.82
2	22	148.26	177.14
3	14	27.78	33.21
4	22	57.09	59.31
5	0	0	0
6	27	51.51	66.57
7	16	35.51	42.06
8	8	15.41	16.52
9	1	0.63	27.04
10	13	23.6	35.19

Significant data of these ten vehicles are recorded each working day of postmen, which constitutes the database of our research. The profile of the database is shown in Table 2.1. The MH hydrogen storage tanks on the vehicles undergone 131 cycle in total and the whole charging time is about 375 hours. For these ten vehicles, the fuel cell operation time is around 450 hours. In this project, the vehicle No. 5 is applied as the reference vehicle without any operation. This large amount of data is of great significant not only in MH hydrogen storage research but also in fuel cell system analysis.

Figure 2.11 show an example of the database recorded during the process of charging the tanks on the vehicle. The first stage of absorption was occurred in the first 1000 seconds, a large amount of gaseous hydrogen was charged into the tanks, which can be seen in Figure 2.11(a). As a result, the pressure grows rapidly which also leads to the rise of temperature, as presented in Figure 2.11(c). When it comes to the second stage, the pressure remained stably as hydrogen turned into hydride form. In spite of the exothermic absorption reaction, the temperature gradually decreases because of the heat transfer between the tank and atmosphere. Figure 2.11(d) shows the variation of temperature during the charging process. As practical application, the absorption process might not be completely carried out and the tank was not fully charged to the end of second stage. For the Mobypost vehicle, two tanks are connected in parallel on board of the vehicle to provide enough hydrogen which have a total mass of about 350 g, while only 300 g of hydrogen is charged into the tank in this example as presented in Figure 2.11(b).

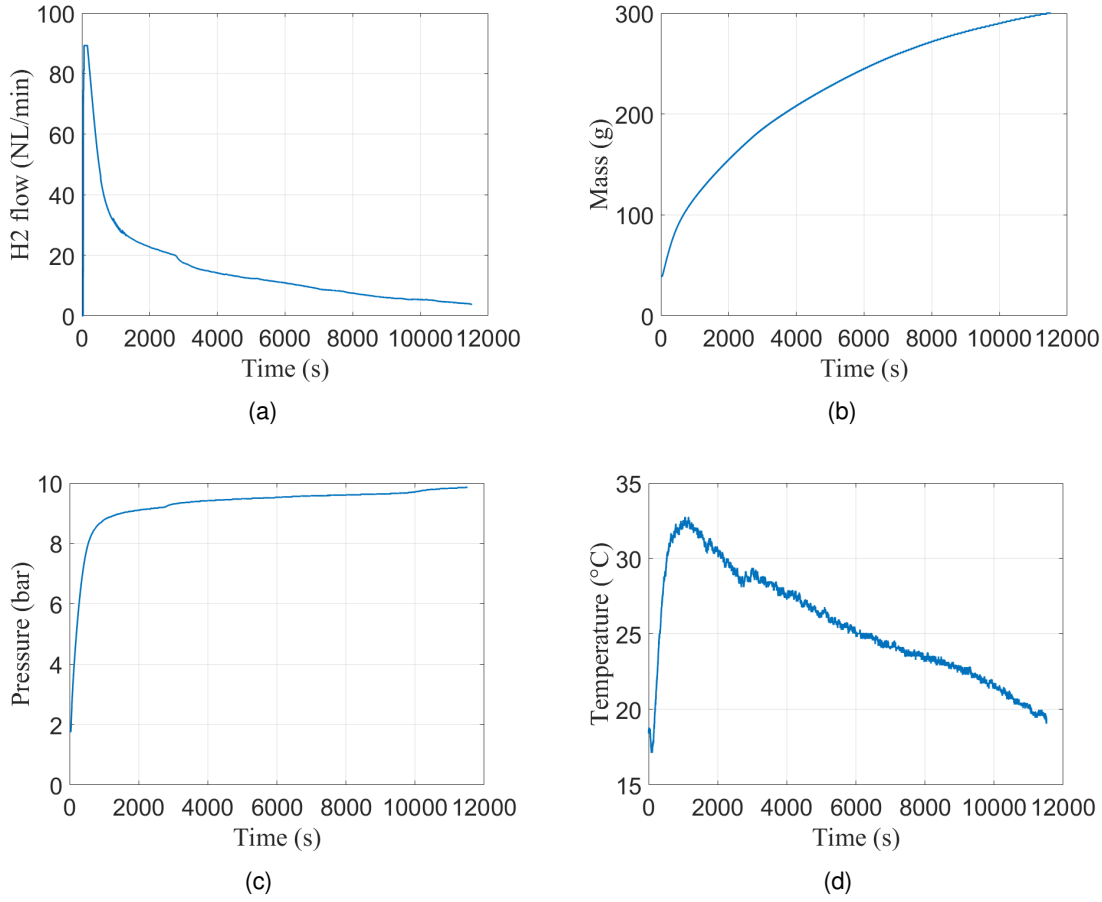

Figure 2.11: Mobypost database profile in charging process: (a) Hydrogen flow rate of charging; (b) The mass of hydrogen absorbed; (c) Pressure variations; (d) Temperature variations.

Figure 2.12 shows the main parameters variation of the tank during the vehicle operation including pressure, temperature, mass of hydrogen and hydrogen flow. The hydrogen flow at the outlet of tank obeys to the request of fuel cell. In Figure 2.12(c), one can see the first stage where the state of tank was turned from its equilibrium state to desorption

state, the gaseous hydrogen was discharged and the pressure decreased rapidly. For the second stage, the hydrogen was desorbed from the MH material and then discharge out of the tank. The pressure reducing slowly until the balance state is achieved between inside and outside of the tank. In Figure 2.12(b), it shows the decrease of hydrogen mass of the tank from 300 g to about 70 g. During the discharging process, a mean value of hydrogen flow about 12 NL/min with a lot of peaks due to the periodic purges of the fuel cell, which is presented in Figure 2.12(a).

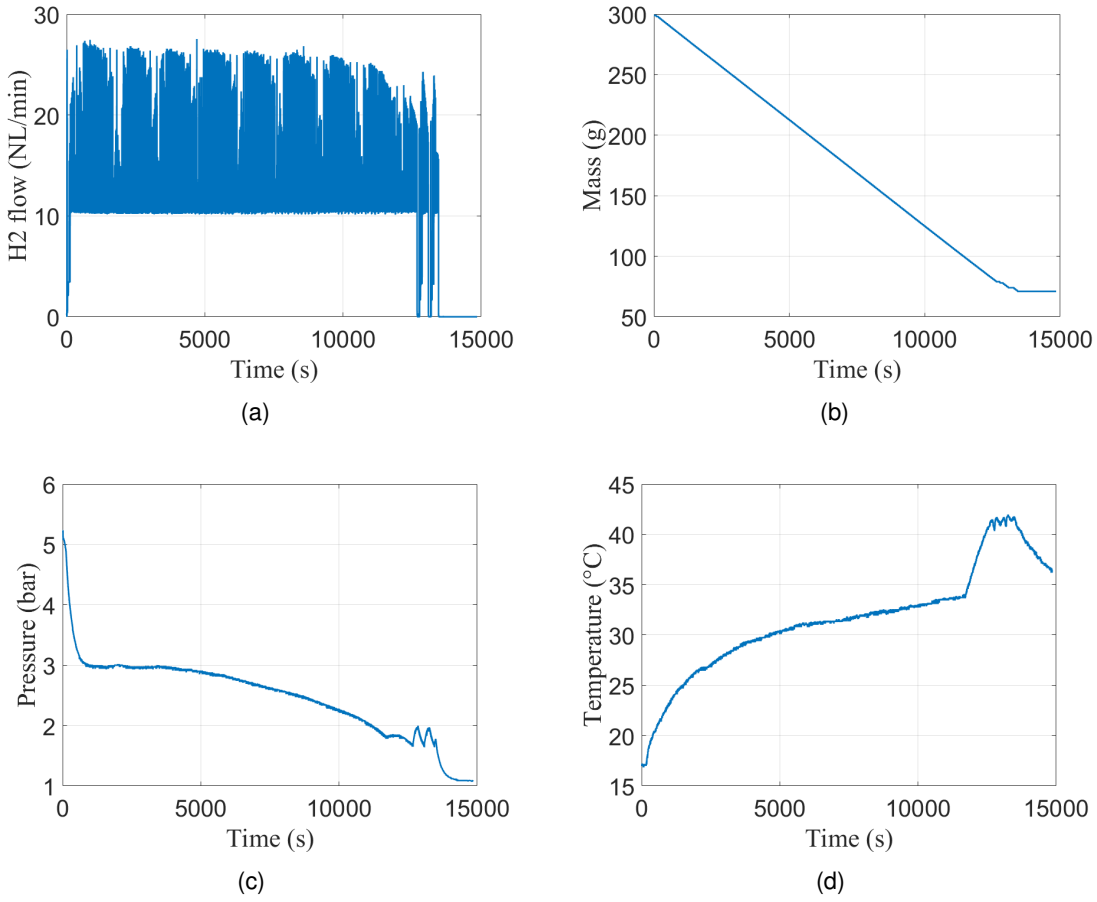

Figure 2.12: Mobypost database profile of the discharging process: (a) Hydrogen flow rate of discharging; (b) The mass of hydrogen remaining in the tank; (c) Pressure variation; (d) Temperature variation.

2.3/ NUMERICAL STUDY OF AN EMBEDDED MH TANK

2.3.1/ STATISTICAL MODEL OF THE CHARGING PROCESS

For the purpose of get the best performance of the on-board MH hydrogen storage tank, fully understanding of the hydrogen absorption and desorption reaction mechanisms as well as the dynamic response during charging and discharging process of a MH tank are of great significance. The database introduced in Section 2.2.2 is used for the analysis of

the dynamic response of the embedded MH tank.

On the Mobypost vehicles, the hydrogen storage system is constituted of the MH tank and heat exchange system as shown in Figure 2.13. The heat exchange system is combined together with tanks to constitute the hydrogen storage system in order to modify the temperature of reaction. The variation of main parameters including temperature, pressure, hydrogen flow rate and mass are analyzed separately.

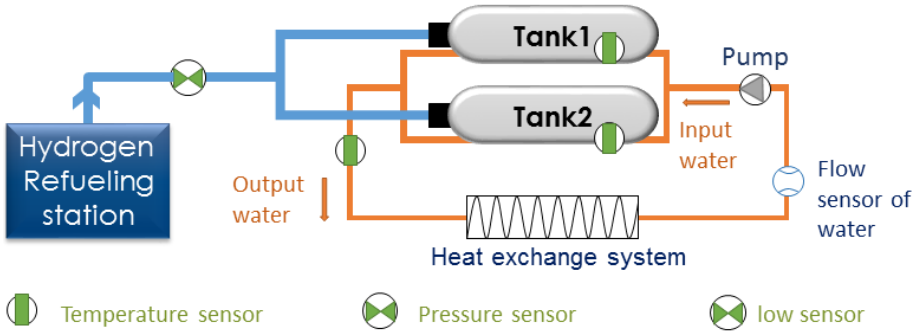

Figure 2.13: Schematic of the charging process.

The charging process is constituted by two stages. In the first stage, the differential pressure between refueling station and on-board hydrogen tank is relatively big, so the hydrogen flow is strong which leads to the rapid growth of temperature and pressure. In the second stage, hydrogen flow keeps in a low value and the reaction carried out in a high speed. Therefore, the density of gaseous hydrogen in the tank increased slowly and the variation of pressure is small. Due to the effect of energy exchange between tank and heat exchange system, the temperature decreases.

Take the moment t_{bp} as boundary point of these two stages, the statistical model of the hydrogen flow rate input to the tank, the modified temperature, pressure, and the hydrogen mass in the tank could be expressed as follows:

$$flow = \begin{cases} k_{f1} + k_{f2} * exp(-\frac{t}{k_{f3}}) & 0 < t \leq t_{fbp} \\ k_{f4} + k_{f5} * (t - t_{fpb}) & t > t_{fbp} \end{cases} \tag{2.1}$$

$$T = \begin{cases} k_{T1} + k_{T2} * exp(-\frac{t}{k_{T3}}) & 0 < t \leq t_{Tbp} \\ k_{T4} + k_{T5} * (t - t_{Tpb}) & t > t_{Tbp} \end{cases} \tag{2.2}$$

$$P = \begin{cases} k_{P1} + k_{P2} * exp(-\frac{t}{k_{P3}}) & 0 < t \leq t_{Pbp} \\ k_{P4} + k_{P5} * (t - t_{Ppb}) & t > t_{Pbp} \end{cases} \tag{2.3}$$

$$mass = \begin{cases} k_{m1} + k_{m2} * exp(-\frac{t}{k_{m3}}) & 0 < t \leq t_{mbp} \\ k_{m4} + k_{m5} * (t - t_{mpb}) & t > t_{mbp} \end{cases} \tag{2.4}$$

2.3.2/ STATISTICAL MODEL OF THE DISCHARGING PROCESS

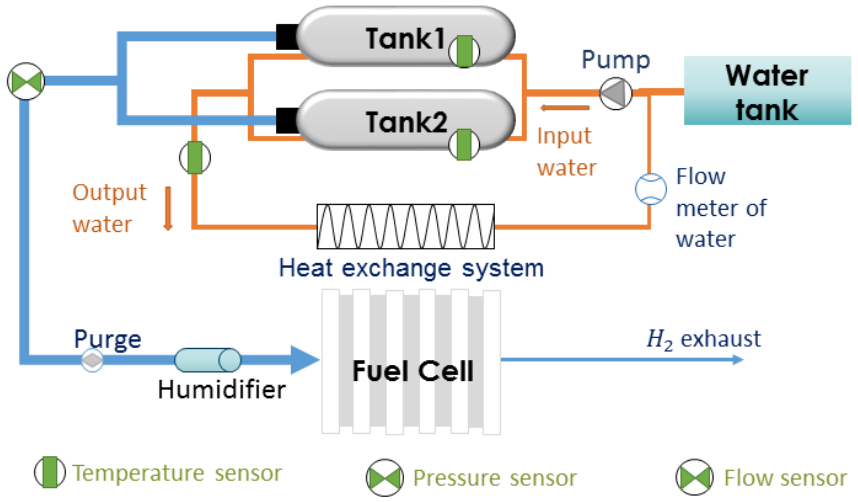

Figure 2.14: Schematic of the discharging process.

During discharging, the hydrogen is desorbed from the tank and supplied to the fuel cell as presented in Figure 2.14. According to the request of fuel cell, the hydrogen flow rate out of tank is relatively stable and the hydrogen mass in the tank reduced continuously. The statistical model of hydrogen mass can be expressed as follow:

$$mass = l_{m1} * t + l_{m2} \tag{2.5}$$

The state variation of temperature and pressure during discharging process could be divided into four stages considering that the MH tank are completely discharged.

No matter the process begins at which hydrogen concentration, pressure dropped quickly in the first stage since the gaseous hydrogen is released from the tank. Meanwhile the temperature of the tank increases rapidly with the heat supplied. During the second stage, the discharging process proceeds smoothly under the collective effect of endothermic reaction and heat exchange. The temperature increases continuously, and the variation of pressure is low. In the third stage, the hydrogen concentration in the tank reaches a lower level which leads to the decrease of pressure. The temperature keeps growth as the results of the temperature control of the heat exchange system. At the end of the third stage, hydrogen pressure reduced to the threshold value which is to low to meet the request of fuel cell. In order to promote the reaction to proceed, the water temperature in the heat exchange system is increased to heat the tank. So in the fourth stage, the hydrogen system starts to work in a new state.

The temperature of circulation water in the heat exchange system growth rapidly with heating, which leads to the increase of temperature of the tank in a higher speed until the hydrogen flow out of the tank paused. Since the dehydrogenating reaction inside the tank is promoted, the gaseous hydrogen desorbed from the MH material leads to the growth of pressure. Meanwhile the temperature of the tank shows a down trend. After stop heating the tank and restart to discharge the hydrogen, the variation of temperature and pressure

show the same trend with the first stage. This process continues only a short period since the hydrogen concentration still low. This stage repeats for several times until the tank is completely discharged. The statistic models for the whole discharging process are expressed as follows:

$$T = \begin{cases} l_{T11} + l_{T12} * exp(-\frac{t}{l_{T13}}) & 0 < t \leq t_{Tbp1} \\ l_{T21} + l_{T22} * (t - t_{Tbp1}) & t_{Tbp1} < t \leq t_{Tbp2} \\ l_{T31} + l_{T32} * (t - t_{Tbp2}) & t_{Tbp2} < t \leq t_{Tbp3} \\ \begin{cases} l_{T41} + l_{T42} * (t - t_{Tbp3}) \\ l_{T43} + l_{T44} * (t - t_{Tbp3}) \\ l_{T45} + l_{T46} * exp(-\frac{t - t_{bp3}}{l_{T47}}) \\ \quad ... \end{cases} & t > t_{Tbp3} \end{cases} \tag{2.6}$$

$$P = \begin{cases} l_{P11} + l_{P12} * exp(-\frac{t}{l_{P13}}) & 0 < t \leq t_{Pbp1} \\ l_{P21} + l_{P22} * (t - t_{Pbp1}) & t_{Pbp1} < t \leq t_{Pbp2} \\ l_{P31} + l_{P32} * exp(-\frac{(t - t_{Pbp2})}{l_{P33}}) & t_{Pbp2} < t \leq t_{Pbp3} \\ \begin{cases} l_{P41} + l_{P42} * (t - t_{Pbp3}) \\ l_{P43} + l_{P44} * (t - t_{Pbp3}) \\ l_{P45} + l_{P46} * exp(-\frac{t - t_{bp3}}{l_{P47}}) \\ \quad ... \end{cases} & t > t_{Pbp3} \end{cases} \tag{2.7}$$

2.3.3/ RESULTS AND DISCUSSION

The database of Mobypost vehicle No. 2 is used to valid the statistical models proposed before. As presented in Figure 2.16 to Figure 2.18, the results of the statistical model identification of the main parameters including temperature, pressure, hydrogen flow rate and mass during charging process are compared to the experimental data.

Coefficients k_n in the statistical models during charging process can be identified using the nonlinear regression method. The results are given in Table 2.2. Considering 20 times of charging processes of vehicle No. 2, the average absolute errors between identified model and experimental data are 0.54%, 1.72%, which are acceptable.

Table 2.2: Identified coefficients of charging model

Coefficient	Flow	Temperature	Pressure	Mass
k_1	6.9	37.65	8.75	180.05
k_2	82	-19.97	-6.81	-119.89
k_3	768.86	384.43	384.43	768.86
k_4	8.19	40.07	8.73	149.6
k_5	-5.3e-4	-5.3e-4	4.5e-5	0.0083

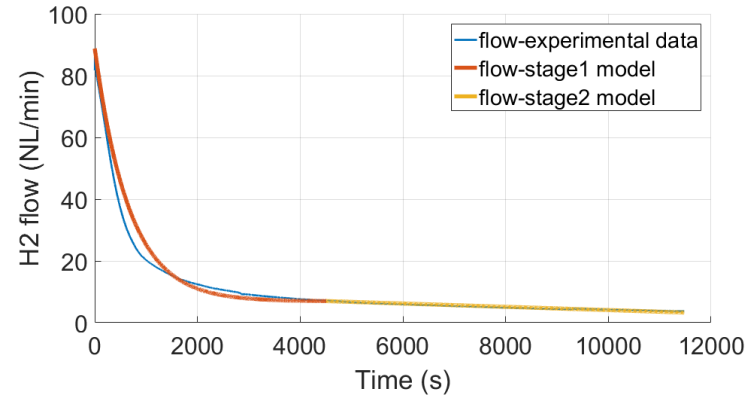

Figure 2.15: Experimental database and statistical model of hydrogen flow in one charging process of the vehicle No. 2.

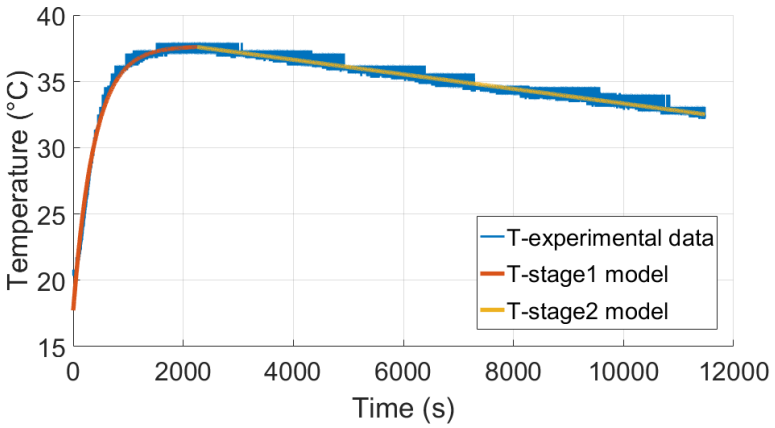

Figure 2.16: Experimental database and statistical model of temperature in one charging process of the vehicle No. 2.

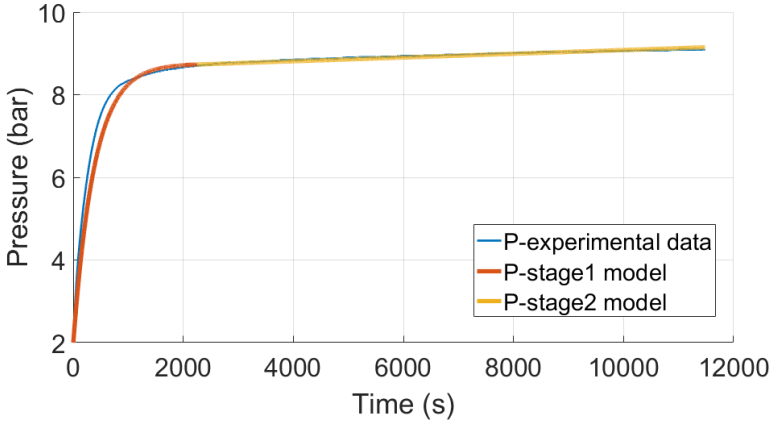

Figure 2.17: Experimental database and statistical model of pressure in one charging process of the vehicle No. 2.

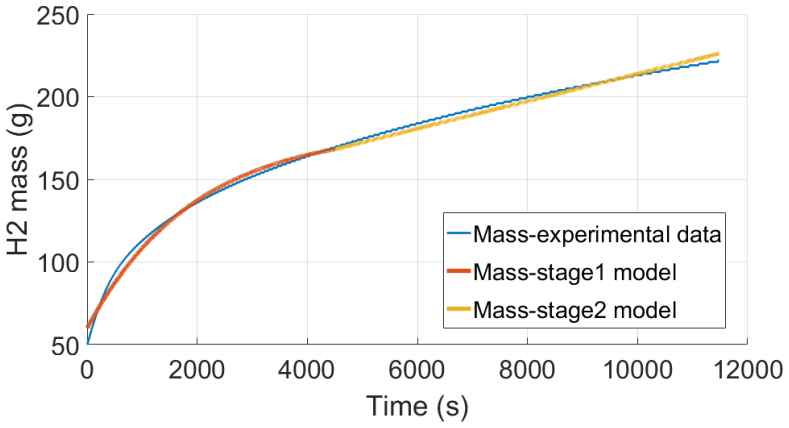

Figure 2.18: Experimental database and statistical model of hydrogen mass absorbed in one charging process of the vehicle No. 2.

The function $y = k_1 + k_2 * exp(-x/k_3)$ has the same characteristics with one order system unit step response function, in which k_1 represent the final stable value of the function, $k_1 + k_2$ represents the initial state and k_3 corresponds to the response time. In one order system unit step response function, the response time T_{res} characterizes the speed of the system transition, and the system trends to stable when it comes to $5 * T_{res}$. As one can see, in the statistical model of temperature and pressure, the speedy increase stage stopped at the time of t_{bp}, so the value of k_3 is about equal to $t_{bp}/5$, which is also be verified in the identification result.

The hydrogen flow rate is caused by the pressure differential. Based on aerodynamics function:

$$flow = (\frac{\Delta P * \rho}{g * S * L})^{\frac{1}{2}} \tag{2.8}$$

in which ΔP is differential pressure, ρ represents the density, g is gravity acceleration, S and L are the parameters of the pipeline. As the refueling station pressure is stable, the responses time of flow is two time of pressure, which means t_{fbp} equals to $2 * t_{bp}$ and k_{f3} equals to $2 * k_{T3}$ and $2 * k_{P3}$.

The hydrogen mass absorbed into the tank is the integral of hydrogen flow, so the relation of the coefficients satisfy to the function that $t_{mbp} = t_{fbp}$ and $k_{m3} = k_{f3}$. The coefficients k_3 could determine the response speed of the system. After fixing the coefficients of k_3, the other coefficients in the statistical model of flow and mass could be identified. The average errors of k_1 and k_2 are 9.53% and 1.13% respectively of 20 times charging processes happened on vehicle No. 2.

Figure 2.21 to Figure 2.22 shows the the identification results of one discharging process. The rad wine line in each picture is the label of heater. Normally the label is 0, which means the heater is turn off. The hydrogen storage system is heated when it turns to 1. The model of each parameter is divided into four stages. The duration of each stages is determined by temperature and hydrogen concentration in the tank.

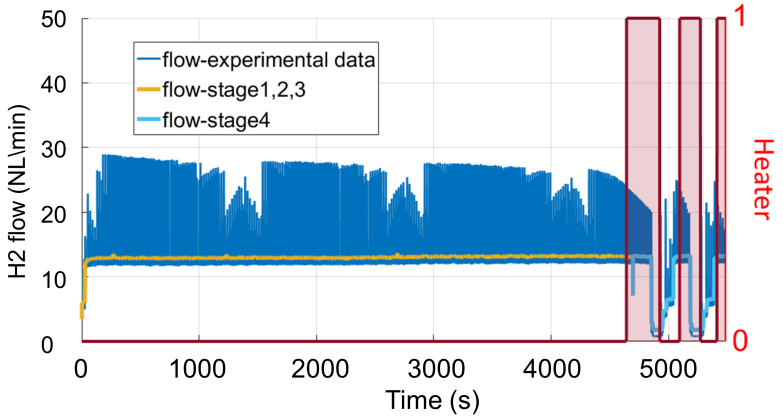

Figure 2.19: Experimental database and statistical models of hydrogen flow rate in one discharging process of vehicle No. 2.

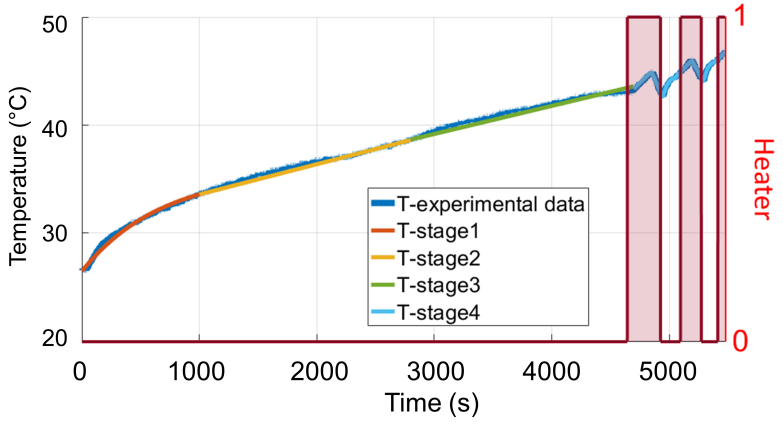

Figure 2.20: Experimental database and statistical models of temperature in one discharging process of vehicle No. 2.

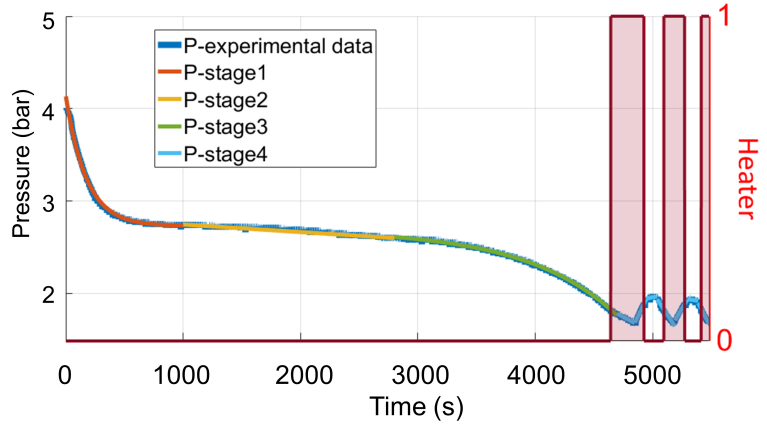

Figure 2.21: Experimental database and statistical models of pressure in one discharging process of vehicle No. 2.

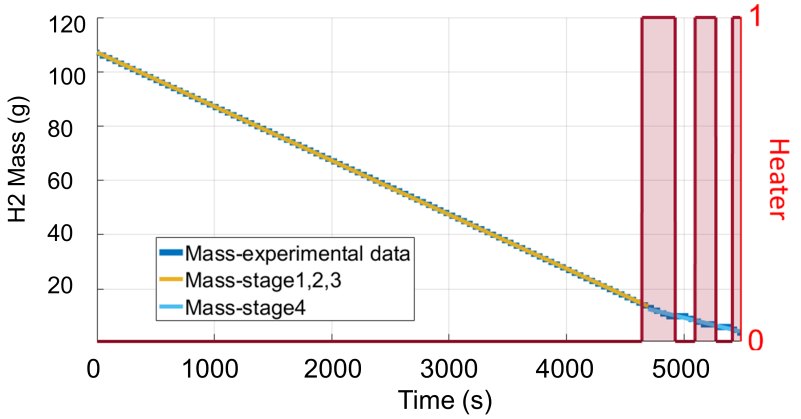

Figure 2.22: Experimental database and statistical models of hydrogen mass remained in the tank during one discharging process of vehicle No. 2.

For the first stage, the originally gaseous hydrogen stored in the tank is released, which lead to the rapidly reduce of pressure. This phenomenon happens in the first stage of all the discharging process regardless of the initial hydrogen concentration. Temperature altered under the influence of the reaction inside the tank and heat exchange system, which affect the duration of the first stage. The second stage is in equilibrium state. It will come to the end when the hydrogen concentration is low. Since the hydrogen desorption process occurs during the postal delivery, in which the flow of hydrogen is based on the operation mission, so that the hydrogen tanks might not be discharged from the fully charged state and end to the completely empty state. In the third stage,

Table 2.3: Identified coefficients of discharging model

Model	Temperature	Pressure	Mass
Stage 1	l_{T11}: 34.65	l_{P11}: 2.73	l_{m11}: 102.647
	l_{T12}: -8.16	l_{P12}: 1.41	l_{m11}: -0.0199
	l_{T13}: 550.56	l_{P13}: 175.26	
Stage 2	l_{T21}: 33.99	l_{P21}: 2.92	l_{m11}: 102.647
	l_{T22}: 0.0027	l_{P22}: 0.00008	l_{m11}: -0.0199
Stage 3	l_{T31}: 39.03	l_{P31}: 2.73	l_{m11}: 102.647
	l_{T32}: 0.0027	l_{P32}: -0.00006	l_{m11}: -0.0199
		l_{P33}: -777.25	
Stage 4	l_{T41}:45.37	l_{P41}: 1.78	l_{m41}: 8.4797
	l_{T42}: 0.011	l_{P42}: 0.00066	l_{m42}: -0.011
	l_{T43}: 40.28	l_{P43}: 14.64	
	l_{T44}: 0.011	l_{P44}: 0.0026	
	l_{T45}: 44.63	l_{P45}: 1.6075	
	l_{T46}: -2.06	l_{P46}: 0.9857	
	l_{T47}: 45.47	l_{P47}: -12.6618	

equilibrium pressure decreased as the result of low hydrogen concentration, which leads to the reduce reaction speed and pressure. Under the collective effect of temperature and concentration, when the equilibrium pressure equals to the pressure, the third stage stops. In actual operation of Mobypost project vehicles, tanks are heated before the reactions termination in order to fully discharge the tanks and obtain more hydrogen. This leads to the start of the fourth stage. During the fourth stage, the heating system works intermittently. When the system is heated, the equilibrium state is broken, and a new state is built. After heating, the variation of parameters shows the same trend with stage 1 until next heating period. Since the hydrogen concentration is quite low, the speed of hydrogen mass released from the tank decreased.

Table 2.3 shown the coefficients l_n of the statistical model of temperature, pressure and hydrogen mass during discharging process, which are identified by using the method of nonlinear regression with smaller errors. The errors of temperature, pressure and mass calculated with the database of 27 times discharging processes of vehicle 2 are lower than 2.3%, 5.3% and 6.5%.

2.4/ CONCLUSION

This chapter focuses on the data based study of the embedded MH hydrogen storage tank. The studied databases are collected from laboratory experiments and Mobypost project separately, which are representative for reflecting the performance of the hydrogenation reaction. The models designed in this chapter are based on the statistical theory to characterize the performance of the main parameters of reaction including hydrogen flow rate, pressure, temperature and hydrogen mass. Coefficients in the statistical models are identified by using the method of nonlinear regression and the errors between database and model results are acceptable. These statistical models provide the detailed and accurate explanation of the charging and discharging process during practical traffic missions. Next chapter will further discuss its performance based on these databases. Another mathematical model will be presented based on the reaction proprieties between MH material and hydrogen. Combining with the dynamic performance discussed in this chapter, the online state of charge estimation method well be proposed.

3

STATE OF CHARGE ESTIMATION OF EMBEDDED MH TANK

3.1/ INTRODUCTION

State of charge (SOC) estimation is always an important issue and challenge for all energy storage devices, namely, batteries, oil tank, hydrogen storage tank. High precise estimating the remaining energy like electric, oil or hydrogen in the devices is of great help on both reliability evaluation and control strategy design. Moreover, an accurate and efficient SOC estimation gives the information of the health condition of a real applied energy storage device, which have a significant impact on the control of practical operation in charging and discharging process. Thus, SOC of the embedded MH hydrogen storage tank should be estimated. The development of an online SOC estimation strategy, which is of great importance for the real on-board operation.

Generally, the hydrogen content of a sample is indicated by the hydrogen to host atomic ratio that:

$$\frac{H}{X} = \frac{n_H}{n_X} = \frac{m_H/M_H}{m_X/M_X} \tag{3.1}$$

where X is the number of moles of the host material and H represents hydrogen. In this equation, n_H and m_H are the number of moles and the mass of hydrogen absorbed in the MH sample respectively. M_X is the molar mass of host material and M_H represents the molar mass of hydrogen. As a result, the mass proportion of hydrogen p_H in the host metal material can be expressed as:

$$p_H = \frac{m_H}{m_X + m_H} = \frac{H/X}{H/X + M_X/M_H} \tag{3.2}$$

which can be used to evaluate the hydrogen storage capacity of the MH material and estimate the SOC of a tested sample.

In practical application of a MH hydrogen storage tank, the stored hydrogen mass can be calculated by the hydrogen flow refueled into or released out of the tank. A gas flow sensor is well developed to measure the gaseous hydrogen. However, in long-term operation along with repeated charging and discharging cycle, the measurement error of sensor is accumulated. The expanded error of hydrogen flow leads to the decline of the SOC estimation accuracy, it might resulting in an erroneous control strategy and an irreversible

damage on the MH hydrogen storage tank. Therefore, an online SOC estimation method is required to measure and calibrate the remaining hydrogen in the tank.

This chapter is arranged as that the applied databases in the research are introduced firstly, and then the attempts for SOC estimation based on these databases are presented respectively. Based on the physical characters of the reaction, a mathematical model is used to simulate the pressure-composition-isotherm (P-C-T) curves and calculate the proportion of hydrogen stored in the MH tank. Then the mathematical models of the dynamic performance of both charging and discharging process are discussed. In addition, an online SOC estimation method is proposed based on the P-C-T character and dynamic performance.

3.2/ P-C-T BASED METHOD FOR SOC ESTIMATION

3.2.1/ MATHEMATICAL MODEL

The hydrogen mass stored in MH tank is one of the most important feature of the hydrogen tank, which dominates SOC of the tank as well. During charging or discharging process, the state of MH including pressure and temperature varied and the trend of these state could be generally inferred form P-C-T isotherms, which show how the equilibrium hydrogen pressure depends on the amount of hydrogen absorbed or desorbed from the solid phase at different constant temperatures.

From the experimental data introduced above in Section 2.2.1, which were collected by controlling the temperature threshold, several P-C-T curves under different temperatures of the studied MH tank could be extracted. For each P-C-T curve, the complete process of both hydrogenation and hydrogen extraction can be described in three phases, namely slowly increase phase, quick increase phase and tend to be constant phase. Moreover, all these P-C-T curves have the same trend. This kind of feature is similar to the probability distribution function. So, the relationship among mass of hydrogen absorbed, pressure and temperature could be identified through the least squares method and the hydrogen mass could be directly described by the following equation. The mathematical model of hydrogen mass could be presented as follows:

$$Mass = k1 + \frac{k2}{1 + e^{(k3*P+k4)}} \tag{3.3}$$

where $Mass$ represents the mass of hydrogen absorbed by the host material; P represents the tank pressure. $k1$, $k2$, $k3$ and $k4$ are the coefficients reflecting the influence of temperature and cycle on the reaction of hydrogen absorption and desorption.

The coefficient $k1 = mass_{ini}(n)$ corresponds to the initial condition of the tank, ideally the tank was empty and $k1$ is zero. Under actual circumstances the tank could not be completely discharged after several times of charging and discharging cycles. Assuming the parameter n to define the number of cycles, the coefficient $k2$ becomes $k2 = mass(n, T)$, which corresponds to the amount of hydrogen mass absorbed into a fully charged tank at the end of the charging process. The latter not only depends on the number of cycles n determined by the effect of ageing, but also corresponds to the temperature T. At the

end of the process, the whole mass of hydrogen in the tank could be presented by $k1+k2$. The coefficients $k3 = f(T)$ and $k4 = g(T)$ are the functions of temperature corresponding to the equilibrium pressure in the tank, which will determine the shape of P-C-T curves.

The SOC of a MH tank at each moment i during absorption can be expressed as the following equation:

$$SOC(i) = \frac{Mass(i) - mass_{ini}}{mass_{end}} \tag{3.4}$$

where $SOC(i)$ represents the SOC of the tank at certain sampling time of i. $Mass(i)$ corresponds to the hydrogen mass being charged into the tank at this sampling time.

Based on Eq. 3.3, through modifying the mathematical model of hydrogen mass, the SOC of the tank can then be expressed as follows:

$$SOC(i) = \frac{1}{1 + e^{(f(T)*P+g(T))}} \tag{3.5}$$

As can be seen in Eq. 3.5, the SOC of a MH tank can be reflected by the pressure and temperature, no matter of the ageing degree. However, the hydrogen mass stored in the tank and the hydrogen concentration inside is tightly corresponding to the MH tank capacity.

In order to modeling the hydrogen capacity of the MH hydrogen storage tank, database of the real operation FCHEV is analyzed, the detail information of which is present in Section 2.2.2. The database indicates the dynamic performance of the embedded MH hydrogen storage tanks, while the model proposed above deals only with the behaviors under certain equilibrium state. Thus, in order to show the influence of the cycling on the P-C-T curves of the tanks, the constant temperature of $34°C$ is considered as the equilibrium state. The data recorded for Mobypost vehicle No. 4 is used, in which the MH tanks undergone 21 times of cycles of charging and discharging. The applied MH tanks on the Mobypost vehicles are of the same technology with the one test in laboratory experiment, so that the mathematical model developed above can assumed to be valid. Therefore, the parameters of $k1$ to $k4$ present the same meaning of the MH tanks' physical characteristics. Under the picked temperature of $34°C$, the parameters $k3$ and $k4$ are easily to be calculated. The detail information about the simulation results and further discussion will be presented in the next section.

3.2.2/ RESULTS AND DISCUSSION

3.2.2.1/ ABSORPTION CASE

From the database test in laboratory experiment, which is presented in Section 2.2.1, the pressure under same temperature can be extracted. Therefore, certain data point on P-C-T curves under different temperature of absorption process can be determined. Here, these picked temperature are of $22°C$, $23°C$, $24°C$ and $25°C$.

Figure 3.1 shows the identification results of the mathematical model for calculating the hydrogen mass in a MH tank during the whole process of absorption under one cycle. As shown by each isotherm curve, the absorption process mainly occurred during the

pressure from 2 bar to 4 bar. When the hydrogen concentration is too low, hydrogen cannot be absorbed. The hydrogenation process will start after the concentration reaches a certain value, which leads to the pressure increasing. After the MH material distributed in the tank was fully charged, the pressure rises steeply with the increased concentration of gaseous hydrogen. The coefficients $k1$, $k2$, $k3$ and $k4$ used to draw these curves of the mathematical model in Figure 3.1 are given in Table 3.1. As one can see, the maximum and the minimum value of the error between proposed model and experimental data are 9.6% and 2.5% respectively, which are acceptable.

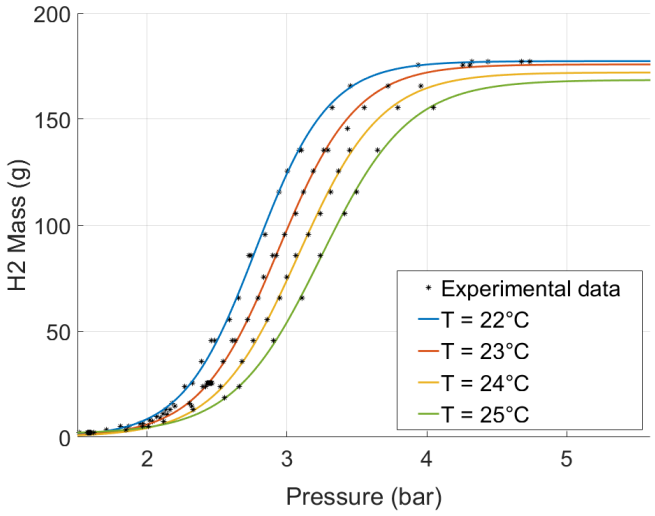

Figure 3.1: Parameter identification of the absorption model for one cycle.

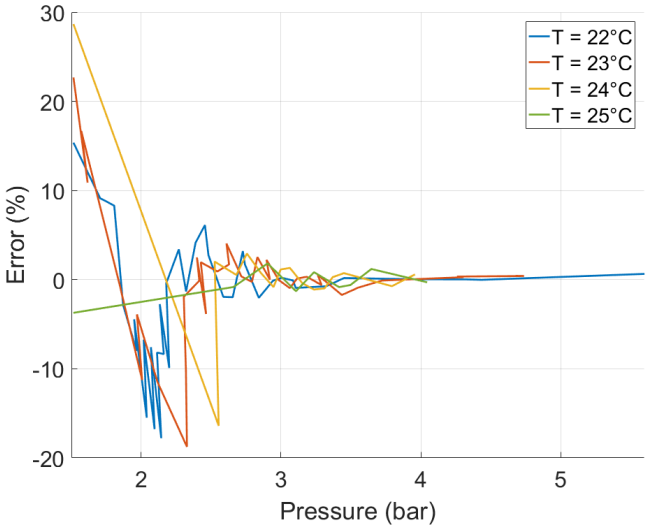

Figure 3.2: Errors of identification of absorption model for one cycle.

Figure 3.2 gives the deviation of under different pressure. One can see that the errors of the proposed model are concentrated in the pressure zone of 1.5 bar to 2.5 bar, where

the hydrogen concentration is not high enough and the main absorption reaction is not carried out.

All these data points are extracted from the same absorption process. As a result, the initial state of the tank are the same. Therefore, the identification results of the coefficient $k1$ are ideally to be the same, which can be seen from the Table 3.1 that the identification results are approximate. The coefficient $k2$ corresponding to the hydrogen mass stored in fully charged MH tank, which can be influenced by the temperature. So, for different operation temperature, the capacity of a MH tank could be varied. The cycle number would effect the capacity as well, which will be discussed below.

Table 3.1: Identified parameters for absorption model.

$T(C)$	22	23	24	25
$k1$	10^{-8}	10^{-14}	10^{-6}	10^{-6}
$k2$	177.3635	175.8193	172.0149	167.0116
$k3$	-3.8324	-3.5680	-3.3795	-3.1786
$k4$	10.6431	10.4728	10.4141	10.3063
Error(%)	9.6	9.1	7.4	2.5

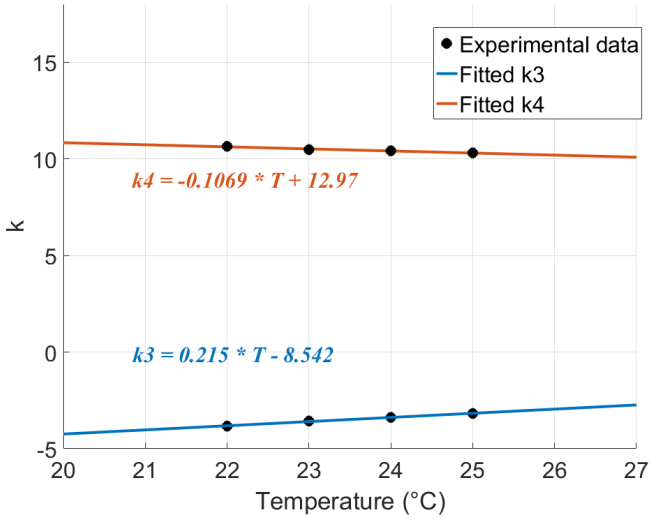

Figure 3.3: Coefficients fitting of k3 and k4 with P-C-T curves for one cycle.

As mentioned in the mathematical model of $Mass$ above, $k3$ and $k4$ reflect the effect of temperature on the equilibrium pressure, which determines the shape of P-C-T curves. The values of equilibrium pressure under each temperature could also be obtained by plotting the equations of the relationship between $k3$ and $k4$ and temperature. Figure 3.3 shows the coefficients variation with different temperatures. The function of $k3$ and $k4$ are identified as follows:

$$k3 = 0.215 * T - 8.542 \tag{3.6}$$

$$k4 = -0.1069 * T + 12.97 \tag{3.7}$$

Figure 3.4 shows the model of the hydrogen mass absorbed under certain temperature and the pressure without considering degradation. It is can be seen that for the first time charged tank, the coefficient of $k1$ is zero and the mass of hydrogen charged is only depending on the temperature and the pressure.

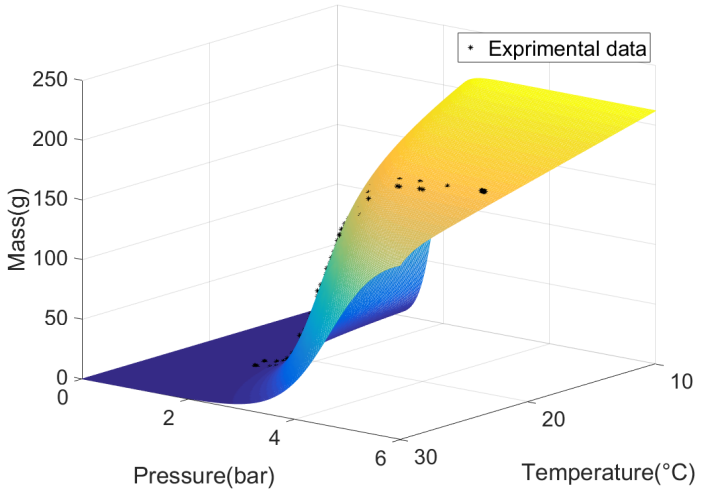

Figure 3.4: Mathematical model of hydrogen mass absorbed into the tank.

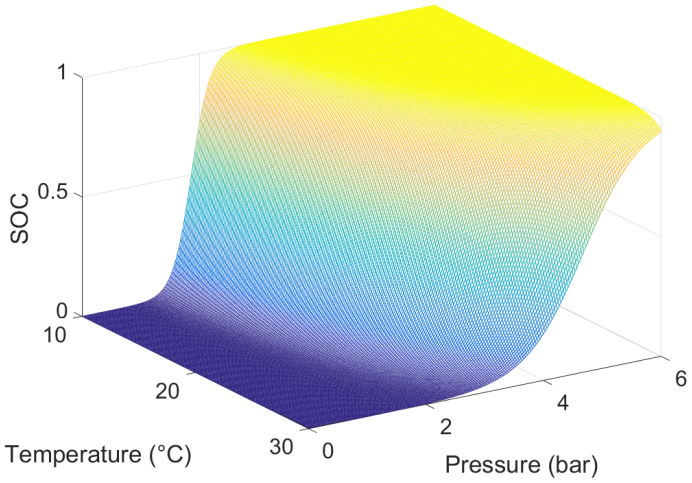

Figure 3.5: SOC model of the MH hydrogen storage tank.

Figure 3.5 shows the state of charge of the tank, which is calculated by the model based on Eq. 3.4. Since the number of cycle only effect the capacity of the tank, the percentage of hydrogen concentration can be calculated by the value of pressure and temperature, namely, the SOC of the tank is not affected by how many times the tank was charged and discharged.

3.2.2.2/ DESORPTION CASE

Similar to the absorption case, the data points of pressure under certain temperature during hydrogen desorption process can be extracted. The results of the mathematical model of hydrogen mass stored in a MH hydrogen storage tank during desorption process under one cycle is presented in Figure 3.6. Obviously, the desorption process is normally carried out in a lower pressure zone than absorption, for the tested tank, between 1 bar to 2 bar. The desorption reaction cannot keep going automatically when the pressure is relatively too low at the end period of discharging process due to the low hydrogen concentration. Special measures are necessary to fully discharge a MH hydrogen storage tank like heating. Hydrogen retention in the tank would lead to the capacity degradation of a embedded tank used for practical operation since the temperature condition cannot achieved, which should be paid particular attention. The coefficients of the model for desorption process are presented in Table 3.2, in which the maximum error is acceptable that the value is 2.5%. As shown in Figure 3.7, the error occurs when the pressure is low, as a result, higher difficulty is inevitable for SOC estimation at low hydrogen concentration.

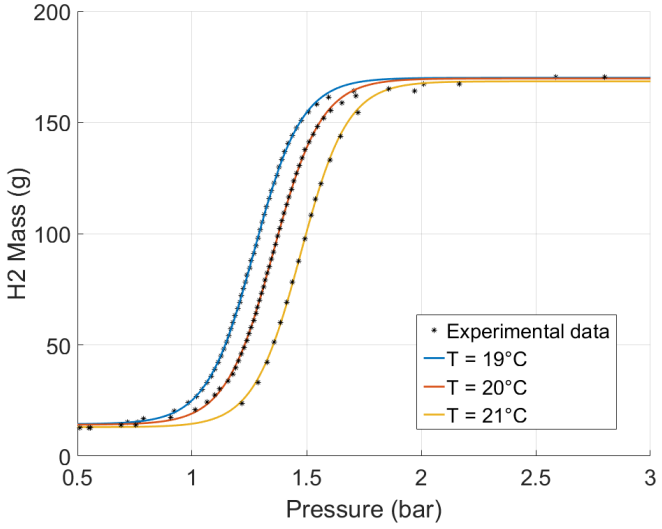

Figure 3.6: Parameter identification of desorption model for one cycle.

Table 3.2: Identified parameters for desorption model

$T(°C)$	19	20	21
$k1$	14.3184	14.0725	13.0102
$k2$	155.7164	155.6490	155.4380
$k3$	-9.5933	-9.5522	-9.7628
$k4$	12.1947	12.9445	14.3836
Error(%)	0.82	1.51	2.47

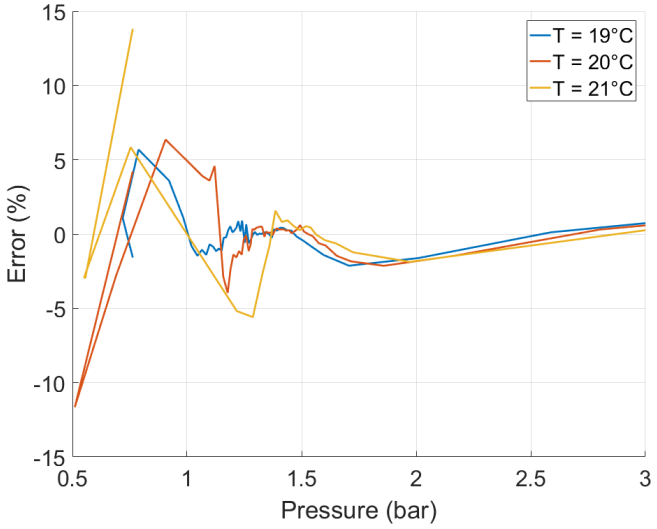

Figure 3.7: Identification errors of desorption model for one cycle.

3.2.2.3/ CAPACITY DEGRADATION

The database of Mobypost project introduced in Section 2.2.2 show the dynamic behaviors of the embedded MH hydrogen storage tanks where we recognize one and second order variations. The tanks undergone several times of charging and discharging cycles with the operation mission. However, the models presented before deal only with the behaviors under certain equilibrium state. Thus, the preprocess and classification of the database is necessary.

Based on the prior knowledge of the trend of the database, useful databases are picked out in order to identify the coefficients of hydrogen mass model in Eq. 3.3. In our study the constant temperature of $34°C$ was considered as the unified equilibrium state. The aim is to show the influence of the cycling on the hydrogen capacity and the mathematical model of the MH tanks. The data corresponding to 21 times of charging process of the Mobypost vehicle No. 4 are used. Knowing that the tanks of Mobypost are of the same technology with the one studied before, the model and coefficients developed in Section 3.2.1 can be assumed to be valid. So, for the coefficients $k3$ and $k4$ corresponding to the temperature of $34°C$ are easily to be computed using the fitting functions of Eq .3.6 and Eq. 3.7. The obtained values are $k3 = -1.23$ and $k4 = 9.34$, which remain constant while the temperature is stable. Otherwise the coefficients $k1$ and $k2$ will change according to the cycle conditions.

Figure 3.8 shows the identified model of hydrogen mass absorbed of different cycles during charging process, of which the data points are collected from Mobypost project database. For each cycle of charge, the values of the equilibrium pressure under different reaction temperature remained stable as the atmosphere temperature did not changed a lot. The charging pressure provide by the refueling station is 10 bar, which of great effect on the reaction temperature and speed the hydrogeneration process. As a result, the main process of hydrogenation occurs when the pressure is between 7 bar and 9 bar. Along with the increased cycle numbers, the performance of the tank undergoes

a sustained degradation that the capacity declined. Due to the operation condition, the tank can not be completely charged and discharged every time, which could lead to the total hydrogen mass supplied by the tank decreasing with the cycle. Assuming that the hydrogen absorption reaction process is evenly distributed in two parallel MH tank, it can be noticed in Figure 3.8 that, for the first cycle, the hydrogen supply capability of one MH hydrogen storage tank is about 163 g while after 21 times of charge and discharge, the supply capability is only about 158 g.

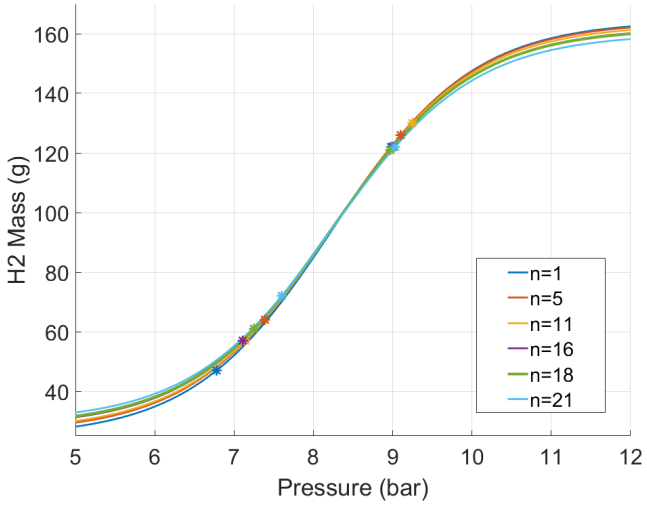

Figure 3.8: Hydrogen mass charged into the tank of Mobypost project vehicle for different cycles.

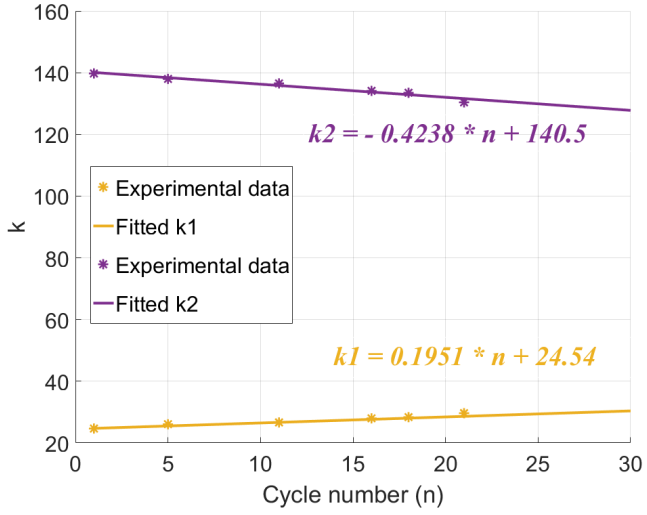

Figure 3.9: Coefficients fitting of k1 and k2 with the number of cycle.

Figure 3.9 highlights how the cycles influence the initial hydrogen mass and the final hydrogen mass in the MH tank. After several cycles of charging and discharging, its capability to storage hydrogen will decrease until no more hydrogen could be absorbed

into the tank or desorped from the tank. The relationship between cycles and hydrogen supply capability could be used to build the ageing model and describe the degradation degree of the tank. The coefficients of the hydrogen mass model in Eq. 3.3 can be expressed as:

$$k1 = 0.1951 * n - 24.54 \tag{3.8}$$

$$k2 = -0.4238 * n + 140.5 \tag{3.9}$$

What should be declared is that the database of Mobypost project is collected in real FCHEVs operation, in which the postmen are responsible for the charging and operation process. Therefore, the experiment is not strict controlled under the premise that the requirement of postal tasks are considered first. As can be seen in Figure 3.8, even the hydrogen capacity of the tank under the first cycle is lower than that had tested in laboratory, namely, about 180 g. This might caused by the inadequate execution of the termination conditions that the postmen driven the vehicle for deliver mission before the tanks are fully charged. Besides, the discharging process stops along with the end of vehicle operation, instead of the completely use of hydrogen, which leads to the hydrogen remaining in the tank before next charging process. Moreover, according to the data sheet provide by the manufacture and the background knowledge from literature, the tested MH tank is possible to be used for around 1000 number of charging and discharging cycles. The database of 21 times of cycle provided by the Mobypost vehicles is not enough for degradation analyses. More test reflecting the degradation situation of the tank is required for improving the accuracy of the coefficient identification results of $k1$ and $k2$.

3.3/ Online SOC estimation with a state classifier

3.3.1/ Framework of the process

For transportation application, the SOC of a MH tank should be carefully estimated. In spite of the summation calculation of the hydrogen flow during a dynamic charging or discharging process provides the hydrogen mass been stored into the tank or released out of a tank, the uncertain information of the initial hydrogen concentration make the result inaccuracy. During charging process, the tank is well controlled at the refueling station and the SOC of the tank can be measured by the pressure difference. However, the discharging process occurred with the vehicle operation don't have such information for SOC estimation. Meanwhile, the remained hydrogen in the tank is of great importance for the embedded energy management system to monitor the mission.

The physical state of the MH tank, namely, pressure and temperature, is effected by the inside hydrogen concentration and the reaction condition. Hence, the SOC of a MH hydrogen storage tank can be estimated through monitoring its pressure and temperature. As discussed in Section 2.4, the variation of the physical state of a tank during absorption process can be separated into two stages and the desorption process can be separated into four stages. In the second stage of both absorption and desorption process, the reaction between MH and hydrogen stay in equilibrium state and the physical state preformed by the tank are mainly dominated by the P-C-T condition, which means that the pressure and temperature in this stage are determined by the hydrogen concentration. Therefore,

the mathematical model proposed in Section 3.2.1 can be used for SOC estimation. In this section, an online SOC estimation method is proposed.

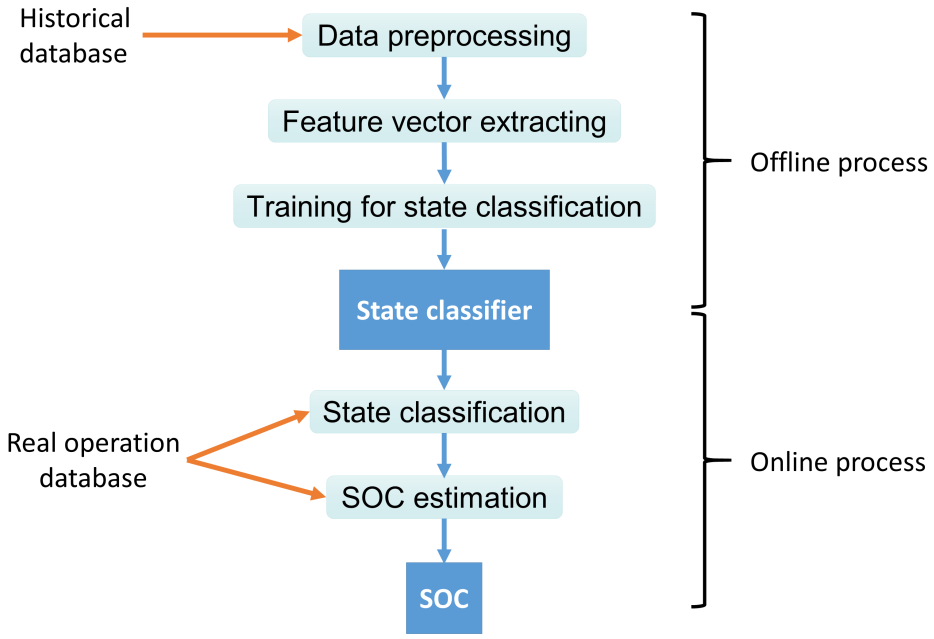

Figure 3.10: Framework of the online SOC estimation with a state classifier.

Figure 3.10 gives the schematic of the framework of SOC estimation procedure. A state classifier is designed to classify the physical state of the tank. After training the state classifier offline using the historical database, the real data recorded during test can be characterized into relating stage, which can be realized online.

In the offline stage, the historical database is analyzed and preprocessed. For the purpose of quick classification, the optimal feature vectors reflecting the characteristics and state should be extracted from the recorded database. The statistical characters including slope, kurtosis, entropy, etc, are of great potential as the feature vectors for classifying. Afterwards, the state classifier is trained by the feature vectors training set. When the trained state classifier comes to the online stage, the feature vectors extracted form the real measured database is able to be classified and therefore the SOC of the tank could be estimated. In this process, classifier is a model set describing the characteristics and features of the database, which can be used to identify the category of unknown data, namely, map the unknown state to a discrete classification set. The data-based classification method includes fuzzy logic identification, neural network, Bayes classify, support vector machine (SVM) and so on. In this work, a joint multi-classifier is designed through combining the Naive Bayes classifier and SVM classifier, the detailed information of which will be presented below.

In the online stage, the feature vectors extracted from real operation database are putted into the joint multi-classifier to recognize the current reaction state. As discussed in Section 2.3 and Section 3.2, the second stage of the hydrogenation reaction is stable, and in this stage, the hydrogen concentration is performed by the dynamic performance like

pressure and temperature. Thus, the remaining hydrogen can be calculated by the proposed mathematical model.

3.3.2/ DESIGN OF THE STATE CLASSIFIER

3.3.2.1/ NAIVE BAYES CLASSIFIER

Based on Bayes statistical theory, Naive Bayes (NB) classifier is developed to identify the category to which the observation belongs to, it has been widely applied in many situations [160]. The feature vectors to be examined are assumed to follow a certain probability distribution and can be reasoned based on these probabilities, thus, the optimal classification decision can be made. Although the independence assumption between the feature vectors is oversimplified, the NB classifier bring a competitive performance compared to other state of the art classifiers in many complex real-world situations [161].

The classification using Bayesian method needs to be carried out under certain conditions, that is, the probability distribution of each category is consistent; the number of categories to be classified is certain. For a given observation simple set S, the feature vectors is assumed to be $A_1, A_2, ..A_n$ with the number of n. Therefore, the sample set to be classified is X with the characters $x_1, x_2, ..., x_n$, in which x_i is the specific value of A_i. The number of categories contained in the observation sample set is c, and $C = C_1, C_2, ..., C_c$. Moreover, the posterior probability of the sample to be classified belonging to a certain class C_i is set as $P(X|C_i)$, and $c(X)$ presents the label of category obtained by the classification. Thus, the NB classifier can be expressed as:

$$c(X) = \underset{C_i=C}{argmax}\, P(C_i)P(X|C_i) \tag{3.10}$$

The NB classification is developed on Eq. 3.10 with a hypothesis that all the features A_i are independent to each other under the condition that the category is given, which means:

$$P(A_i|C, A_j) = P(A_i|C), \forall A_i, A_j, P(C) > 0 \tag{3.11}$$

In NB classification method, the probability and category label of each features can be learned independently at the same time. The posterior probability calculated by a NB classifier for certain category is:

$$P(C = c|A_i = a_1, ..., A_n = a_n) = \alpha P(C = c) \prod_{i=1}^{n} P(A_i|C = c) \tag{3.12}$$

where a_i is the probability of each category, which remained constant. The category of the unknown sample set with the highest posterior probability can therefore be predicted.

Generally speaking, the optimal classification result should satisfy the following condi-

tions:

$$p(c_i|a_1, ..., a_n) = \frac{p(a_1, ..., a_n)|c_i}{p(a_1, ..., a_n)} p(c_i) \tag{3.13}$$

$$p(c_i|a_1, ..., a_n) > p(c_j|a_1, ..., a_n); j \neq i \tag{3.14}$$

The advantages of the NB classifier model includes:

- The algorithm logic is simple and easy to implement;
- The time and space overhead during the classification process is small;
- The performance of the algorithm is stable. The classification results varies little for different characteristics, namely, the model is robust.

The NB classification method is widely used thanks to its high efficiency, high precision, and solid theoretical foundation. It is based on the conditional independence hypothesis that the effect of the attribute on a given class is independent to other features. The smallest misclassification rate can be achieved by NB classifier under the establishment of the conditional independence assumption.

However, in practical applications, the prior probability and the class conditional probability density of each category are difficult to achieve, which limits the scope of application of the NB classifier.

3.3.2.2/ SVM CLASSIFIER

Support Vector Machine (SVM) is a robust machine learning model that shows high accuracy with different classification problems, which is widely used for various embedded applications. Based on the VC dimension theory and structural risk minimization principle in statistical learning theory, SVM is originally proposed for the classification problem of the two-type patterns in the case of linear separability. For the given observer set $S = (\boldsymbol{x}_i, y_i), ..., (\boldsymbol{x}_i, y_i) \subset \boldsymbol{\chi} \times -1, +1$, in which $\boldsymbol{\chi} \subset \boldsymbol{R}^n$ is the input feature space and $y_i \in -1, +1$ is the label of the sample. The objective of training is to construct a decision function that would classify the test sample as accurately as possible.

As presented in Figure 3.11, two classes of sample are fully separated by a classification hyper-plane expressed as $\boldsymbol{\Gamma} = \overline{\boldsymbol{w}} \cdot \boldsymbol{x} + \overline{b} = 0, \overline{\boldsymbol{w}} \in \boldsymbol{R}^n, \overline{b} \in \boldsymbol{R}$. Assumed that the minimum distance of these two categories in the sample to the classification hyper-plane $\boldsymbol{H}$ is $d^+ = mind_i|y_i = +1$ and $d^- = mind_i|y_i = -1$, two parallel hyper-plane $\boldsymbol{H}_1$ and $\boldsymbol{H}_2$ are therefore determined. The other parallel hyper-plane $\boldsymbol{H}_0$ located in the middle of $\boldsymbol{H}_1$ and $\boldsymbol{H}_2$ have optimal classification property thanks to the equal distance of separating the two categories. The distance between hyper-plane $\boldsymbol{H}_1$ and $\boldsymbol{H}_2$ is named as the classification interval Δ of hyper-plane $\boldsymbol{H}_0$. Under the presupposition of correctly classifying all learning samples, the hyper-plane $\boldsymbol{H}_0$ is considered as the optimal classification hyper-plane if Δ is the maximum classification interval [162].

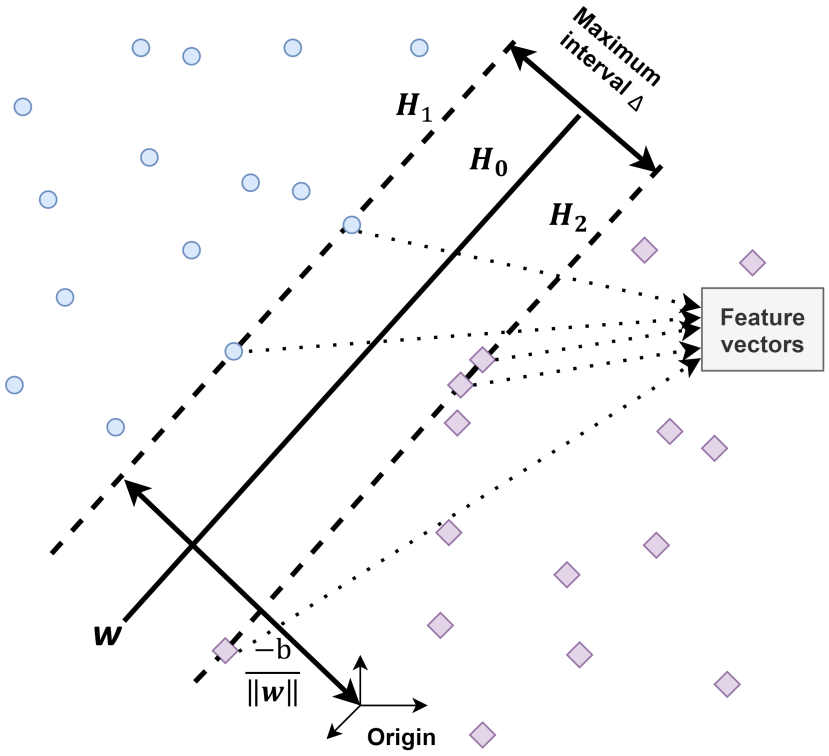

Figure 3.11: Maximum interval classification hyper-plane.

For the linear separability situation, the formulation of searching the optimal hyper-plane can be considered as the quadratic programming problem. The classifier can be expressed as:

$$f(\boldsymbol{x}) = sgn(\boldsymbol{w}^* \cdot \boldsymbol{x} + b^*) = sgn(\sum_{i=1}^{i} \alpha_i^* y_i (\boldsymbol{x} \cdot \boldsymbol{x}_i) + b^*) \tag{3.15}$$

in which α is the lagrange multipliers for each sample and α^* is the optimal value. The sample satisfies to the condition that $\alpha^* > 0$ is defined as the support vector, which located on the boundary of the classification interval. As can be seen in Figure 3.11, the hyper-plane $\boldsymbol{H}_1$ and $\boldsymbol{H}_2$ are the interval boundary hyper-plane, the samples on which are support vectors.

Replacing the hyper-plane with a hyper-surface, then searching for a maximum spacing hyper-surface which can classify all samples correctly is the effective way of solving the linear unclassifiable problem. Such classifier is remarked as the support vector machine. It is generally expressed as:

$$f(\boldsymbol{x}) == sgn(\sum_{i=1}^{i} \alpha_i^* y_i K(\boldsymbol{x} \cdot \boldsymbol{x}_i) + b^*) \tag{3.16}$$

SVM classification is a supervised learning model for analyzing data in classification and regression research. The accuracy of classification is guaranteed for the high dimensional spaces and complex interaction characteristics. However, it can only be used for two category classification problems, which limits the application in complex state classi-

fication.

An effective multi-classification strategy can be realized that decomposing the multi-classification problem into several number of two-classification problems through decomposition and reconstruction. These two-classification problems can be solved respectively, and the optimal results can then be determined. For the multi-classification problem with the category number of c, the SVM classifier is constructed between each category. Therefore, $c(c-1)/2$ SVM classifiers is required. The training samples of each SVM classifier are two related categories. The voting method is used to determine the classification results that the category got the maximum votes is the class to which the sample belongs. This kind of multi-classifier has significant advantages. Since each SVM classifier only considers two types of samples, the training process is simple to achieve. Using the majority voting method for making the final decision is easy to implement with a high speed. Meanwhile the classification accuracy is high. However, when there are many categories to be distinguished, the number of SVM classifiers increases sharply, which affects the training and test speed, the accuracy might be decreased as well.

3.3.2.3/ JOINT MULTI-CLASSIFIER

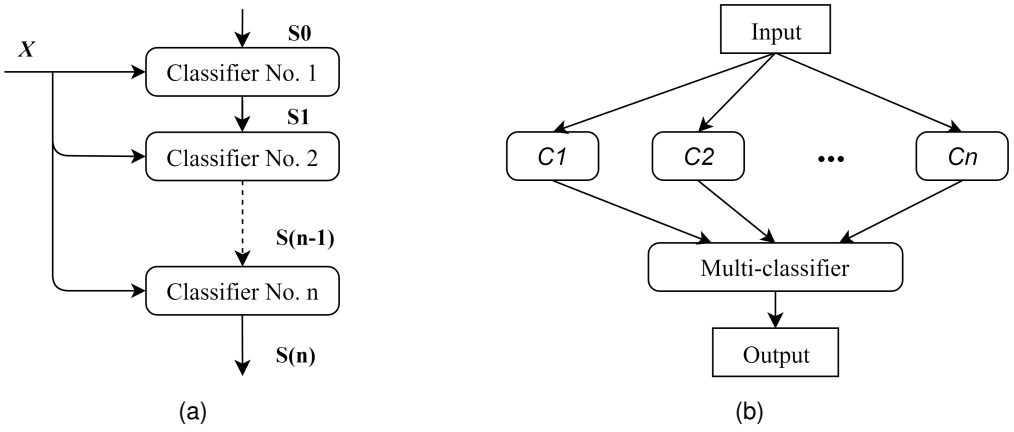

Figure 3.12: Structure of the multi-classifier: (a) Series multi-classifier; (b) Parallel multi-classifier.

The integration method of multi-classification contains two types that the simple classifiers are connected in series and in parallel, the structure of them are presented in Figure 3.12. In the series multi-classifier, the previous simple classifier provides the classification information to the next one, which means the results of the previous simple classifier and the other input information are combined as the input of the next simple classifier. While in parallel multi-classifier, each simple classifier operates separately. Thus, its speed of classification is significantly increased than that of series multi-classifier. Moreover, the results of each simple classifier can be complementary. However, if the simple classifiers and the combination rules are not properly selected, the results of the parallel multi-classifier may not rise but fall.

As discussed above, in order to fully demonstrate the advantages while suppressing the weakness of the single basic classifier, a joint multi-classifier is designed for classification.

NB classification method and SVM classification method are used to construct the this joint multi-classifier for the state classification of the MH hydrogen storage tank operation process.

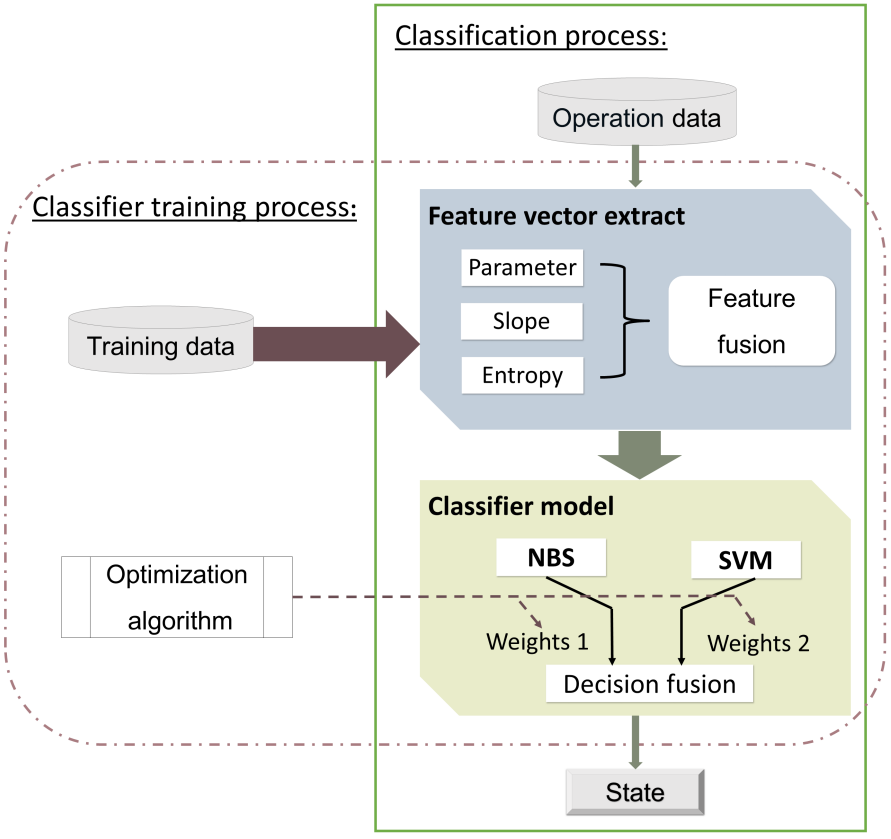

Figure 3.13: Flow chart of joint multi-classification.

The flow chart of the joint multi-classification is presented in Figure 3.13. The SVM classifier and NB classifier are trained by the historical data respectively, then the results of each simple classifiers are learned and remembered. An optimization algorithm is used to search for an optimal weight for the weighted summation of each simple classifier output result on the measurement layer. The final classification result is therefore be determined. In this process, the combination weight is effected by the classification ability of simple classifiers and state characteristics of the analyses system.

3.3.3/ Simulation results and discussion

3.3.3.1/ Training for joint multi-classification

The variation of the physical state during charging and discharging process of the embedded MH hydrogen storage tank are studied separately. The real operation data of ten process are picked randomly form Mobypost project database. In order to reflect the characteristics of each physical state in different stage, feature vectors are selected for classification.

There are two stages in charging process as discussed in Section 2.3.1. The time domain features of these data based on statistical characteristics are typical for the performance since the recorded data is time sampled. The energy density variation could also present the characteristic of the data. Therefore, in this work, kurtosis feature and entropy feature are picked for classification feature vectors, the parameter index of them are presented in Table 3.3. The discharging process can be separated into four stages as mentioned in Section 2.3.2. Except for the feature vectors extracted from the database of temperature, pressure and flow, the index of heater is added for classification training.

Table 3.3: Parameter index

Name	Formula
Kuitosis	$\frac{1}{N}\sum_{i=1}^{N}(x_i-\overline{x})^4/RMS^4$
Entropy	$-\sum_i P(x_i)\,log_b P(x_i)$

The optimal weight is searched during classifier training process using Grid Search (GS) method. GS is an exhaustive search method that all the candidate weight set are tested to find out the best preforming one as the final result. As a result, the optimal weight with highest classification precision can be obtained. Since the number of categories is not too much, the disadvantage of time consuming can be ignored.

3.3.3.2/ CROSS VALIDATION OF THE CLASSIFIER

K-folds cross validation method is applied for testing the classification accuracy of the designed joint multi-classifier. Figure 3.14 gives the flow chart of this process. The sample set is combined by n group of data from real operation process, in which $(n-1)$ processes are set as the training set and the other one is set for testing at one iteration procedure. After repeating the procedure for n times, the average value of the mean square error of all the iteration is regarded as the error of the classifier.

In our test, nine group of data are picked for classification validation in both charging process and discharging process. The highest accuracy of state classification using joint multi-classifier are 91.3% and 83.2% respectively. In charging test, with the combine weight of NB classifier and SVM classifier are 0.4 and 0.6 separately, while in discharging test, the combine weights are 0.5.

Actually, both two single classifiers have a good consequent on the state classification of hydrogenation and dehydrogenating process, and the classification accuracy rate of the tested databases have reached more than 70%. The NB classifier has a simple structure, thus the time required for classifier training and for state classification of each group of test data are short. While the multiple SVM classifier is composed of several single SVM classifiers, in which each state category in the data is trained in pairs and takes a relatively long time. However, the correct recognition rate of the test database by the joint multi-classifiers is higher than that of each single classifier, which make it has higher application value. In the joint multi-classifier training, the GS algorithm needs to perform multiple iterations when seeking the optimal weight, which leads to a significant

increase in training time compared to the single classifier. However, the classification time for each set of test data is still short, which can meet the time limit in practical applications.

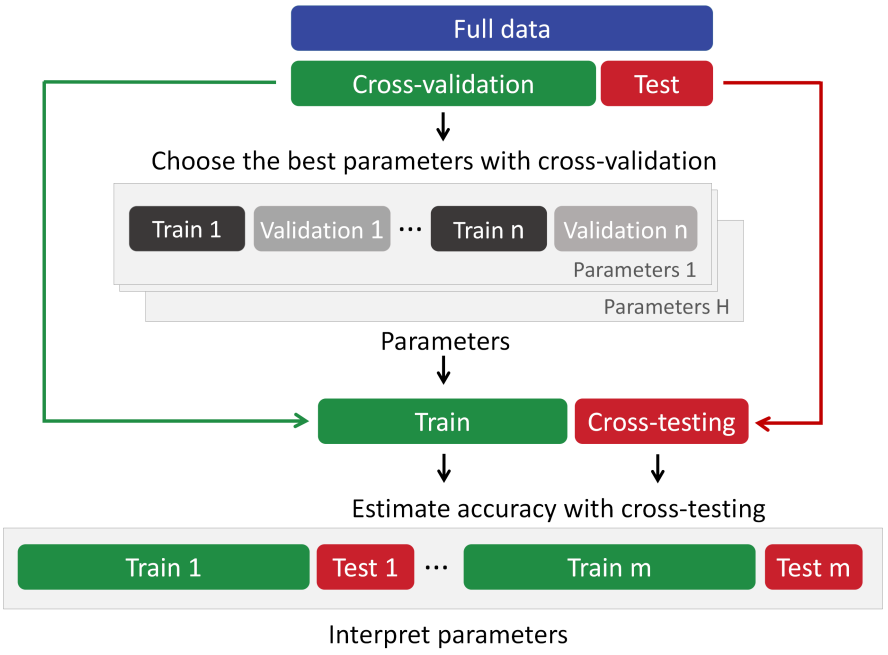

Figure 3.14: Flow chart of cross validation.

3.3.3.3/ ONLINE SOC ESTIMATION

As discussed above, the online SOC estimation during charging and discharging process are quite difficult but important. In this section, the proposed online SOC estimation algorithm is validated. For both charging and discharging process, ten group of data are picked from the Mobypost project database respectively for training and validating the joint multi-classifier, then exploited for online state classification. In the picked database of discharging process, the data was recorded in a continuously vehicle operation process, before that the hydrogen storage tank is fully charged at refueling station. Therefore, the recorded data of remaining hydrogen mass is calculated by the released hydrogen flow rate. For the purpose of protecting the fuel cell, the hydrogen storage tank is controlled to be closed when the estimated remaining hydrogen mass is less than 10%.

Figure 3.15 and Figure 3.16 give the example of the online state classification result of charging and discharging test. Obviously, the classification error is merely appears in transition of the first stage to the second stage in charging test while concentrated in the first stage and the third stage in discharging process. In the second stage, the performance of the classifier is stable and excellent.

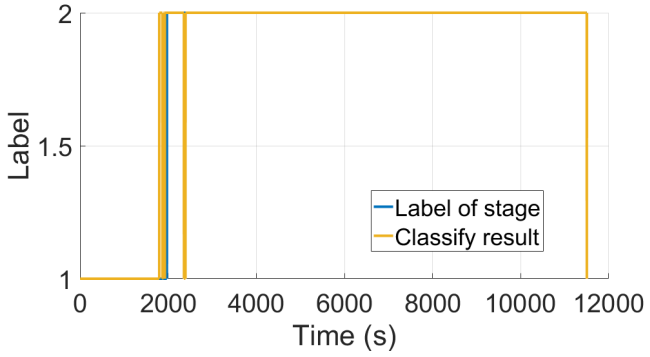

Figure 3.15: Online state classification result of a charging process.

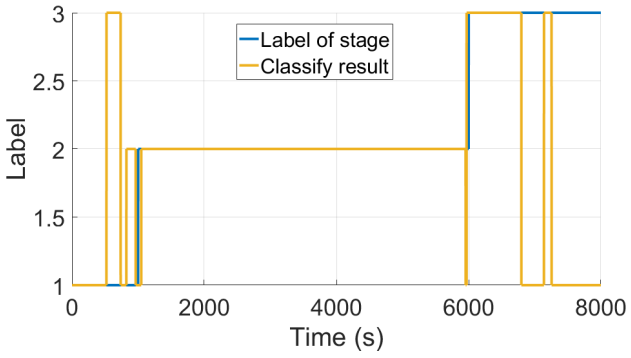

Figure 3.16: Online state classification result of a discharging process.

The classification result can be used to estimate the SOC of the embedded MH hydrogen storage tank. Based on the mathematical model proposed in Section 3.2 and performed in Figure 3.5, the SOC of the tank can be estimated by the data point recognized as second stage. Since the degradation of the MH hydrogen storage tank is not taken into consideration, the hydrogen remaining in the tank at the period of recognized second stage can be estimated.

Figure 3.17 gives the estimation result during charging process, in which the period of recognized first stage is calculated by the recorded data of hydrogen flow rate. Compared to the value of hydrogen mass in the tested database, the online SOC estimation results shows a great agreement with the error of 0.2%. As introduced in Section 2.3.1, the hydrogen flow rate filling into the tank is mainly dominated by the pressure difference so that at the beginning period the flow rate is quite high, which might lead to high kinetics and effect the absorption speed. Therefore, the estimated SOC is low than the calculated value in the head of the second stage. Besides, the real operation data is recorded every second, and the testing time for one group of data is less than 0.1 ms. Thus, this online SOC estimation with high accuracy and low time consumption is of practical value.

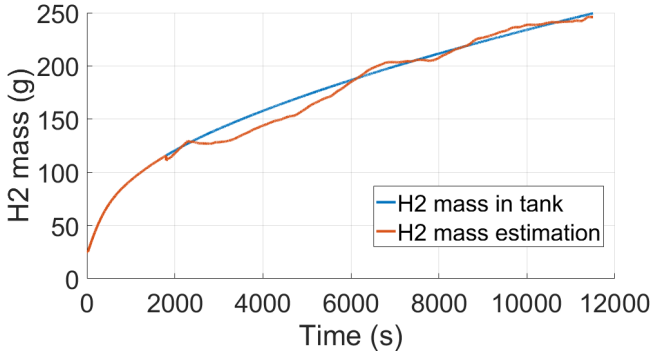

Figure 3.17: Online SOC estimation result during charging process.

Due to the lack of database of discharging test for larger scale of temperature, the P-C-T based mathematical model for SOC estimation can not be defined precisely, namely, the SOC can not be estimated online during discharging in spite of the good result of online state classification. Therefore, more experiment should be preformed to complete the model, which will be introduced in Section 6.3.

3.4/ CONCLUSION

In this chapter, the designed mathematical models are based on the statistical theory to characterize the performance of the main parameters of reaction including pressure, temperature, hydrogen flow rate and hydrogen mass. Then the P-C-T based SOC estimation method is proposed on the basis of the main physical character of the reaction process. More data in large range of temperature distinguish and long time operation will of great help to complete and improve the model. In addition, an effective online SOC estimation method is proposed through designing a joint multi-classifier to recognize the stage of reaction, and then combining with the mathematical model, the remain hydrogen in the tank is estimated on real time.

From next chapter, the dynamic performance based on the physical reaction will be studied. More detailed information about the reaction and thermal variation will be discussed.

4

Dynamic modeling and parameter analysis of MH tank

4.1/ Introduction

In practice using of metal hydride (MH) basd hydrogen storage, packed bed reactors for MH material are usually utilized to take advantage of the porous and discontinuous structure of the reactant metal alloy to increase the slide gas interface and promote the reaction [163]. Besides of the structure and distribution of the MH inside the container, many other variables such as operation temperature, hydrogen pressure, hydrogen flow rate and concentration have significant impact on the performance of a MH hydrogen storage tank. Mathematical modelling is a useful tool to identify and predict the state of MH during absorption and desorption as well as to determine the relationship between different effective factors with the aim of finding the best performance of a MH hydrogen storage system [155].

Attempts have been made to identify the relationship between different operating and design variables. Many different mathematical models are designed to simulate the reaction kinetics, equilibrium conditions, heat and mass transfer inside the tank during absorption and desorption process [119–124]. The first two-dimensional numerical model is presented 20 years earlier to emphasize the effect of the shape, pressure and cooling system [125], which is widely applied in the later research. The three-dimensional models are more exhaustively designed to figured out the permeability and the thermal conductivity of the hydride [126, 164].

Dhaou et al. [128] presented the P-C-T curves under three temperatures of both absorption and desorption process. The relationship between the equilibrium pressure of reaction, hydrogen composition in the MH and temperature is expressed by these P-C-T curves, which are of great interest since the difference between hydrogen pressure and equilibrium pressure constitutes a driving force for the reaction. They also proposed an analytic expression of the equilibrium pressure by polynomial interpolation based on experimental data. As a deterministic factor of the reaction direction, equilibrium pressure shows a great dependent on temperature and hydrogen concentration. Based on the analysis of equilibrium pressure, a deep discussion was made on the effect of operating parameters, including hydrogen flow, temperature of the cooling fluid and volume of metal in the tank [129, 130]. The mass and heat transfer during operating process are

simulated to analysis the effects of these parameters to the efficiency of the reaction and supply capacity of the hydrogen storage system [131, 132].

However, in the practical application of hydrogen storage system with MH, an extremely meticulous mathematical model with numerous complex elements is unnecessary, for which could lead in excessive calculations and errors. Meanwhile, although the previous studies show great performance in simulating the dynamic response of the absorption and desorption process and evaluate variables of reaction kinetics, the proposed models are just validated in simulation and laboratory experiments. The real operation condition of the on-board hydrogen storage system is not fully considered. Furthermore, the effect of the parameters on the efficiency of both absorption and desorption process is highly demanded in practical application.

This chapter presents a dynamic modeling process for the embedded MH hydrogen storage system on FCEHVs. Starting from the dynamic response model, particle swarm optimization (PSO) algorithm is used to identify and investigate the parameters of this model. The modeling method will be detailed in the second section. In the third section, PSO is introduced and the identification process with PSO algorithm will be presented. The section four is dedicated to validate the proposed model through a comparison study between simulation result and real measurement data.

4.2/ MODELING PROCESS

4.2.1/ CONFIGURATION OF THE STUDIED SYSTEM

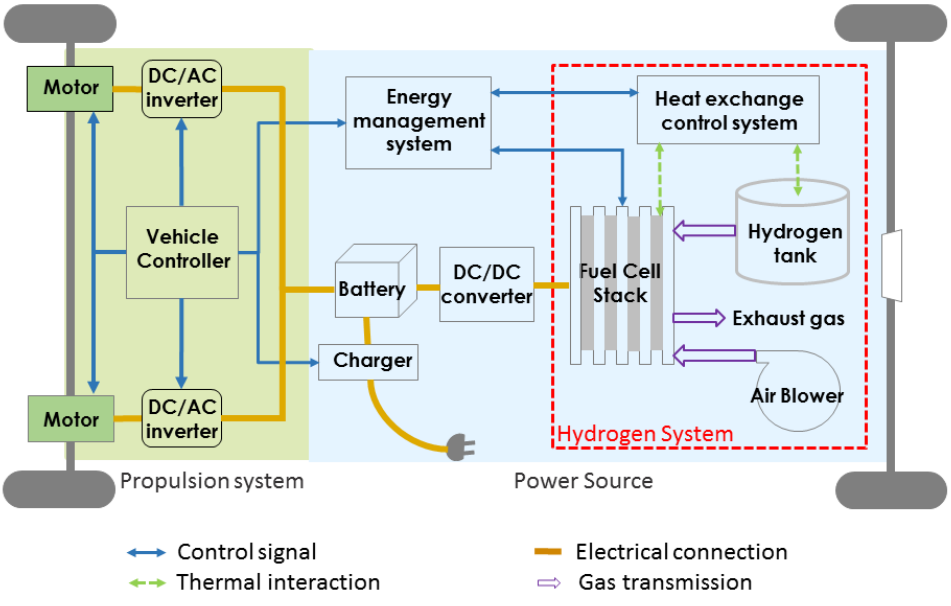

Figure 4.1: Schematic of the hydrogen storage and application system.

As shown in Figure 4.1, the studied system is the same with the Mobypost project vehicles introduced in Section 2.2.2. Fuel cell stacks act as the first power source to charge the batteries and the used hydrogen during fuel cell operation is stored in the MH hydrogen storage tanks. The configuration of the on-board hydrogen storage and application system is also present in the red square in Figure 4.1, including MH hydrogen tanks, fuel cell stacks, circulation water of temperature control system and the sensors of each significant parameter. The heat exchange system is combined by the circulation water channel, which is arranged around the storage tank to control the thermal condition.

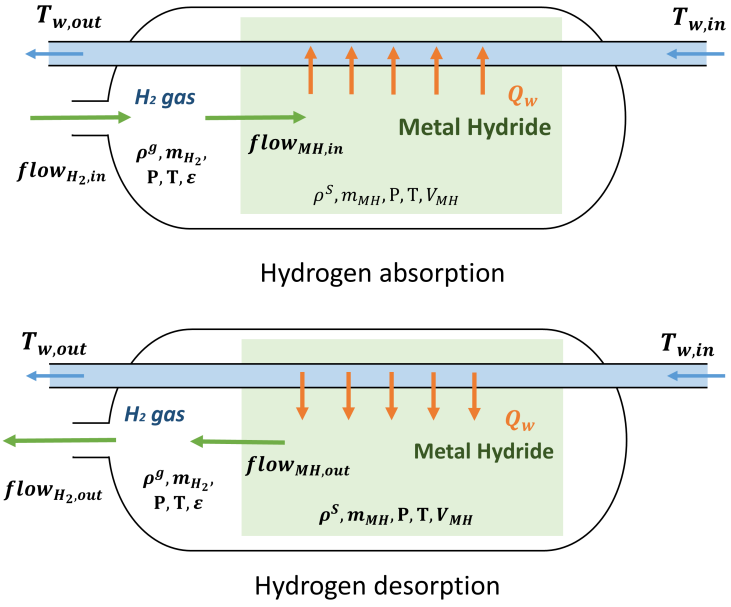

Figure 4.2: Schematic diagram of absorption and desorption process in a MH hydrogen storage tank.

Figure 4.2 shows the process of charging and discharging of a bottle-like geometry modeled MH hydrogen storage tank, which matches the real vessels available in the practical application. During the operation process, the thermodynamic state of the tank modified with the reaction situation and state of charge (SOC) inside the tank. As an exothermic reaction, heat generated and released during charging process. The cooling system to remove the heat is necessary since the high temperature suppresses the progress of the exothermic reaction. On the contrary, heat transfer system should provide heat to the tank to release hydrogen from the hydride formation during discharging process.

During charging process, the MH hydrogen storage tanks are filled in hydrogen refueling station with a stable pressure hydrogen providing. When the vehicle is driven, constant hydrogen flow is discharged from the MH tanks to support the fuel cell operation. The thermal situation is managed to control the desorption reaction. In this section, the dynamic model is focus on the discharging process based on the real operation database. Since the used MH hydrogen storage tank is a seal container filled with uncertain material and structure, the dynamic model of the tank is like a gray box with unknown parameters.

4.2.2/ DYNAMIC MODEL OF THE HYDROGEN STORAGE SYSTEM

4.2.2.1/ MODEL ASSUMPTIONS

The overall performance of the MH hydrogen storage tank is determined by the hydrogen storage capacity and the cycling numbers. However, its dynamic performance, namely, the parameters of pressure, temperature and hydrogen concentration distribution are also of great significant. Figure 4.1 also shows the model structure of the on-board hydrogen storage system charging and discharging process, considering the heat exchange with circulated water. During the operation process, the thermodynamic state of the tank modified with the reaction situation and the SOC of the tank. In order to design a simplified model for practical use and reduce the compute processing time, assumptions and simplifications are usually made [129, 165–168].

1. Stable test temperature is guaranteed;
2. The physical properties of the system are also assumed to be stable;
3. Hydrogen is considered to be an ideal gas;
4. The MH hydrogen storage tank degradation homogeneous;
5. The modeled geometry has a bottle-like shape as shown in Figure 4.1 that matches the real MH tank for vehicle application;
6. The MH characteristics such as thermal conductivity, porosity and volume remain constant during reaction;
7. The MH physical characteristics of thermal conductivity, porosity and volume remain constant;
8. The heat convection inside the tank is neglected, which means the temperature of the tank interior and its surface are assumed to be the same;
9. Heat radiation on the MH tank is ignored, namely, the heat transfer only appears between tank and circulation water;
10. The model is developed incorporating the mass conservation and thermal energy balances in the hydrogen storage system to describe the dynamic performance of discharging process.

4.2.2.2/ STATE MODEL

The state in the tank is assumed to follow the ideal gas equation all the time during charging and discharging process:

$$P = \rho^g RT \tag{4.1}$$

in which P and T are represent the pressure and temperature inside the tank, ρ^g is the density of gaseous hydrogen in the tank, R is the universal gas constant.

Based on the continuity of MH material, the mass flow rate variation of the desorped hydrogen can be expressed as:

$$\dot{m}_{MH} = (1-\varepsilon)\frac{\partial \rho^s}{\partial t} \tag{4.2}$$

where ρ^s is the density of hydrogen stored in the hydride, and ε presents the porosity of the MH structure distributed inside the tank. Thus, the variation rate of hydride hydrogen density can be presented as:

$$\dot{m}_{MH} = m_{MH}/V_{MH} \tag{4.3}$$

Due to the mass conservation of gaseous hydrogen, the mass flow rate of gaseous hydrogen in the tank varies as:

$$\dot{m}_{H_2} = \Big(\frac{V_{tank}}{V_{MH}} - 1 + \varepsilon\Big)\frac{\partial \rho^g}{\partial t} \tag{4.4}$$

in which $(\frac{V_{tank}}{V_{MH}} - 1 + \varepsilon)$ is the empty space inside the tank dominated by the distribution of the MH material.

The mass flow rate of gaseous hydrogen is influenced by two parts. During the charging process, the hydrogen is pushed into the tank and absorbed by the MH material, therefore the mass flow rate of gaseous hydrogen is:

$$\dot{m}_{H_2} = f_{in} - \dot{m}_{MH} \tag{4.5}$$

When discharge the tank, the hydrogen is released out, which results in the decrease of gaseous hydrogen mass inside the tank. Meanwhile, the desorpted hydrogen from MH material leads to the increase of the gaseous hydrogen mass. Thus, the mass flow rate of gaseous hydrogen in the tank during desorption process can be expressed as:

$$\dot{m}_{H_2} = \dot{m}_{MH} - f_{out} \tag{4.6}$$

The hydrogen mass flow rate generated from the MH material $\dot{m}_{MH}$ is dominated by the equilibrium pressure. As introduced in Eq. 1.5, the reaction proceeds to the right side to form the hydride or to the left to generate hydrogen depending on the relation between pressure and equilibrium pressure. When the pressure inside the tank higher than the equilibrium pressure for absorption, hydrogen is absorbed. Hence, the mass flow rate of hydrogen absorbed by MH material can be calculated by:

$$\dot{m}_{MH} = C_a * exp\Big(-\frac{E_a}{RT}\Big) ln\Big(\frac{P}{P_{eq}}\Big)(\rho_s^s - \rho^s) \tag{4.7}$$

in which C_a is the constants of absorption rate, E_a is the relative activation energy of absorption.

While the pressure inside the tank is lower than the equilibrium pressure for desorption, hydrogen generated from the hydride composed by hydrogen and MH material. Its rate

can be calculated as:

$$\dot{m}_{MH} = -C_d exp\Big(-\frac{E_d}{RT}\Big)\Big(\frac{P - P_{eq}}{P_{eq}}\Big)(\rho_s^s - \rho^s) \tag{4.8}$$

where C_d is the constants of desorption rate, E_d is the relative activation energy desorption.

The other situation that the current pressure is between absorption and desorption equilibrium pressure, the reaction stay in balance and no more hydrogen can be absorbed or released. That is to say:

$$\dot{m}_{MH} = 0 \tag{4.9}$$

When modeling the discharging process, the applied equilibrium pressure could be fitted from the P-C-T curves of the MH tank and be formed as [169] :

$$P_{eq} = f(r)exp\Big(\frac{\Delta H}{R}\Big)\Big(\frac{1}{T} - \frac{1}{T_r}\Big) \tag{4.10}$$

in which ΔH is the reaction enthalpy corresponding to the MH material in the tank, T is the current reaction temperature and T_r is the reference temperature. Equilibrium state of the reaction not only effected by temperature but also influenced by the hydrogen concentration that represent by r, which is calculated by the hydrogen to metal ratio:

$$r = \frac{H}{H_{max}} = \frac{2(\rho^s - \rho_0^s)M_{MH}}{\rho_0^s M_{H_2}} \tag{4.11}$$

Researchers measured the equilibrium pressure of hydrogen desorption on several material by experiments and approximates $f(r)$ as a ninth-order polynomial function that [169]:

$$f(r) = \sum_{n=1}^{9} p_n * r^{(10-n)} + p_{10} \tag{4.12}$$

4.2.2.3/ THERMAL MODEL

The thermal condition in the system is controlled by the circulation water. Though the assumption of uniform temperature does not exactly describe the actual phenomena, the difficulty in estimating the exact value of the heat transfer coefficient also arises in multi-dimensional numerical modeling. Therefore, an overall heat transfer coefficient is introduced to investigate the effect of heat transfer rate. The energy exchanges between MH material and circulation water could be expressed as:

$$\Big(\frac{V_{tank}}{V_{MH}} - 1 + \varepsilon\Big)C_{pg}\frac{\partial(\rho^g T)}{\partial t} + (1-\varepsilon)C_{ps}\frac{\partial(\rho^s T)}{\partial t} = Q + \dot{m}_{MH}\Delta H \tag{4.13}$$

in which C_{pg} and C_{ps} are the heat capacity of hydrogen an MH material separately.

The overall heat exchange between the MH tank and the circulation water is developed based on the energy balance. The amount of heat transfer can therefore be expressed

as:

$$Q = \frac{Q_w}{\dot{m}_w} C_{p,w}(T_{w,in} - T_{MH})(1 - e^{-A}) \tag{4.14}$$

where $\dot{m}_w$ represents the water flow rate across the tank and $C_{p,w}$ is the water heat capacity. T_w represents the temperature of water, that the temperature of input water to the tank is $T_{w,in}$ and the output water temperature is $T_{w,out}$. T_{MH} is the temperature of the MH material during reaction.

Therefore, the variation of circulation water temperature after heat transfer can be expressed as:

$$T_{w,out} = T_{MH} + (T_{w,in} - T_{MH}) * e^{-A} \tag{4.15}$$

in which A is the heat exchange coefficient.

4.2.2.4/ INITIAL AND BOUNDARY CONDITIONS

It is necessary to specify appropriate initial state and boundary conditions of the model, and these conditions are normally determined by the shape and structure of the tank, the operating conditions and the efficiency of the associated cooling system.

Initial conditions are typically taken as identical throughout the whole system. The initial temperature is taken to be the same with the atmospheric temperature and the initial pressure is often chosen to be equal to the equilibrium pressure at the initial temperature and hydrogen to metal ratio:

$$T_0 = T_{atm} \tag{4.16}$$

$$P_0 = P_{eq} \tag{4.17}$$

Besides, the initial MH density is set to be ρ_{ini}. It might be equal to the hydrogen saturated MH density or lower if the metal is only partially filled.

Generally, the boundary conditions of a MH hydrogen storage tank can be classified into three types [170]: adiabatic wall, heat transfer wall and mass transfer boundary. In our model, the mass transfer boundary is taken into consideration, namely, the operation stops when the tank is fully charged or completely discharged. In addition, a Danckwerts' boundary condition is applied to make sure that the flow rate is continuous across the boundary [170].

The above equations for the dynamic response of the MH hydrogen storage system are applied as a gray box with unknown parameters in our study. It is incomplete and the parameters need to be identified.

4.3/ PSO-BASED PARAMETER IDENTIFICATION

4.3.1/ PSO METHOD

PSO algorithm is an evolutionary computation for obtaining an optimal solution by searching for the best position in space through information sharing and collaboration among particles, which is inspired by social behavior of flocks of birds and fish looking

for food [171]. Observers found that every bird could find its best direction to search for food through the information shared among the whole group. They took the birds in the group as particles:

$$X_i = (x_{i1}, x_{i2}, ..., x_{iD}) \tag{4.18}$$

Then they summarized that through update the particles' velocities and positions with the best experience for enough generations, the optimal positions of the particles could be approached. The velocities and positions are expressed as:

$$V_i = (v_{i1}, v_{i2}, ..., v_{iD}) \tag{4.19}$$

$$X_i = (x_{i1}, x_{i2}, ..., x_{iD}) \tag{4.20}$$

The experience information including the position of each particle P_{best} and the information of the whole group G_{best}. For each generation, the particles update their velocity and position according to the following functions:

$$\begin{aligned} v_{id}(n+1) = w * v_{id}(n) + c_1 * rand_1 * (p_{id}(n) - x_{id}(n)) \\ + c_2 * rand_2 * (p_{gd}(n) - x_{id}(n)) \end{aligned} \tag{4.21}$$

$$x_{id}(n+1) = x_{id}(n) + v_{id}(n+1) \tag{4.22}$$

where w is the inertia weight; c_1 and c_2 are the acceleration constants; $rand_1$ and $rand_2$ are two random values in the range of $[0, 1]$. The iteration index of each generation is $n = 1, 2, ..., n_{max}$, and n_{max} is the maximum iteration times, which could be defined at the initial step of the process. The fitness function F is designed to evaluate the the current position in each iteration.

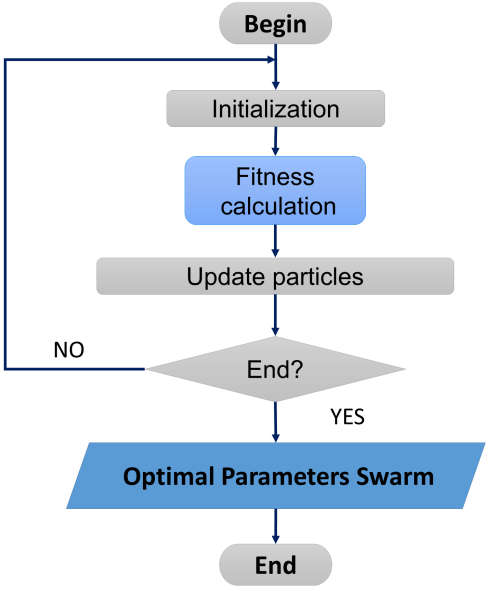

Figure 4.3: Flowchart of PSO algorithm.

Figure 4.3 presents the flow chart of PSO algorithm, which is described in detail as below:

- Step 1: Set the size and range of the particle swarm under the request of application.
- Step 2: Set the iteration index to zero, then initialize the velocity V_0 and position X_0 of the particles randomly to start the process.
- Step 3: Calculate the objective function value of the current parameter swarm to evaluate the fitness.
- Step 4: Evaluate the previous performance and determine the new global optimal particles. The current best position$P_{best}(n)$ and global best $G_{best}(n)$ are updated as follow:

$$P_{best}(n) = \begin{cases} X_i(n) & \text{if } F(X_i(n) < F(P_{best}(n-1)) \\ P_{best}(n-1) & \text{if } F(X_i(n) \geqslant F(P_{best}(n-1)) \end{cases} \tag{4.23}$$

$$G_{best}(n) = \begin{cases} G_{best}(n) & \text{if } F(X_i(n) < F(G_{best}(n-1))) \\ G_{best}(n-1) & \text{if } F(X_i(n) \geqslant F(G_{best}(n-1))) \end{cases} \tag{4.24}$$

- Step 5: Update the velocity of particles based on Eq. 4.21 and move the particles to the new position according to Eq. 4.22.
- Step 6: Analysis the current state to investigate whether the end criterion is satisfied or not, which could be the sufficiently great fitness F_{min} or the maximum iteration number n_{max}. If the end criterion is not reached, loop to step 3. Proceeding the identification process until the optimal parameter swarm is found out.

4.3.2/ IDENTIFICATION PROCESS

Since the MH hydrogen storage tank used on the vehicle is a seal container filled with unknown material and structure, the tank is a like gray box in our model with some uncertain parameters as mentioned above. PSO method can be applied to identify the parameters of the MH tank model for on-board hydrogen storage system.

As the diagram shown in Figure 4.4, PSO algorithm is applied for the parameter identification in our study. For the purpose of identifying the parameters in the on-board MH hydrogen storage system, the parameters are considered as the particles. Thus, the optimal particles' position represents the results of parameter identification.

The fitness function is determined to evaluate the accuracy of parameters. Fitness is the errors between model simulation results and real operation data. Generally, the optimal parameters are obtained when the fitness value is small enough. As a consequence, the fitness function is set as:

$$F = \sqrt{\frac{1}{N}\sum_{i=1}^{N} f(S(i), E(i), \Phi)^2} \tag{4.25}$$

where $S(i)$ and $E(i)$ represents the dynamic model simulation results and the related measurement results from the real operation database respectively. N is the size of the simulated and experimental data, and the set of parameters need to be identified is:

$$\Phi = [M_{MH}, C_{ps}, \Delta H, \rho_s^0, \varepsilon, A, C_d, E_d] \tag{4.26}$$

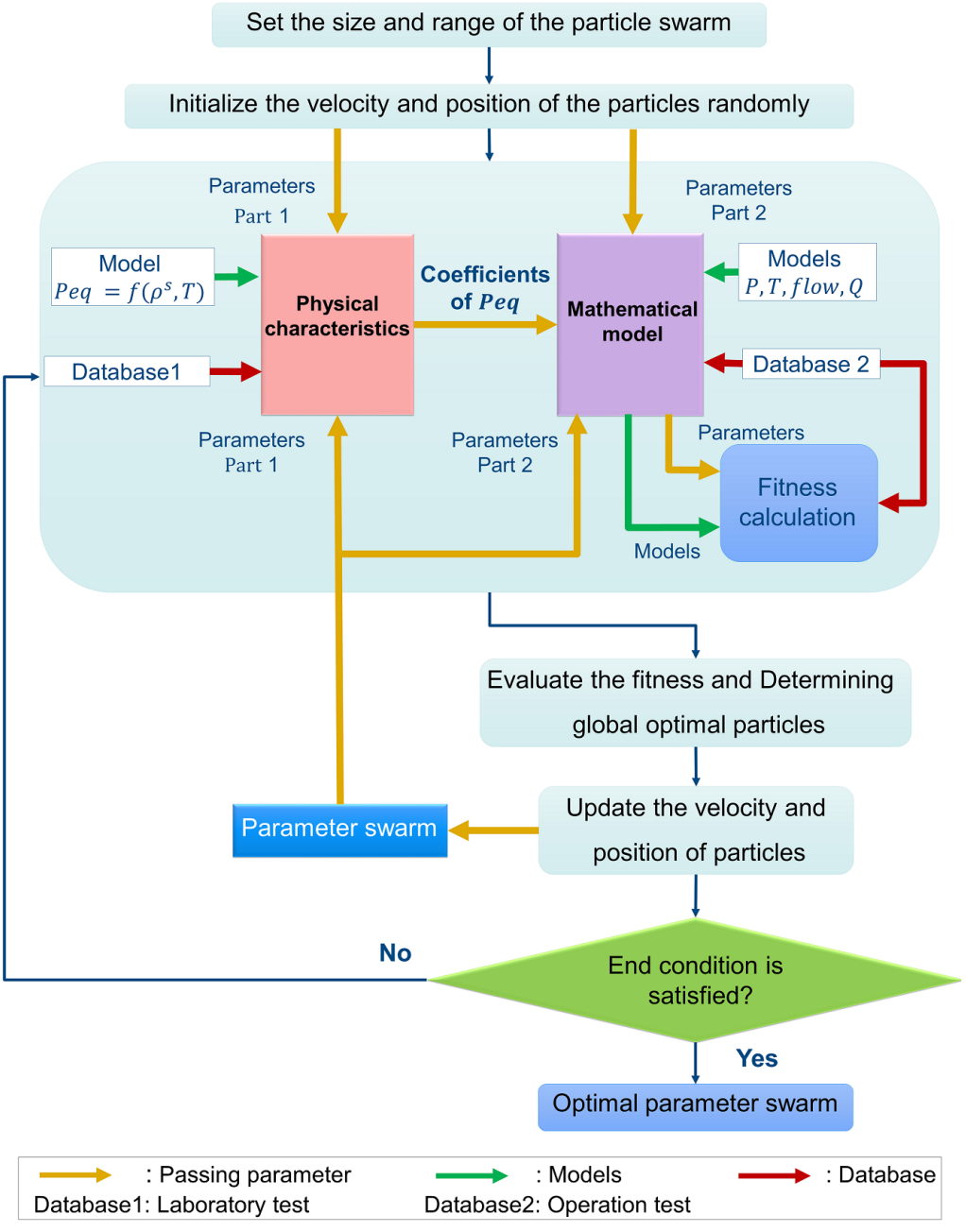

Figure 4.4: Schematic of the applied identification method with PSO algorithm.

In this work, the calculation of fitness F is divided into two parts: physical characteristic measurement of the tank and dynamic response simulation of the operation system,

which is shown in Figure 4.4. The first part is the measurement of physical characteristics analysis of the tank, which corresponds to the equilibrium pressure. From the database of the laboratory test, P-C-T curves of the tank could be extracted for identifying the parameters M_{MH} and ΔH of equilibrium pressure P_{eq}. The second part is the investigation of the dynamic model of the embedded MH hydrogen storage system. The behaviors of this system can be observed from the database of the real operation test. By combining the mathematical model of the dynamic response and the equilibrium pressure obtained in laboratory test, the fitness value F of the current parameter swarm can then be calculated.

The previous performance of particles is evaluated by fitness. The parameters will be updated and the procedure of PSO will loop to fitness calculation, unless the end criterion is satisfied. The end criterion is generally set as the fitness falls below the threshold, or, the iterations exceed the maximum number. Finally, the optimal parameter swarm can be obtained as the identified parameters.

The result of the parameter identification based on PSO algorithm will be discussed in next section.

4.4/ RESULT AND DISCUSSION

4.4.1/ PCT TEST RESULTS

The proposed method for parameter identification of the embedded MH hydrogen storage system using PSO algorithm is verified through the analysis of the dynamic model and operation data. The results are evaluated by the fitness value of PSO and the errors of variables. This process is implemented by MATLAB software [172]. In order to verify the equilibrium pressure model of the tank shown in Eq. 4.10, the database of the laboratory experiments introduced in Section 2.2.1 is investigated.

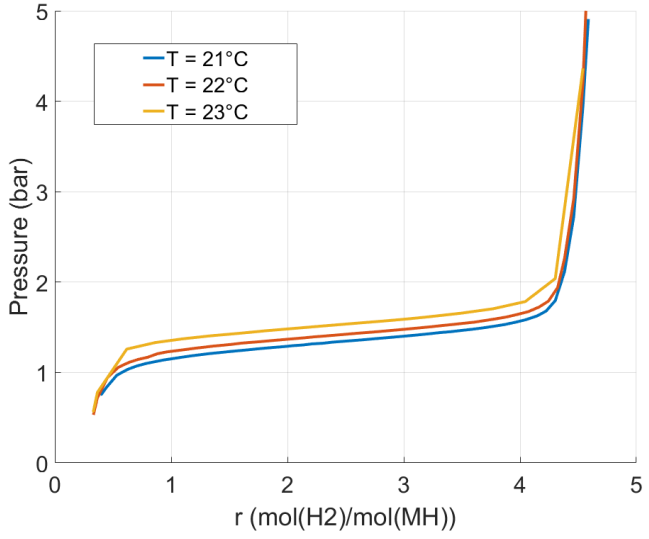

Figure 4.5: P-C-T curves of the tested MH hydrogen storage tank.

Figure 4.5 presents the P-C-T curves of the hydrogen desorption process under three different temperatures 21°C, 22°C and 23°C, which are extracted from the laboratory database. These curves show the equilibrium state of the reaction inside the tank. The equilibrium pressure changes with temperature and hydrogen concentration, which is consistent with the equation of P_{eq} in Eq. 4.10. The effect of hydrogen concentration on equilibrium pressure has been approximated by a ninth-order polynomial function as Eq. 4.12. This polynomial function is fitted depending on the identified parameters of the tank and the database of P-C-T curves from laboratory experiment. Table 4.1 gives the coefficients $p_0, p_1, ..., p_{10}$ of $f(r)$, which are calculated when the optimal parameters are obtained in this study.

Table 4.1: The polynomial function coefficients of equilibrium pressure.

Coefficient	Value	Coefficient	Value
p_1	0.0191	p_6	-97.2922
p_2	-0.3869	p_7	121.3925
p_3	3.3691	p_8	-93.9727
p_4	-16.5014	p_9	41.5605
p_5	50.0302	p_{10}	-5.6286

4.4.2/ PSO-BASED PARAMETERS IDENTIFICATION RESULTS

Thanks to the robustness to control variables and high computational efficiency, PSO algorithm is applied to identify the parameters of the dynamic model of desorption process. For the purpose of accelerating the convergence speed and optimization rate, the range of the parameter is narrowed based on the prior information from experiments and literature, which are presented in Table 4.2.

Table 4.2: Parameters optimization with PSO method.

Parameter	Symbol(Unit)	Range	Reference
Metal molecular weight	M_{MH} (g/mol)	[200,600]	[115, 173, 174]
Metal heat capacity	C_{ps} $(J/kg/K)$	[100,400]	[115, 173, 174]
Reaction enthalpy	ΔH (J/kg_{H_2})	[2E7,4E7]	[115, 173, 174]
Empty density	ρ_0^s (kg/m^3)	[7000,7400]	[159]
Porosity	ε	[0.2,0.7]	[166, 175, 176]
Heat transfer coefficient	A	[0.1,0.7]	[166]
Desorption rate constant	C_d $(1/s)$	[2,15]	[125, 166, 177]
Activation energy	E_d (J/mol)	[15000,30000]	[125, 166, 177]

In the initialization, the particle swarm is defined under the request of parameter identification for the on-board hydrogen storage system. The performance of the studied system is directly affected by the MH material, the structure inside the tank and the efficiency of the

heat exchange system. Therefore, the particles are defined to be the parameters given in Table 4.2. Among the parameters, M_{MH}, C_{ps} and ΔH are the significant properties of hydride material, ρ_0^s and ε describe the internal structure of the tank, and A represents the effect of the heat exchange system. In addition, C_d and E_d signify the direction and efficiency of the reaction. As a more complex procedure associated with the whole operation of the vehicle, the desorption process is the main object of our analysis. The end criteria of PSO is set as maximum iteration number reached to avoid over calculation.

Table 4.3: Value of the optimal parameters with PSO method.

Parameter	Optimal value
Metal molecular weight	417
Metal heat capacity	285
Reaction enthalpy	30605000
Empty density	7144
Porosity	0.4
Heat transfer coefficient	0.3524
Desorption rate constant	10.82
Activation energy	21682

Table 4.3 gives the results of the parameter identification of the hydrogen storage system using PSO algorithm. Among the database of real operation, 14 qualified desorption process are tested and the average value of the identified parameters for these 14 set are adopted as the final result.

A discharging process on a real operation FCHEV is taken as the example to present the results and discussion in detail. The vehicle was operated in 3rd July with the atmosphere temperature of $27°C$. This process lasted for about 1.6 hours until the hydrogen is fully released from the storage tank. The MH hydrogen storage tanks applied in the operation test are brought from the market with limit information. The tanks are bottle-shaped with the weight of 19 kg and the volume of 4 L. The on-board hydrogen storage system is equipped with two tanks in parallel with the hydrogen capacity of about 300 g, and a temperature control system designed as the configuration shown in Figure 4.1.

As shown in Figure 4.6, the hydrogen flow discharged from the tank is controlled to be relatively stable for the protection of fuel cell, the performance of the system can then be evaluated by the variations of pressure, temperature and hydrogen capacity.

Figure 4.6 to Figure 4.9 show the comparison between real operation data and simulation results applying the identified parameters.

The fitness is calculated by the optimized parameters, simulation results and real operation data according to Eq. 4.25. The simulation errors of pressure, temperature and hydrogen mass are 7.5%, 4.4% and 3.5% respectively. The curves of simulation results and operation data match well, as the result that the identified parameters are validated.

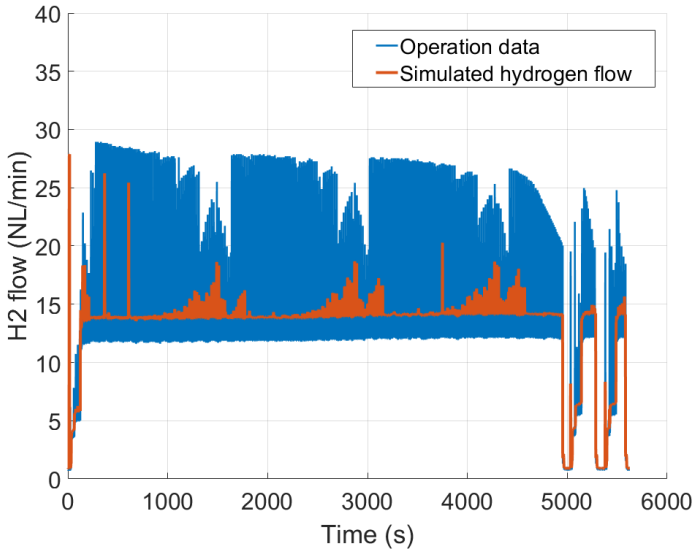

Figure 4.6: Real operation data and simulation value of hydrogen flow.

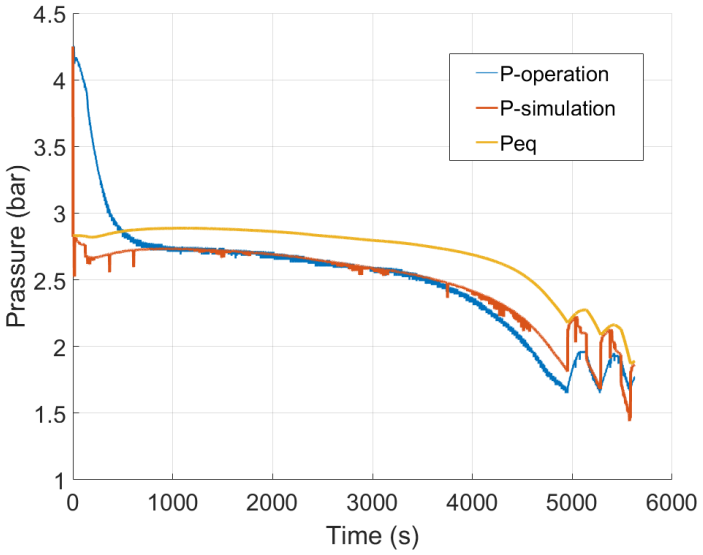

Figure 4.7: Real operation data of pressure and simulation result with optimal parameters

As shown in Figure 4.7, the pressure drops during the discharging process of the tank since the hydrogen concentration decreased. Before operation, the state inside the tank is stable and under equilibrium. The hydrogen under gaseous state satisfies to the ideal gas state equation:

$$PV = nRT \tag{4.27}$$

Thus, at the beginning of the operation the pressure satisfies with:

$$P_0 = k * Mass_0 * T_0 \tag{4.28}$$

where $P_0, Mass_0$ and T_0 is the initial value of pressure, hydrogen mass and temperature respectively. The range of coefficient k is $[0.0012, 0.0015]$ tested by all the discharging process in the database of operation.

At the initial stage of operation, the discharging process is dominated by the differential pressure between hydrogen tank and fuel cell. The pressure of the tank drops rapidly due to the release of gaseous hydrogen. The dehydrogenating reaction starts until the pressure reaches to the current equilibrium state, and this stage is considered as response period. During this period, the state of the MH inside the tank changes form seal equilibrium to desorption equilibrium. According to the analysis of the database, the response period lasts for about 1000 s, no matter of the initial hydrogen capacity inside the tank.

Since the proposed model mainly focuses on the reaction process of MH with some idealized hypotheses, the response period is not simulated comprehensively. In addition, this period is relatively short to the entire operation process. Therefore, the model with identified parameters using PSO algorithm in our study can be applied to describe the dynamic response of hydrogen discharging process.

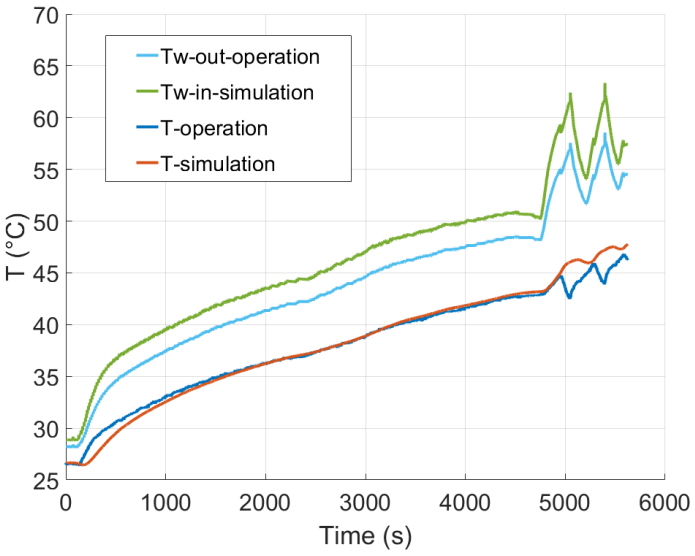

Figure 4.8: Real operation data of temperature and simulation result with optimal parameters.

Figure 4.8 shows the variation of temperature of both circulation water and MH tank during operation. The dehydrogenating reaction inside the tank is an endothermic process. Hence, the heat exchange system is used to improve the efficiency by providing high temperature circulation water during operation. After heat transfer, the lower temperature circulation water is exported. As a consequence, the temperature of the tank is increased as well. The simulation results show the consistency with the real operation data.

In addition, in our operation test, the circulation water of the heat exchange system is also used to fully discharge the tank. When the hydrogen concentration decreases and the pressure drops to a value lower than what is required of the fuel cell application, the higher temperature water is brought into the circulation channel to heat the tank. As a result, the pressure of desorped hydrogen raises, which keeps the discharging process

going on. This stage could also be presented by the mathematical model with the identified parameters. The simulation results show the same tendency with the operation condition. The deviation might be the consequence of the temperature sensors' location. The temperature in the dynamic model is assumed to be the internal temperature of the tank, while operation database is measured by the surfaced sensors.

Figure 4.9 presents the operation data and dynamic model results of the hydrogen mass inside the tank. In order to protect the efficiency of fuel cell, the discharging process is suspended when the hydrogen pressure is too low. Thus, the tanks are not totally discharged.

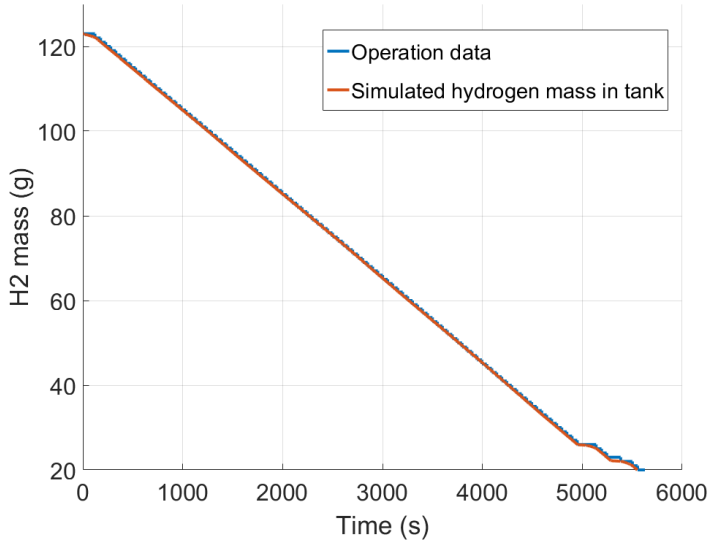

Figure 4.9: Real operation data of hydrogen mass and simulation result with optimal parameters.

4.4.3/ HEATER OPERATION

In the studied hydrogen storage and application system, the circulation water of the heat exchange system is also of great help to fully discharge the tank. When the hydrogen concentration is low, the hydrogen generation reaction speed decreases, which leads to the hydrogen pressure drops to a value lower than the requirement of the fuel cell application. Thus, higher temperature water is brought into the circulation channel to heat the tank for the purpose of promoting the dehydrogenating reaction and furthering the discharging process.

In the practical operation, an extra heater is used to increase the temperature of circulation water. Figure 4.10 gives the schematic of the detailed water circulation system, on which one can see the water circulation direction clearly. The circulation water is stored in a tank and embedded on the vehicle. The pump is turned on when the operation starts. Thus, the water keeps flowing inside the pipe follow a sequence of hydrogen tank, heat ex-changer with fan, heater, and then go back to the next round of circulation.

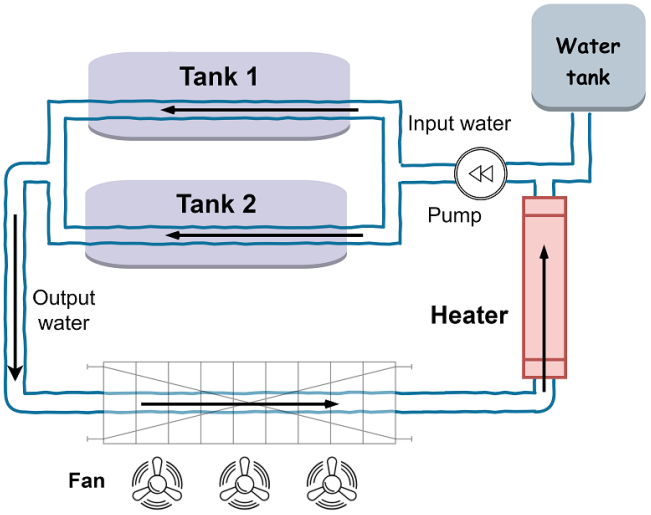

Figure 4.10: Schematic of water circulation system with a heater.

Normally, the heater is turned off under the condition that hydrogen pressure and flow rate satisfy to the requirement of fuel cell operation. The heat exchange treatment leading to the fluctuation of temperature and pressure is monitored by heat ex-changer and fan. The heater starts to warm the water when the hydrogen pressure is lower than a set threshold. For the current stage, the controller of the heater used on the vehicle is under On/Off strategy. The continuous simulation of the dynamic model could cause the response delay. Replacing it by an analog controller like Proportional or Proportional-Integrator Controller on the vehicle could be of great help to improve the smoothing of the curve and then decrease the error. Besides, the location of temperature sensors leads to a time response delay between the operation test and simulation model as well. The operation database is measured by the surfaced sensors while the temperature in the dynamic model is assumed to be the internal temperature. A more complicated model considering the heat conduction applied to simulate this phenomenon could improve the accuracy.

4.4.4/ Effect on vehicle design and application

As a parameter used for expressing the condition of heat exchange system, A represents the heat exchange coefficient. During the discharging process, the heat transmits between hydrogen tank and water circulatory system, which affects the temperature variation rate and the reaction speed inside the tank. Under real operation condition, the heat generated by the reaction of fuel cell influences the tank temperature as well. As introduced above, the heat radiation is ignored, its influence is therefore be contained in the parameter of the dynamic model. The value of A can be identified using PSO method.

The efficiency of heat exchange system mainly affects the temperature variation of the tank. Figure 4.11 shows the results of this analysis that the temperature of the tank could be dramatically different when the parameter A is modified. The generating rate of hydrogen changes correspondingly.

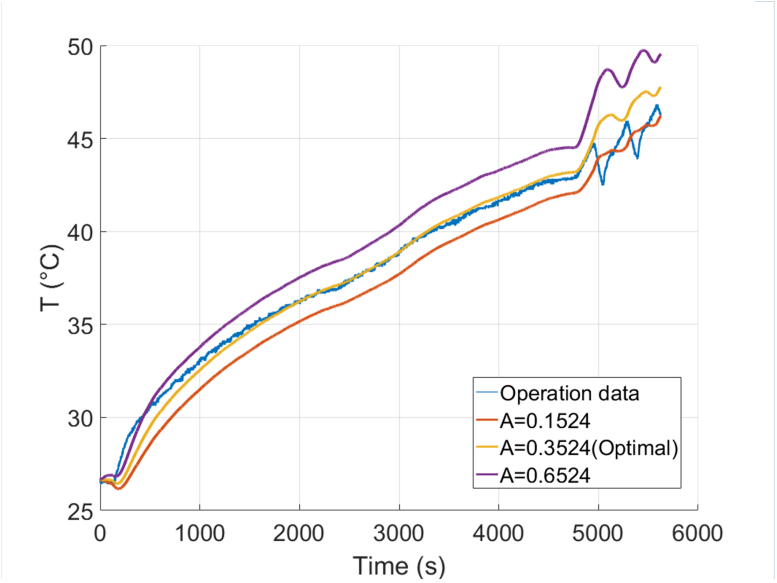

Figure 4.11: Simulation results of temperature with different exchange coefficient.

When we design and manufacture a fuel cell vehicle, the applied hydrogen storage tank is generally commercially available that it is inappropriate to open it up or modify the structure. The only measure we can take is to improve the efficiency of the tank and achieve its best performance during operation. Under this situation, the design of the heat exchange system is of great significant. The optimal heat transfer coefficient A can be realized through modifying the flow rate or change the liquid of the circulatory system.

4.5/ CONCLUSION

This chapter discussed the dynamic performance of the practical application of an embedded MH hydrogen storage tank. Since the material and structure of the MH inside a commercial tank is unknown, it has been considered as a gray box for the modeling process. The PSO algorithm is applied to search for the optimal parameter set for the purpose of identifying the missing parameters. For all the operation conditions with different environmental temperatures, the simulation results of the dynamic model with the optimal parameters show a great agreement with the real operation data, and the errors are lower than 9%. This deviation, between simulation result and operation data, is mainly caused by the activated heater. It can be reduced through two strategies: The first one is to include the heater in the model by considering the heat conduction and heat radiation. The second strategy is to improve the current control algorithm to smooth the pressure waveform at the end of the discharging process of the tank.

In the next chapter, detailed information about the thermal condition and energy transfer will be studied on the basis of the context of this chapter. One interesting application will be the energy management of the system associating the MH tank and fuel cell generator including heat exchange smoothing and ageing aspects.

5

THERMAL MANAGEMENT OF THE PEMFC-MHT SYSTEM

5.1/ INTRODUCTION

As discussed in the first chapter, the fuel cell vehicles are expected to play an important role in the future clean energy transportation for its renewable energy source and zero carbon emissions [178]. On these vehicles, fuel cell is an energy conversion device converting the chemical energy into electrical energy taking hydrogen as the source. Based on the advantages of relatively high power density, high energy density and environmental friendly byproduct, the fuel cell power system has considered to be the promising alternative to the tradition power generation technologies for transportation application [13, 14, 179].

Proton-exchange-membrane (PEM) fuel cell introduced in chapter one is one type of fuel cell technologies with high power density and compactness. Meanwhile, it operate at relatively low temperature ($-20°C$ to $100°C$), which contributes to a fast starting from idle to full load operation [180]. Thus, PEM fuel cell is more suitable for the embedded application on the long-range transportation.

MH hydrogen storage tanks provide a low pressure charging, transportation and operation method for on-board hydrogen storage and application. Due to the advantages of safety, pollution-free, and reusable, the MH hydrogen storage tanks have been widely developed and applied on fuel cell vehicles [95]. The hydrogen flow rate drawn from a MH tank is strongly influenced by the heat transfer rate at reaction zone [181]. Faster reaction kinetics is one of the most important and essential attributes of MH alloys. The reaction kinetics of the hydride bed is strongly influenced by the rate at which the heat can be removed/supplied from/to the reaction bed [182]. Often, the heat transfer rate is the controlling variable that determines the hydrogen gas flow rate can be extracted from a tank. Hence, increasing heat transfer rates is important for optimizing the design of MH hydrogen storage applications [183]. The absorption reaction is accompanied by the released heat which needs to be removed from the system, on the contrary that additional heat needs to be supplied for the desorption process. Therefore, removing or providing extra heat from or to the MH reaction bed is an important factor for ensuring efficient hydrogen storage or generation.

Multiple studies have addressed the issue of heat transfer in MH based hydrogen storage.

Foam and expanded natural graphite are attempted to add to the MH reaction bed for the purpose of improving the thermal conductivity of MH tank [184–187]. Moreover, extra heat transfer enhancements like fins, cooling tubes, cooling coils, etc, are introduced to facilitate effective heat transfer [124, 176, 188, 189]. Recently, combinations of these techniques have been employed, yielding favorable results [190]. Garrison et al. studied the effect of a concentric cooling tubes equipped with transverse fins and longitudinal fins respectively on a sodium alienate system [191]. The results pointed to a configuration involving multiple cooling tubes at small distances as the most viable. Besides, Ferekh et al. compared the performance of metal fins versus metal foam and found that metal foam based design was superior to the fin based design [187].

During hydrogen discharging process, a particularly thermal management strategy is necessary to obtain the desired hydrogen flow from the MH hydrogen storage tank. For an integrating system, the generated heat from fuel cell could act as the thermal source for hydrogen desorption [192]. Thus, the components in the fuel cell system are thermally coupled tightly. The heat pipes are applied to increase the hydrogen desorption rate from the MH tanks using the fuel cell heat [193,194]. Heat exchange fans and circulation water have also been introduced to this integrate system for thermal management [195, 196]. This reaction heat has a great bearing upon the system performance as it controls the MH reaction bed temperature, which in turn controls the equilibrium pressure.

In FCHEV powertrain, another energy sources, namely, batteries, super capacitors, etc, are applied to provide or absorb the fast peak power under the vehicles short-term accelerations or brakes. Therefore the fuel cell is maintained in high efficiency operation mood at partial loads [197, 198]. The durability of the currently available energy devices is a central issue holding back the critical achievement of the FCHEVs [199]. In addition to the development of materials technology and structure designing of the devices, the effective control strategies on the operating conditions are proved to be possible to mitigate the deleterious effects of degradation [13]. However, the performance and limitation of the hydrogen storage containers are not taken into account. The self regulation ability of the fuel cell system coupled with the hydrogen storage system need to be recognized and valued. So an active thermal management strategy is proposed to maintaining the performance and extending the life span of fuel cell along with time in this chapter.

This chapter is organized as follows: Section 5.2 gives the configuration and dynamic model set in detail, including the structure of the studied integrate hydrogen system, the dynamic model of the MH hydrogen storage tank, the PEM fuel cell, the heat ex-changer and air below. The dynamic performance of this integrating system of PEM fuel cell and MH hydrogen storage tank system (PEMFC-MHT system) is simulated and the model set is validated by the database collected form the real operation FCHEVs. In Section 5.3, the degradation model of both MH tank and PEM fuel cell are introduced to present the influence and phenomenon of the ageing system. Section 5.4 provide an thermal management strategy for long-term operation. The function of this strategy is simulated by 1000 hours. Then the fuel efficiency and economy of the hydrogen storage and application system are applied for evaluation. The last part gives a rapid summary of the main contribution and some prospects of this chapter.

5.2/ PEMFC-MHT SYSTEM FOR ON-BOARD HYDROGEN STORAGE AND APPLICATION

5.2.1/ CONFIGURATION OF THE COUPLING SYSTEM

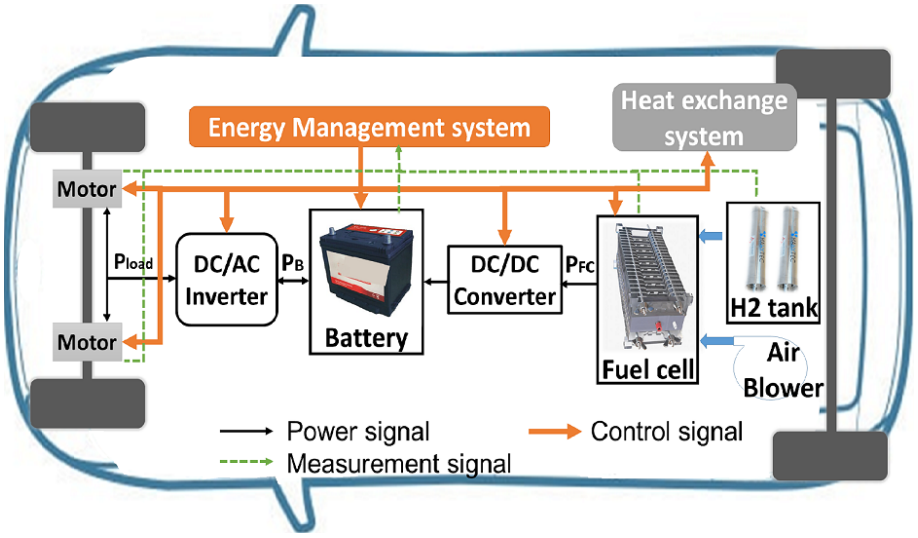

Figure 5.1: Architecture of the tested vehicle.

Commonly used FCEHV configuration mainly includes fuel cell system and battery as power source. As shown in Figure 5.1, a series hybrid configuration is studied in this research including hydrogen storage tank, fuel cell, batteries, electric machine, mechanical drive line and controllers. The fuel cell system is connected to the batteries via a DC/DC converter and operates as a range extender to increase the driving distance and level up the speed. Under this condition, the fuel cell is possible to be held in a relatively steady state and controlled to operate in its max efficiency region [41, 43, 44].

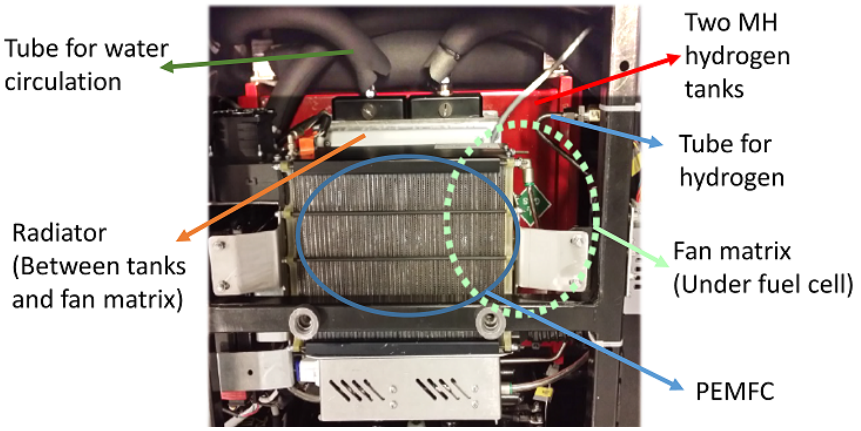

Figure 5.2: PEMFC-MHT system on the studied vehicle.

Figure 5.2 presents the photo of the embedded PEMFC-MHT system on the tested vehicles, its detailed schematic is then shown in Figure 5.3. Such system, namely, an on-board PEMFC-MHT system, is combined by PEM fuel cell, MH hydrogen storage tank, air blower, radiator, fan matrix and circulation water. Through the reaction of oxygen and hydrogen, PEMFC transforms the chemical energy into electric energy and serves as the main source of the FCEHV powertrain. An air blower is applied to provide enough oxygen for the reaction. Hydrogen is stored in the MH tanks through hydrogenation reaction and carried on the vehicle. To supply the proper hydrogen flow, the reaction speed and operation temperature are controlled through the heat ex-changer. A copper tube for circulating water is installed to control the temperature and regulate the equilibrium pressure of the MH reaction bed. The extra heat generated by the PEMFC is exploited for raising the circulating water temperature through the radiator and fan matrix. The heat transfer condition is depicted in Figure 5.3. This schematic is also the configuration of the mathematical model used in our study, which will be discussed in Section 5.2.2.

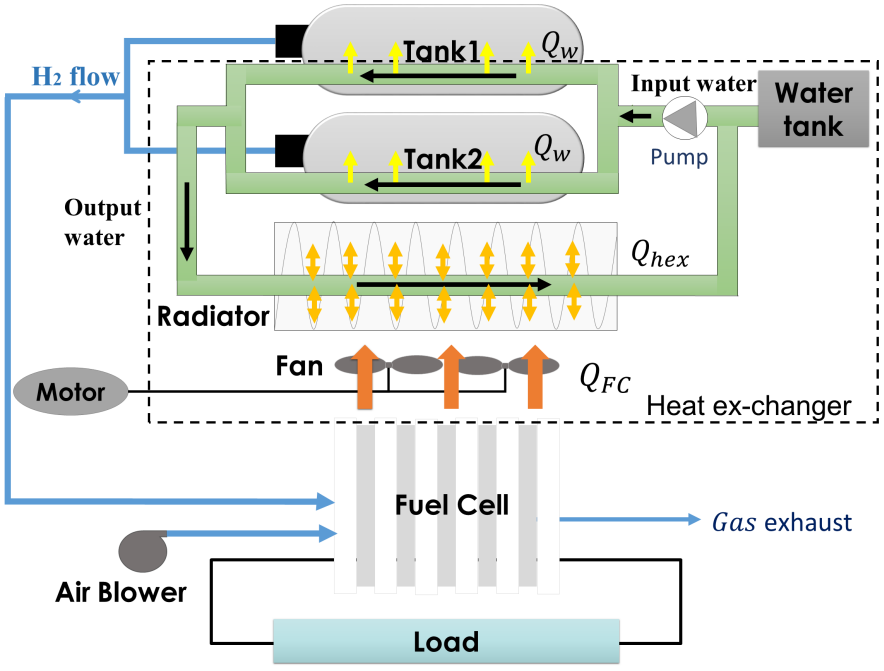

Figure 5.3: Schematic of PEMFC-MHT system on tested vehicles.

5.2.2/ Modeling process

5.2.2.1/ Model assumptions

This mathematical model of PEMFC-MHT system is applied to describe the dynamic responses of the embedded MH hydrogen storage tank and PEM fuel cell. The polarization curves under different operation condition of fuel cell, the reaction kinetics and equilibrium conditions of hydrogen storage tank and the heat transfer and exchange situation among the system are modeled and simulated in detail. In order to design a simplified model for practical use, some assumptions are made as following [129]:

- 1. Stable test temperature is guaranteed;
- 2. The degradation of fuel cell has no extreme effect to the operation during a short period, namely, operation less than 10 hours;
- 3. The degradation happening on each area of the fuel cell stack is held on the same degree;
- 4. The MH hydrogen storage tank degradation is homogeneous;
- 5. The modeled geometry has a bottle-like shape as shown in Figure 5.3 that matches the real MH tank applied on the FCHEVs;
- 6. Used hydrogen is considered to be an ideal gas;
- 7. The MH physical characteristics of thermal conductivity, porosity and volume remain constant;
- 8. The heat convection inside the tank is neglected, which means the temperature of the tank interior and its surface are assumed to be the same;
- 9. The equipment in heat ex-changer remain constant operation efficiency.

5.2.2.2/ PEMFC STACK MODEL

During operation, PEMFC releases water by combining hydrogen and oxygen and generate the required electrical energy. For the applied mathematical model, four factors determine the output of PEMFC for operating load [71, 200], which are presented as follows:

The reversible potential is calculated by the Nernst equation:

$$E_{nernst} = E_0 + \frac{RT}{2F} * ln\Big(\frac{P_{H_2} * P_{O_2}^{\frac{1}{2}}}{P_{H_2O}}\Big) \tag{5.1}$$

where E_0 is the theoretical real voltage, T is the fuel cell operating temperature, P_{H_2},P_{O_2} and P_{H_2O} are the effective pressure of hydrogen, oxygen and gaseous water. F represents the Faraday constant.

The activation over voltage is obtained by:

$$V_{act} = \frac{-RT}{2\alpha F} * ln(\frac{i}{i_0}) \tag{5.2}$$

in which α is change transfer coefficient and i_0 is the exchange current density. i is the current density of fuel cell stack.

The ohmic over voltage is determined as:

$$V_{ohmic} = i * S_{cell} * R_{ohmic} \tag{5.3}$$

in which S_{cell} is the cell active area and R_{ohmic} represents the ohmic resistance.

The concentration voltage drop could be calculated as:

$$V_{conc} = BT * ln(1 - \frac{i}{i_L}) \tag{5.4}$$

where i_L represents the limiting current.

Thus, the output voltage of a single PEMFC is:

$$V_{FC} = E_{nernst} - V_{act} - V_{ohmic} - V_{conc} \tag{5.5}$$

Taking N_{cell} as the number of cells, the power generated by the embedded fuel cell and used for load can be calculated as [193]:

$$P_{FC} = N_{cell} * V_{FC} * i * S_{cell} \tag{5.6}$$

Meanwhile the heat generation rate of the operating fuel cell stack can be calculated. The value of the voltage is $1.48V$ when the water product is in liquid form and $1.25V$ is used in vapour form [168, 193].

$$Q_{FC} = N_{cell} * (1.48 - V_{FC}) * i * S_{cell} \tag{5.7}$$

$$Q_{FC} = N_{cell} * (1.25 - V_{FC}) * i * S_{cell} \tag{5.8}$$

5.2.2.3/ MH HYDROGEN STORAGE TANK MODEL

In the PEMFC-MHT system, the hydrogen supply flow rate of the MH tank should be adequately controlled to meet the requirement of fuel cell operation. Unlike the high pressure tank, the hydrogen flow rate released from a MH tank in this integrate hydrogen system is controlled by thermal management. Thus, the dynamic responses of the MH hydrogen storage tank to the PEM fuel cell demands could be expressed as the state alteration such as pressure or temperature. The model is developed incorporating the mass conservation and thermal energy balances in the hydrogen storage system [166, 167], for describing the reaction kinetics, mass and energy transfer during FCHEVs operation process.

The model introduced in Section 3.2 are applied to describe the dynamic performance of the MH hydrogen storage tank, as presented in Table 5.1.

Table 5.1: Model equations of MH hydrogen storage tank

Model	Equation
State equation	$P = \rho^g RT$
MH continuity	$\dot{m}_{MH} = (1-\varepsilon)\frac{\partial \rho^s}{\partial t}$
Hydrogen mass conservation	$\dot{m}_{H_2} = \left(\frac{V_{tank}}{V_{MH}} - 1 + \varepsilon\right)\frac{\partial \rho^g}{\partial t}$
Reaction kinetics	Absorption: $\dot{m}_{MH} = C_a exp\left(-\frac{E_a}{RT}\right) ln\left(\frac{P}{P_{eq}}\right)(\rho_s^s - \rho^s)$
	Desorption: $\dot{m}_{MH} = -C_d exp\left(-\frac{E_d}{RT}\right)\left(\frac{P-P_{eq}}{P_{eq}}\right)(\rho_s^s - \rho^s)$
Equilibrium pressure	$P_{eq} = f(r) exp\left(\frac{\Delta H}{R}\right)\left(\frac{1}{T} - \frac{1}{T_r}\right)$
Energy balance	$\left(\frac{V_{tank}}{V_{MH}} - 1 + \varepsilon\right) C_{pg}\frac{\partial(\rho^g T)}{\partial t} + (1-\varepsilon) C_{ps}\frac{\partial(\rho^s T)}{\partial t} = Q + \dot{m}_{MH}\Delta H$
Heat transfer	$Q = \frac{Q_w}{\dot{m}_w} C_{p,w}(T_{w,in} - T_{MH})(1 - e^{-A})$
Water temperature	$T_{w,out} = T_{MH} + (T_{w,in} - T_{MH})e^{-A}$

5.2.2.4/ MODEL OF AIR BLOWER

The oxygen required by fuel cell is extracted by a blower from atmosphere. The flow rate determined by the fuel cell operating condition is:

$$f_{air} = \frac{S * M_{air}}{4 M_{O_2} * F} * I_{FC} \tag{5.9}$$

where S is the stoichiometric ratio, M_{air} is the number of air moles [201].

As a main auxiliary component for the PEMFC-MHT system, the power consumption of the air blower is calculated as follows [202]:

$$P_{blower} = \frac{C_{pair} * T_{atm} * f_{air}}{\eta_{blower}} * ((\frac{p_{sm}}{p_{atm}})^{(\gamma-1)/\gamma} - 1) \tag{5.10}$$

In this equation, T_{atm} is the atmospheric temperature, η_{blower} is the blower coefficient, γ is the ratio of the specific heats of air, p_{sm} is the pressure inside the supply manifold and p_{atm} is the atmospheric pressure.

5.2.2.5/ MODEL FOR HEAT EX-CHANGER

Figure 5.3 also presents the simplified thermal circulation in this PEMFC-MHT system. The thermal radiation from the relatively high-temperature PEM fuel cell and the heat generated by operating Q_{FC} are transferred to the radiator through fan matrix. The fan

speed is controlled by the motor and the function between the fan torque τ and the motor speed N can be expressed as [203]:

$$\tau = k * N^2 \tag{5.11}$$

Under this situation, the electrical power of the motor provided to fan could be determined by introducing an empirical model that:

$$P_{Fan} = \frac{2\pi * k}{60(aN^2 + bN + c)} * N^3 \tag{5.12}$$

The transfer efficiency of the fan λ_{Fan} is depending on the fan torque that:

$$\lambda_{Fan} = m * \tau \tag{5.13}$$

Therefore, under ideal situation, the heat absorbed by the heat ex-changer can be calculated as:

$$Q_{exc} = \lambda_{Fan} * Q_{FC} \tag{5.14}$$

In the PEMFC-MHT system, the radiator is applied to heating the circulation water. A transfer function is applied to indicate the time response of temperature variation. Based on specific heat function that:

$$T_{w,in} = (T_{w,out} - \frac{Q_{exc}}{C_{pw} * m_w}) * (1 - exp(-\frac{t}{R_s})) \tag{5.15}$$

in which $T_{w,in}$ presents the temperature of the water input to the tank and $T_{w,out}$ is the water temperature at the outlet of tank. R_s represent the response time of the transfer function.

Inside the tank, the energy exchanges between MH tank and circulation water, which could be expressed as:

$$\Big(\frac{V_{tank}}{V_{MH}} - 1 + \varepsilon\Big)C_{pg}\frac{\partial(\rho^g T)}{\partial t} + (1-\varepsilon)C_{ps}\frac{\partial(\rho^s T)}{\partial t} = Q + \dot{m}_{MH}\Delta H \tag{5.16}$$

The overall heat exchange between MH tank and circulation water is developed based on the energy balance. The amount of heat transfer can therefore be expressed as:

$$Q_{tank} = \frac{Q_w}{\dot{m}_w} c_{p,w}(T_{w,in} - T_{MH})(1 - e^{-A}) \tag{5.17}$$

As a result, the temperature of circulation water changes after heat transfer can be expressed as:

$$T_{w,out} = T_{MH} + (T_{w,in} - T_{MH})e^{-A} \tag{5.18}$$

where A is the coefficient of heat exchange between MH material and water.

5.2.3/ DYNAMIC SIMULATION OF THE MODEL

The model of the purposed PEMFC-MHT system is verified by the real tested FCHEVs through the contradistinction between dynamic performance simulation and recorded operation database. The parameters applied for simulation are presented in Table 5.2 and Table 5.3. This process is implemented by MATLAB software [172].

Table 5.2: The properties applied in PEM fuel cell model [80, 200]

Properties		Value	Unit
F	Faraday constant	96485	C/mol
T	Temperature of the cell	55	$^{\circ}C$
α	Change transfer coefficient	0.1	-
S_{cell}	Active area in single cell	62	cm^2
N_{cell}	Number of cells	40	-
β	Degradation coefficient	3.5×10^{-3}	-

Table 5.3: The parameters applied in simulation [202, 203]

Parameters		Value
S	Stoichiometric ratio	2
γ	Specific heats ratio of air	1.4
η_{blower}	Efficiency of air blower	0.8
p_{sm}	Pressure inside the supply manifold	2 atm
k	Coefficient of fan torque	4.03×10^{-11}
a	Coefficient of fan power	-5.6×10^{-8}
b	Coefficient of fan power	5.3×10^{-4}
c	Coefficient of fan power	-0.38

On the tested vehicle, the configuration of drive train is distributed as Figure 5.1. The fuel cell system is applied as the first power source to charge the batteries. A PEMFC stack of 1.1 kw, composed by 40 single fuel cells, is installed on the vehicle and operated under the temperature of $55^{\circ}C$. The database for model validation is collected when the atmosphere temperature is $17^{\circ}C$. The FCHEV is continuously operated in three separate phases, with the fuel cell mode turns on all the time during operation.

Figure 5.4 presents the results of the embedded PEM fuel cell response to the power load. Under this stable driving condition, the load power required by batteries stay constant. The output power of fuel cell system is observed to follow the trail of the load with some delay. Such delay happens due to the current response, which caused by several elements. In one part, the fuel cell is controlled to operate under a relatively high temperature, the heater for fuel cell is turned on when the fuel cell mode starts, while it takes amount of time for the operating temperature to reach the predetermined value. Low operating temperature effects the performance of PEM fuel cell. In the other part, a

certain concentration of hydrogen and oxygen is necessary for the reaction. The dynamic behavior of the MH hydrogen storage tanks causes the time delay as well. During the response period, the voltage appeared to be higher than demand. It is due to one of the characteristics of fuel cell that is expressed as the polarization curve.

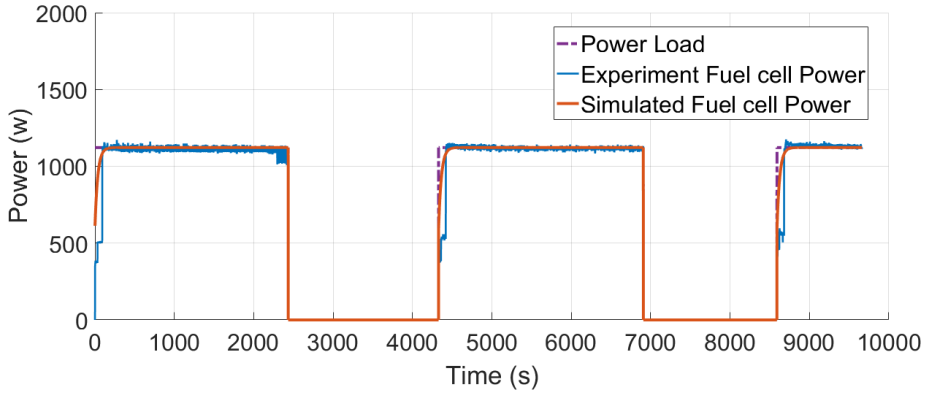

(a)

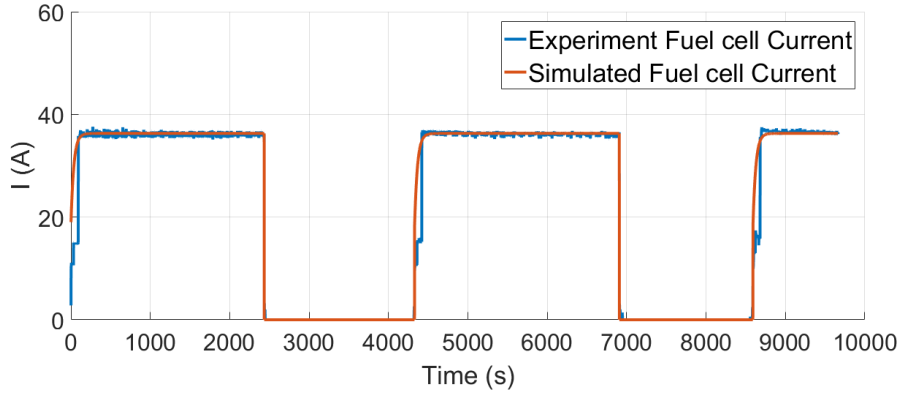

(b)

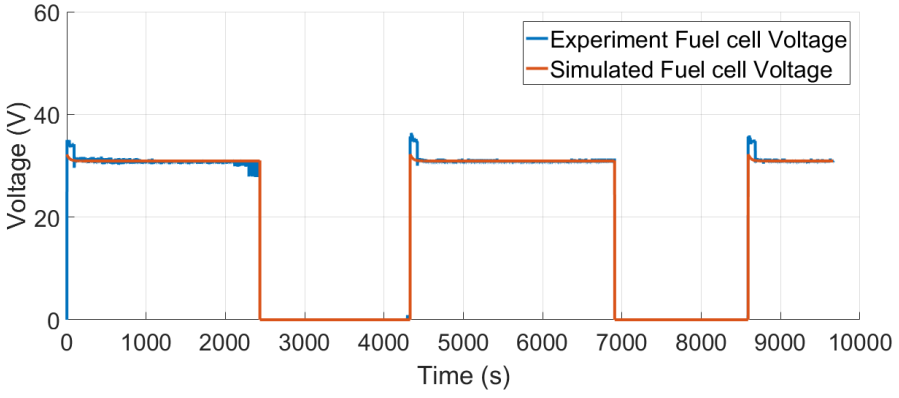

(c)

Figure 5.4: Fuel cell operating condition under required power load.

Figure 5.5 to Figure 5.7 presents the dynamic performance of the MH hydrogen storage tank during the tested vehicle operation process. As one can see from Figure 5.5, the

hydrogen flow tracks to the requirement with a time delay at each desorption phase, and it last for around 200 s. During this period, the hydrogen flow rate is mainly dominated by the pressure difference, that caused the gaseous hydrogen releasing from the tank.

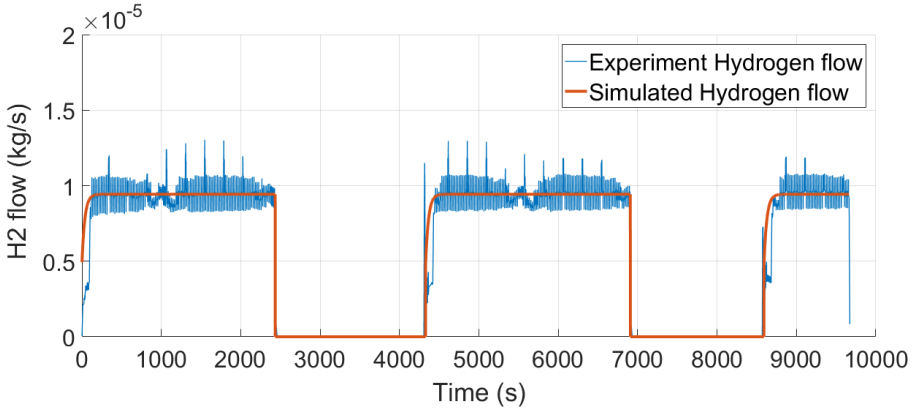

Figure 5.5: Hydrogen flow rate of MH tank under required power load.

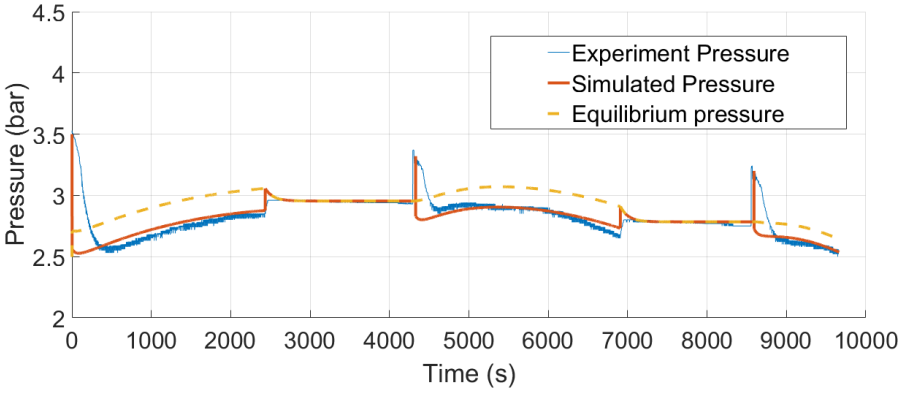

Figure 5.6: The pressure of MH hydrogen storage tank under required power load.

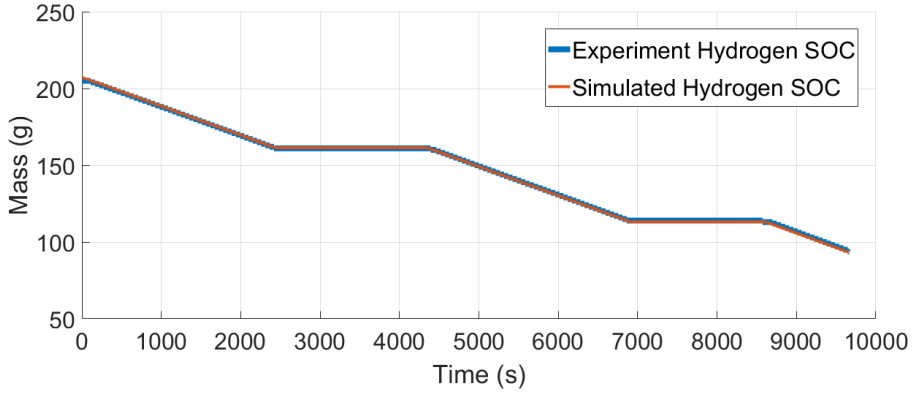

Figure 5.7: Hydrogen mass remained in the MH hydrogen storage tank required power load.

Figure 5.6, shows the pressure and equilibrium pressure variation condition. The equilibrium pressure corresponding to the hydride concentration and temperature, which has been explained in Eq. 4.10. Thus, at the start period, hydrogen cannot be desorbed from the MH autonomously, additional heat is required. Thanks to the gaseous hydrogen releasing and the heat delivering from the circulation water, the pressure drops and the equilibrium pressure raises. Therefore, the prerequisites of the dehydrogenating reaction are achieved and the hydrogen desorption process begins. For the remaining period, the desorption rate follows the requirement well and the simulated pressure tracks the real operation data within reasonable deviation. Figure 5.7 presents the estimated hydrogen mass remained in the tank.

The extra heat generated by PEM fuel cell during the electrochemical reaction is exploited for hydrogen desorption from MH material. Figure 5.8 represents the heat production and transformation under the management of the heat ex-changer. The simulation results indicate that the transferred heat from PEMFC to MH hydrogen storage tanks is adequate to arouse and maintain the desorption reaction. After short period of delay, the stable operating PEM fuel cell provides continuously constant heat, which is simulated to be 600 W. Around 30% of heat is delivered by fan matrix to the radiator, so the circulation water temperature is raised, for the purpose of hydrogen desorption. According to the simulation results, the heat absorbed by the radiator is enough for hydride reaction consumption, even though there is an inevitable time delay of the heat transfer process.

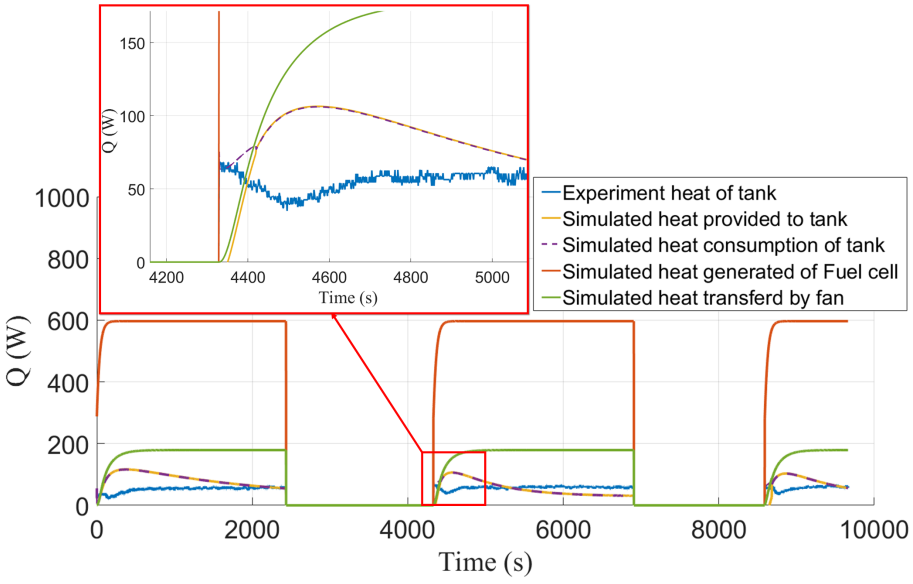

Figure 5.8: Heat generated and transferred in the fuel cell system.

Figure 5.8 also presents the consumed heat of the tank in actual test. At least 60 W of heat is required for hydrogen desorption. The simulated heat provides to the tank not only applied for the dehydrogenating reaction, the circulation water absorbs the energy and it is heated as well. The heat radiation to the environment is also considered. The temperature variation during the simulated process are presented in Figure 5.9, which performed the results of the thermal management of the heat exchange system. At the beginning of hydrogen desorption process, a surplus of heat is provided to the tank,

which causes the temperature of circulation water and tank raised rapidly. When the reaction has stabilized, the growing rate of temperature gradually decreases. During the suspend phase between two operation process, the temperature decreases gradually to the ambient temperature. The temperature response speed of the water and tank are unequal due to the different specific heat capacity.

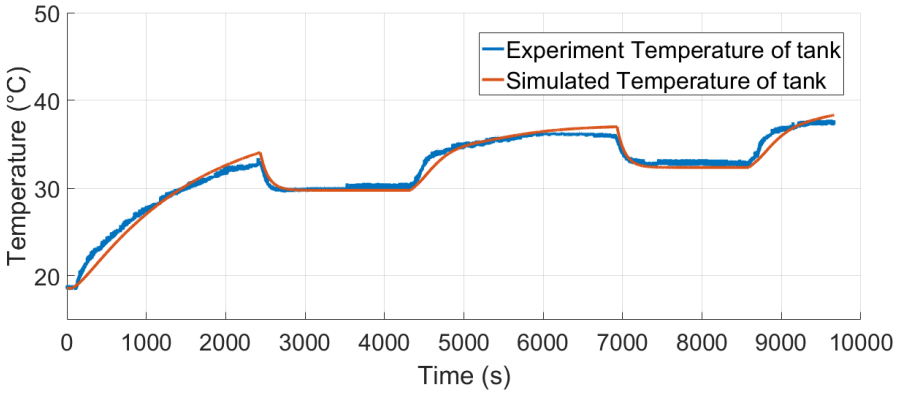

Figure 5.9: Temperature variation along time.

What worth to mention is that the heat for hydrogen desorption is not just provided by the fuel cell. In real operation situation, the circulation water plays the same role once in a while. As shown in the detail part of Figure 5.8, when the heat provided to the tank is less than the reaction consumption occasionally, the rest part of energy is absorbed from the circulation water. Thus, the water temperature dropped rapidly during this short period, which is shown in Figure 5.9.

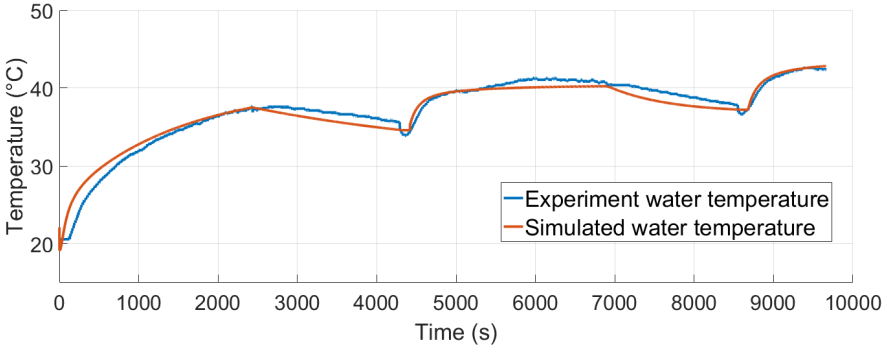

Figure 5.10: Temperature of circulation water variation along time.

5.3/ DEGRADATION OF THE COUPLING SYSTEM

5.3.1/ DEGRADATION MODEL OF THE MH HYDROGEN STORAGE TANK

The practical applications of the MH hydrogen storage tank have a high requirement for long-term hydrogen absorption/desorption cycling, which leads to the degradation of

hydrogen storage properties [204]. The degradation rate k of the tank capacity during cycling is calculated according to the following empirical equation [148, 205]:

$$C_n = C_{n-1} * exp(-kn) \tag{5.19}$$

where C_n is the hydrogen storage capacity at the cycle number of n. As shown in Figure 5.3.1, the degradation rate reaches the highest at the first 30 cycles, and then reduces along with the further cycling. In the first 100 times of charging and discharging process, the hydrogen capacity is obviously degraded, while after 200 cycles the performance steady decline. Figure 5.3.1 presents the hydrogen storage capacity variation of the MH tank during the life span. The reduction of capacity occurs with the growing number of charging and discharging cycles. The storage tank meets its end of life for transportation application after about 2500 cycles since more than 25% capacity degradation happens [206].

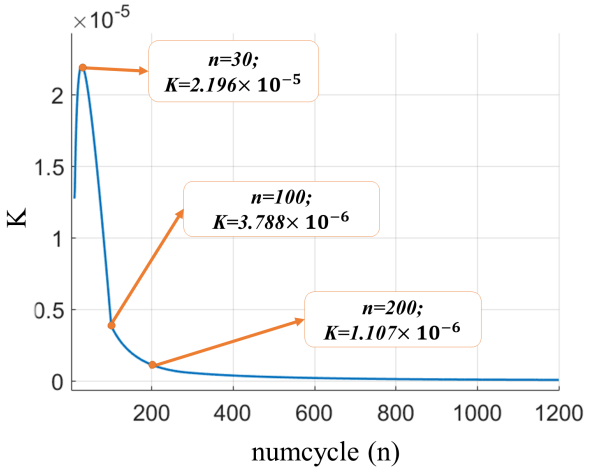

Figure 5.11: MH degradation rate against cycle numbers.

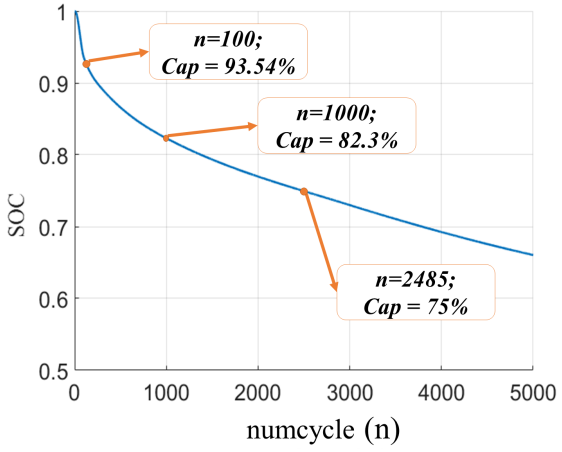

Figure 5.12: SOC degradation of the MH hydrogen storage tank.

5.3.2/ DEGRADATION MODEL OF THE PEM FUEL CELL

The PEM fuel cell degradation takes place with a high number of stops and starts which applies a relatively high load on fuel cells and leads to the output voltage drops. This dwindles the performance and efficiency of the fuel cell stack.

The semi-empirical degradation model of PEM fuel cell used in this thesis is based on the model first developed in [80]. For a given current, the effect of ageing and degradation on stack voltage could be estimated separately:

$$R_{ohmic}(t) = R_{ohmic0} * (1 + g(t)) \tag{5.20}$$

$$i_L(t) = i_{L0} * (1 - g(t)) \tag{5.21}$$

The parameter $g(t)$ reflects the time relation of the change in the resistance and limiting current, where $g(t) = \beta t$ and β approximates to constant.

5.4/ THERMAL MANAGEMENT FOR LIFE SPAN EXTENDING OF THE PEMFC

5.4.1/ PROBLEM FORMULATION AND OBJECTIVE FUNCTION

The stack voltage drop is the most principle performance which leads to the power degradation of the fuel cell system after long time operation. Raising the hydrogen flow rate is an effective approach to maintaining the performance of fuel cell and extending its lifespan [207].

The mass flow rate of hydrogen required by PEM fuel cell can be calculated using the fuel cell model. The following equation is applied considering a hydrogen utilization factor of 0.95 [71].

$$f_{FC} = 1.05 \times 10^{-8} * \left(\frac{P_{out}}{V_{out}}\right)/0.95 \tag{5.22}$$

The hydrogen mass generation rate of the MH tank is dominated to meet this requirement through appropriate thermal management strategy. In practical on-board system, the tank thermal variation is mainly depending on the efficiency of the heat transfer fan. Therefore, through effectively control, the long-term performance of the PEMFC-MHT system could be improved.

5.4.2/ CONTROLLER DESIGN

Figure 5.13 presents the block diagram of the thermal management in the PEMFC-MHT system achieved by controlling the speed of fan matrix. As a simple but useful and efficient control logic, PID control algorithm is applied. The electrical power responsed by fuel cell in this PEMFC-MHT system is denoted as the control variable. The objective of the controller is adjusting the hydrogen mass flow rate released of the tank to meet the

requirement of PEM fuel cell. The input of the diagram is the electrical power required by battery, which should be provided by the PEMFC-MHT system. Proportion, integration and derivative coefficients in the PID controller are adjusted to minimize the error between the required power and real response power. The control parameter $u(t)$ determines the heat transfer coefficient from fuel cell to radiator.

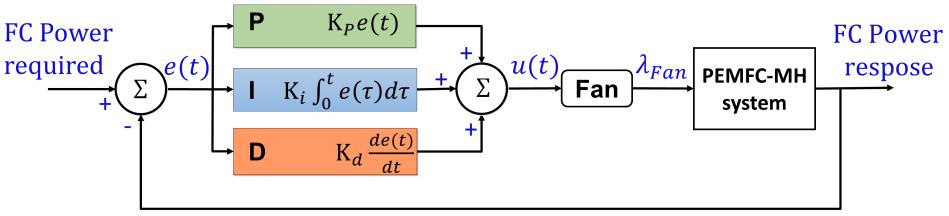

Figure 5.13: Block diagram of a fuel cell system with a PID controller.

In the physical system, the transfer coefficient is dominated by the speed of fan. Modifying the fan speed will let us to control the amount of heat transferred between PEM fuel cell and MH tanks. With more heat supply, the speed and quantity of hydrogen extracted from MH tank will increase and then, the power delivered by the fuel cell is improved correspondingly. We consider here, that, the PEM fuel cell is always well supplied by the oxygen.

In long-term operation of the PEMFC-MHT system for transportation application, the aged PEM fuel cell cannot fully response to the load power. Thus, the error $e(t)$ in this diagram represents the degradation degree of the PEM fuel cell. As mentioned above, the power-train of the studied system is in series so that the load power of fuel cell corresponding to charging the batteries is constant. The error due to the variation of load demand is not considered as the degradation of PEM fuel cell.

5.4.3/ Results and discussion

5.4.3.1/ Simulation results

The long-term operation controller (LTOC) designed above is introduced to modify the fan speed for the purpose of maintaining the power response and decreasing the degradation degree of the PEM fuel cell after long time using of vehicle.

Figure 5.14 and Figure 5.15 shows the effect of the thermal management strategy that the fan speed increased 2.2%, which leads to the transfer efficiency raising 4.6% according to Eq. 5.11. As a consequence, more energy is transferred from PEM fuel cell to MH hydrogen storage tank to accelerate the dehydrogenate reaction and obtaining more hydrogen.

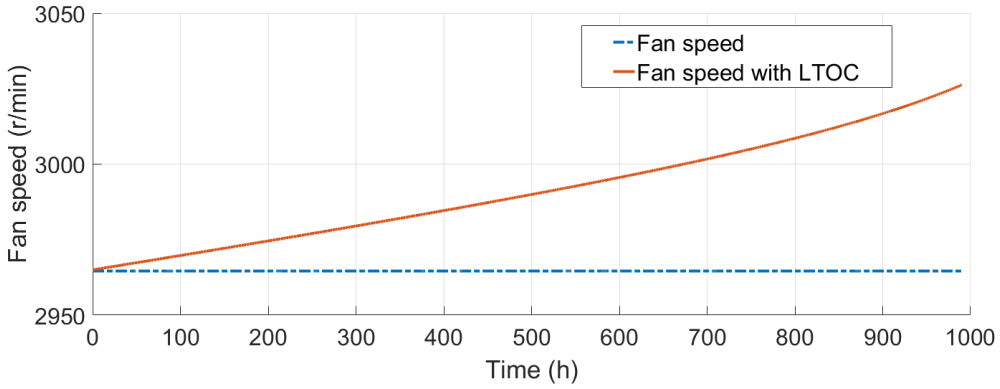

Figure 5.14: Fan speed without and with LTOC.

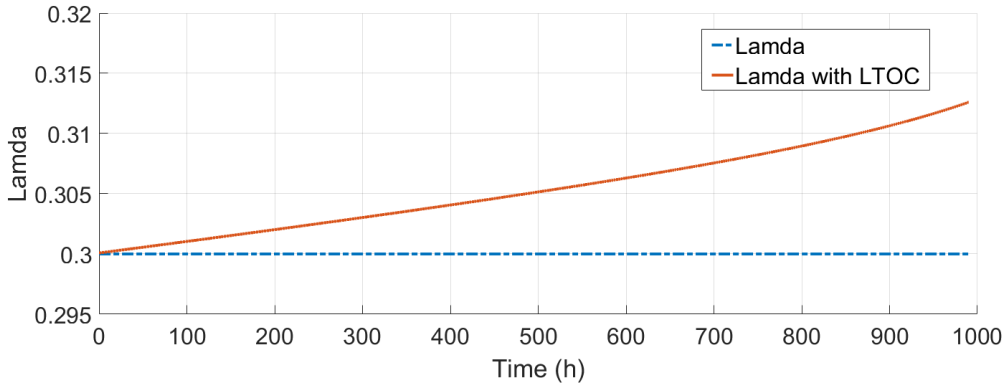

Figure 5.15: Heat transfer efficiency without and with LTOC.

Figure 5.16 presents the variation of hydrogen discharging flow rate during 1000 hours of vehicle operation. Under the adjustment of the heat exchange system, 11% more hydrogen is desorbed from MH hydrogen storage tank and provided to PEM fuel cell. Thus, the efficiency of the PEMFC-MHT system is improved and the degradation rate is reduced, which contribute to meet the requirement of load and maintain the output power. What have to be aware of is that the response time of the hydrogen desorption from the MH hydrogen storage tanks to meet the requirement cannot be ignored, the fuel cell starting time as well. Therefore, during this time, the power of PEM fuel cell cannot response to the load in the simulation results. However, although the starting counts of fuel cell have a serious impact on degradation, the results of thermal control are not changed, for the reason that the driving cycle is not additionally considered in our simulation.

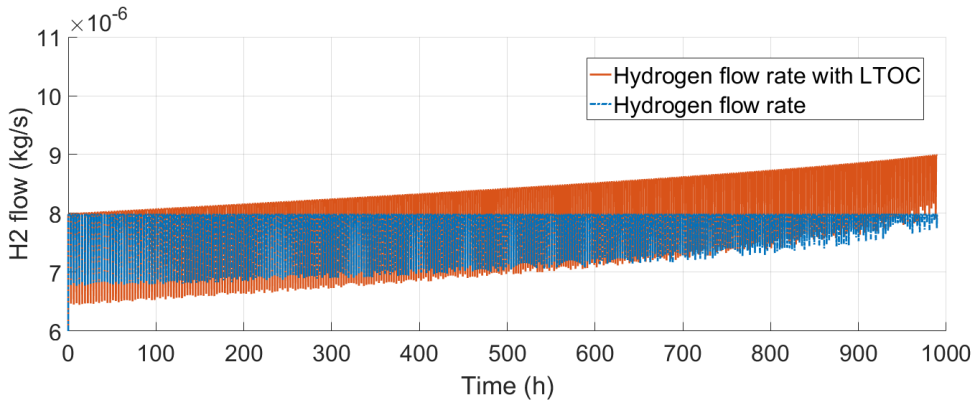

Figure 5.16: Responses hydrogen flow rate from MH tank without and with LTOC.

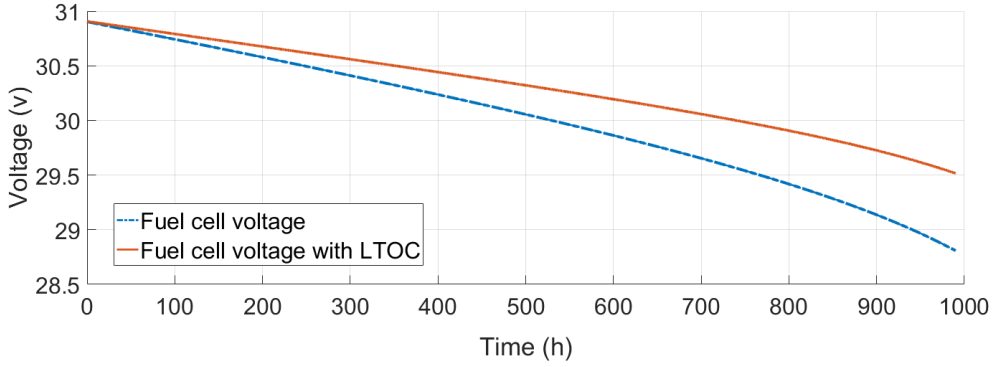

Figure 5.17: Fuel cell voltage along with time without and with LTOC.

The output voltage is widely used to demonstrate the degradation phenomenon of fuel cell. Figure 5.17 shows that with the thermal management strategy, the degradation of voltage is reduced from 6.8% to 4.4% after 1000 hours of operation. Thus, in the case of a constant mission profile, 2.4 % of power degradation is prevented.

Figure 5.18 presents how the hydrogen capacity of the MH tank modified during 1000 hours. Obviously the capacity presents a drop trend with time. Due to the growing discharging hydrogen flow rate, the thermal management strategy helps to maintain the efficiency of fuel cell while accelerate the degradation of MH hydrogen storage tank. During this long time, the number of charging and discharging cycle of the on-board MH tank is 348 and 369 separately, and the degradation rate of the MH tank capacity is about 11.2% and 11.5%. The influence will be discussed at both fuel efficiency and fuel economy part.

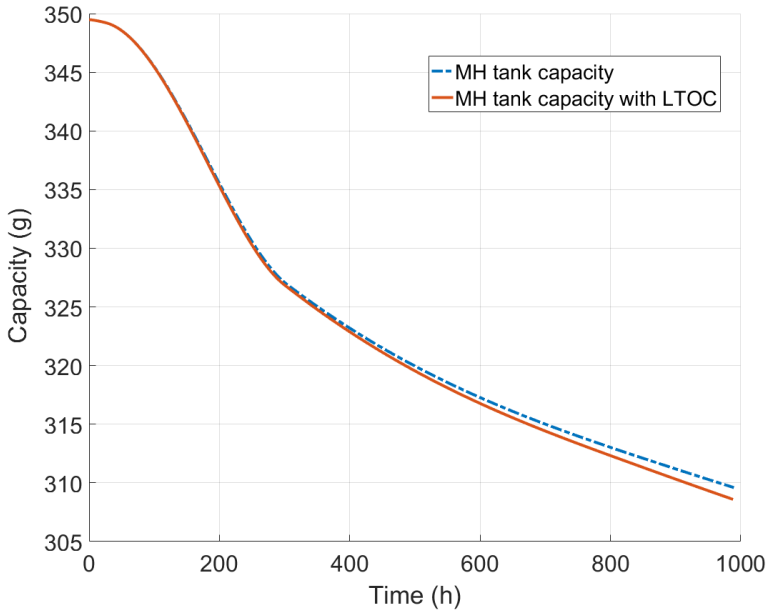

Figure 5.18: MH tank capacity degradation along time.

5.4.3.2/ FUEL EFFICIENCY

Fuel efficiency is a significant criterion for a fuel cell system. Normally the efficiency of an energy conversion is defined as the ratio between the useful energy output and the energy input [208]. Thus, for the applied PEMFC-MHT system, the fuel efficiency could be calculated as follows [201]:

$$\eta_{FCS} = \frac{P_{FCS}}{P_{H_2}} = \eta_{TH} * \eta_{AUX} \tag{5.23}$$

where η_{TH} is the theoretical efficiency that indicates the energy conversion efficiency of the fuel cell stack; η_{AUX} presents the auxiliary efficiency of the system.

In this paper, the air blower and fan are the main auxiliary equipment which affect the fuel efficiency of the system. Therefore, the fuel efficiency in Eq. 5.24 could be rewrite as:

$$\eta_{FCS} = \frac{V_{FC}}{1.25} * \frac{P_{FC} - P_{blower} - P_{fan}}{P_{FC}} \tag{5.24}$$

Figure 5.19 presents the fuel efficiency calculation results of the applied PEMFC-MHT system at different stage of operation. The fuel efficiency reduces due to the fuel cell and MH tank degradation. The introduced PID controller for thermal management is proved to be effective to reduce the power and voltage decline. However, the raised speed of fan leads to the extra auxiliary power consumption. As shown in Figure 5.19, at initial time, the PEMFC-MHT system operated at the optimal efficiency zone, which is about 40.8%. The degradation of fuel cell seriously impacts the efficiency of the system that reduced to 33.8%. The thermal control of the hydrogen supply tank helps to reduce the degradation degree of fuel cell, meanwhile the fuel cell efficiency of the PEMFC-MHT

system is improved to 37% after 1000 hours. The auxiliary power affection on efficiency is relatively low that reducing the efficiency less than 0.5%. Thus, the proposed method on thermal management of the PEMFC-MHT system is effective on fuel efficiency, that 3.2% has been raised.

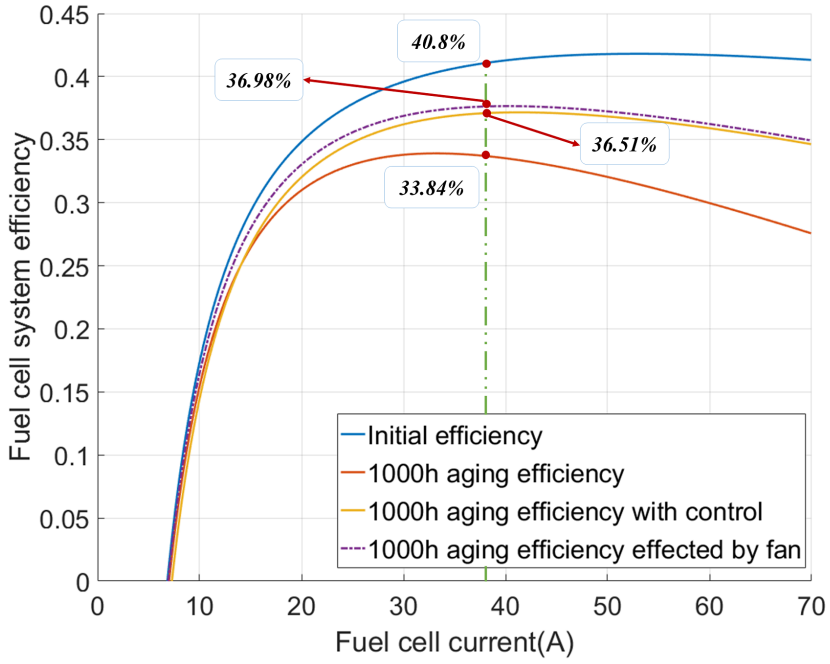

Figure 5.19: Fuel cell system efficiency along with current.

5.4.3.3/ FUEL ECONOMY

Fuel economy is also an important criterion to judge a fuel cell system. According to the 2020' automotive fuel cell system target defined by the US Department of Energy [206], the cost function of a fuel cell system could be calculated as follows:

$$Cost = Cost_{D_{FC}} + Cost_{D_{MH}} + Cost_{H_2} \tag{5.25}$$

In the cost function, the fuel cell degradation speeding $Cost_{D_{FC}}$ is depends on the fuel cell degradation degree D_{FC} and the fuel cell cost $FC_{cost} = 600\$$. Similarly, the degradation of MH hydrogen storage tank D_{MH} expends $MH_{cost} = 380\$$ [209]. The hydrogen cost is calculated by the hydrogen consumption M_{H_2} and the unit price $H_{2cost} = 3.5\$/kg_{H_2}$ [210]. Therefore:

$$Cost = D_{FC} * FC_{cost} + D_{MH} * MH_{cost} + M_{H_2} * H_{2cost} \tag{5.26}$$

For the proposed PEMFC-MHT system, the effects of the thermal management strategy on the ageing degree of PEM fuel cell and MH hydrogen storage tank are opposite. The degradation of PEM fuel cell is decelerated while the MH hydrogen tank undergoes an accelerated ageing. Meanwhile, more hydrogen has been consumed. However, the operation cost of the fuel cell system in 1000h are around 199.08 $ and 178.44 $ sepa-

rately. As a consequence that the thermal management strategy is worth to apply on the PEMFC-MHT system since 10.4% of economy could be saved.

5.5/ CONCLUSION

The objective of this chapter was to develop a thermal management strategy for reducing the degradation of a long-term operating on-board PEMFC-MHT system. The system integrates PEM fuel cell and MH hydrogen storage system through a heat exchange system. A mathematical model describing the dynamic behavior of PEM fuel cell and MH tank is presented, the thermal coupling among the components through fan and circulation water were modeled as well. A database recorded from real operation mission of FCHEVs is applied to validate the model. The simulation results show a great agreement considering the same operation condition assumption. Meanwhile, the strong dependence of the dynamic response of the MH tank to the thermal condition supplied by the PEM fuel cell is presented.

The ageing model presenting the degradation phenomenon for PEM fuel cell and MH tank are replenished to the dynamic model. The voltage of PEM fuel cell reduced along with operating time, and the capacity of MH tank decreased after cycling of charging and discharging. A thermal management strategy is proposed that the fan speed is modified by a PID controller. As a consequence, the output power of the PEMFC-MHT system can be maintained by raising the hydrogen supply rate from the MH tank. 1000 hours of stable operation has been simulated. In this procedure, the voltage degradation of PEM fuel cell is reduced from 7% to 3%, which is helpful to extending the remain useful life. The raised hydrogen consumption speedy the capacity decline of the MH tank, the degradation rate is increased from 11.1% to 11.6% after 1000 hours, which is acceptable. The fuel efficiency and economy are calculated for determining the effect of the proposed thermal control strategy. For the long-term operation of the applied integration PEMFC-MHT system, the fuel efficiency has been raised 3.2% and 10.4% of fuel economy could be saved in 1000 hours.

This chapter also presents a new idea for fuel cell system design. For automobile application, the choice of the load power of PEM fuel cell and the number of the MH hydrogen storage tank could be optimized for the purpose of extending the lifespan of PEM fuel cell, which could maintaining the output power, the fuel efficiency and fuel economy at the same time. Since the degradation mechanism of PEM fuel cell and MH tank are different, the synchronous of ageing degree has a great impact on the performance of the entire FCHEV. This should be taken into consideration in fuel cell system sizing as well.

6

EXPERIMENTAL VALIDATION

6.1/ INTRODUCTION

In order to further experimentally validate the studies of MH hydrogen storage in the previous chapter, extra experiments are required. Thus, a test bench is design and built on the fundamental of the previous experimental platform in our laboratory. In this chapter, the experimental platforms are generally introduced. Then, the detailed configuration of the test bench is presented. Moreover, for the purpose of validate the research in above chapters, different experimental procedures are designed. At last, the experimental results are presented and discussed in detail respectively.

6.2/ EXPERIMENTAL PLATFORM

Figure 6.1: Experimental setup of the test bench.

In the laboratory, a test bench is built to validate models and thermal condition proposed above. As presented in Figure 6.1, two MH hydrogen storage tanks are connected in parallel for testing. The hydrogen flow supplied in the laboratory is 7.8 bar with the maximum

flow rate of 120 NL/min. The discharged hydrogen is released to atmosphere via the air circulation system in the test room. During the test, thermal condition is controlled by fan matrix, heater and circulation water. The fan matrix is used for heat dissipation when the temperature is too high, while the heater is used to warm the circulation water to provide more energy to the reaction. In addition, an extra radiator is used to simulate the heat generated by a fuel cell stack during operation on a vehicle. The heat generation power is adjustable from 500 W to 1800 W.

The tested MH tank are the same with the embedded one on the Mobypost vehicles introduced in Section 2.2.2, which are shown in Figure 6.2. The commercial properties provided by the manufacture are presented in Table 6.1.

Figure 6.2: Applied MH hydrogen storage tank.

Table 6.1: MaHyTec proprieties

Type	RHGV 3181L
Tradename	MHT-HyCube-12 kg
Mass	19 kg
Volume	4 NL
Operating temperature	$-20°C - 85°C$
Maximum pressure	10 bar
Maximum absolute pressure	5 bar
Maximum flow	35 NL/min
Life span	3 $years$

Figure 6.3 presents the measurement system in the test bench. The hydrogen flow charged into the tank and released form it are measured by an EL-FLOW base mass flow meter $F-111AC$ from Bronkhorst High Tech which has a range from 0 to 120 NL/min. An electrical valve with a pressure sensor is installed at the outlet of the tank. When the MH tanks are open and the electrical valve is closed, the pressure measured by sensor is regarded as the pressure inside the tank. This pressure sensor is an industrial pressure transmitter $ATM.1ST$.

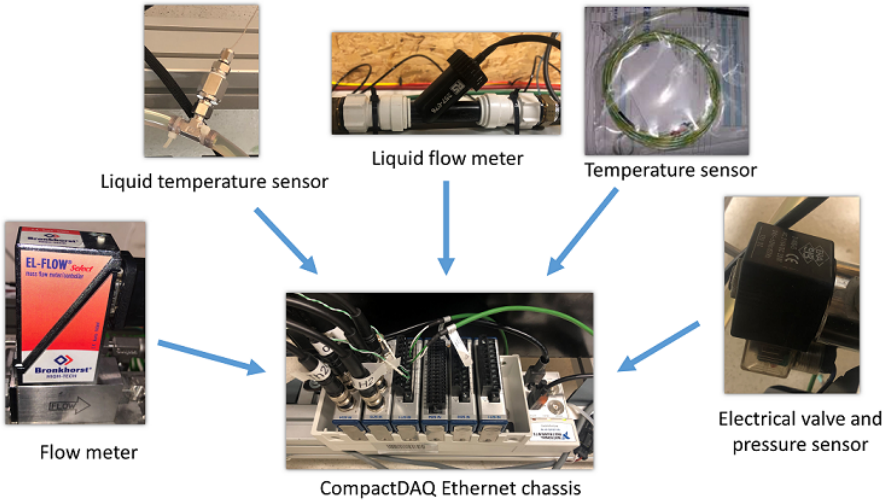

Figure 6.3: Sensors of the measurement system in the test bench.

The gas flow sensor and pressure sensor are installed at the tank outlet. Two temperature sensors are attached at the surface of the MH tanks and the measured results are considered as the reaction bed temperature. The circulation water temperature is measured at both inlet and outlet of the tank with a thermal sensor $K410-1$. A liquid flow detector is applied to test the speed of water flow. The control and data acquisition system is programmed in $LabVIEW$ and the communication between the analogical and digital signals is achieved using the National Instruments (NI) $cDAQ-9178$ device. Software program was achieved under $LabVIEW$ in order to acquire data measurement.

Through this test bench, pressure at the outlet of the tank, temperature at the surface of the bottles and the hydrogen flow rate can be measured and then used to validate the models and management strategies.

6.3/ VALIDATION OF P-C-T BASED MODEL

6.3.1/ EXPERIMENT PROCESS

The experiments for testing the characteristics of the used MH hydrogen storage tank are designed and carried out on the test bench. At the same time, the proposed P-C-T based mathematical model for SOC estimation in Section 2.3 is validated.

The charging process starts from when the tank is empty. The pressure of the supplied hydrogen in the laboratory is constant at 7.8 bar, the hydrogen flow rate filling into the tank is dominated by the pressure difference. In order to avoid high kinetics and limit the temperature variation speed, the valve opening area is controlled manually so that the flow rate is limited under 10 NL/min. Due to the exothermic absorption reaction and pressure raising, the temperature of the tank increases with the hydrogen filling. An upper limit temperature is set as 26$^{\circ}C$. The charging process is stopped when the temperature reaches the threshold. By heat convection, the tank temperature drops to ambient with the help of fan matrix. When the temperature fall to the low limit threshold 22.5$^{\circ}C$, the

valve is opened and the charging process restarts. This process is repeated until the tank is fully charged, namely, the pressure in the tank reaches 7.8 bar and no more hydrogen can be filled into the tank.

Similarly, the discharging process test is controlled by the temperature threshold of 18°C to 24°C. The hydrogen flow rate released from the tank is determined by the pressure difference between the atmospheric pressure and the hydrogen pressure in the tank. The temperature drops during discharging due to the endothermic desorption reaction and the pressure variation. The heater operated to accelerate the temperature recovery. In the end of test, the pressure inside the tank equals to atmospheric value and the hydrogen flow rate is zero. During the experiment, the physical states are measured by these sensors and then recorded for analyse.

6.3.2/ RESULTS AND DISCUSSION

6.3.2.1/ CHARGING CASE

Figure 6.4 to Figure 6.6 show the physical state measured during charging test. As the equilibrium temperature is extracted from Figure 6.4, corresponding data of pressure and capacity can be regarded as part of the P-C-T curves.

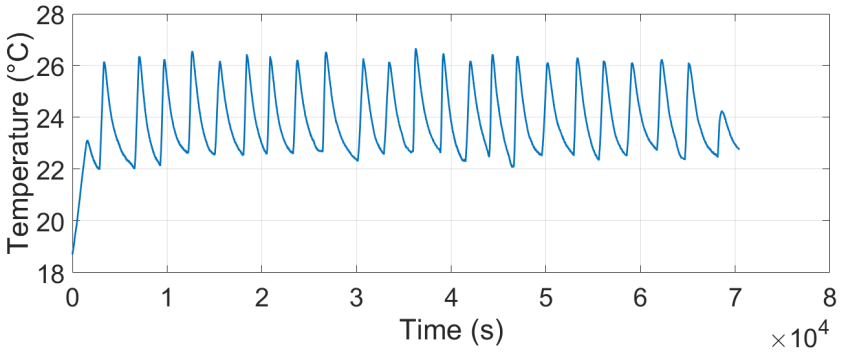

Figure 6.4: Temperature variation during experiment.

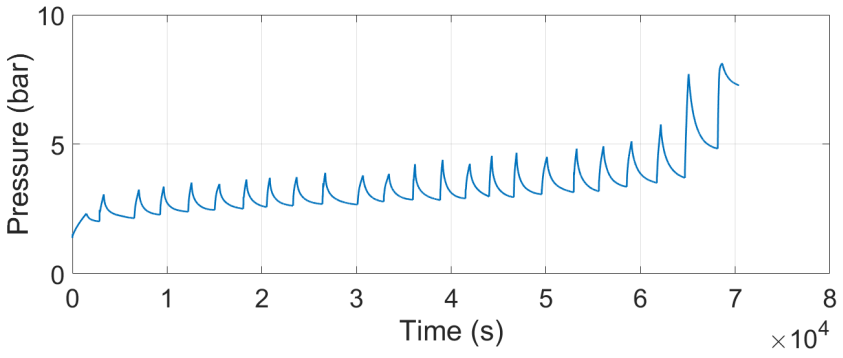

Figure 6.5: Pressure variation during experiment.

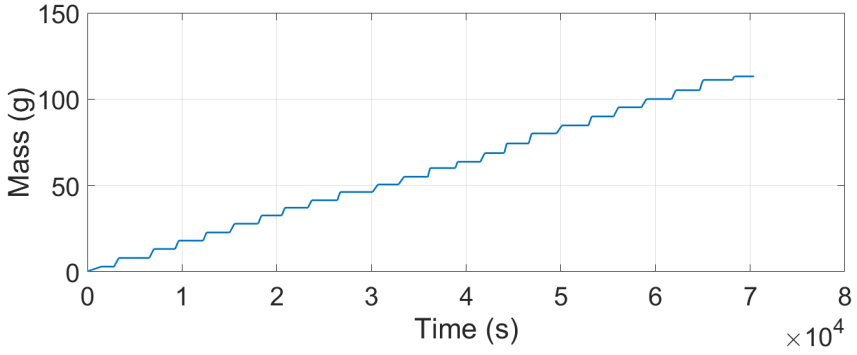

Figure 6.6: Hydrogen mass charged into the tank during experiment.

The P-C-T based SOC estimation model during charging process is proposed in Eq. 3.5 and presented in Figure 3.5. Here, Figure 6.7 gives the comparison between the proposed model and the experiment result on the test bench. The experimental data picked from the pause stage of the charging test process are combined to be the equilibrium state of the tested MH tank during charging, which is shown as the red part on Figure 6.7. Comparing to the proposed model, the average absolute error is 0.24, which means the SOC model of this MH hydrogen storage tank is reliable.

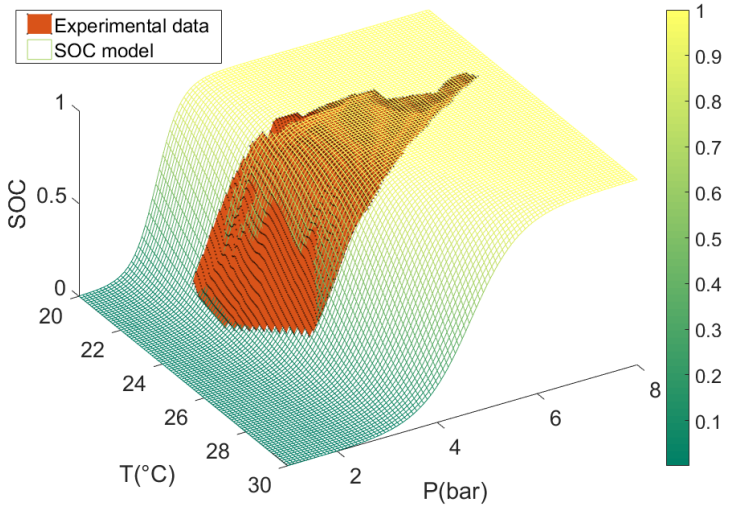

Figure 6.7: P-C-T based SOC model.

In addition, the experimental setup of the database introduced in Section 2.2.2 and the test bench are different. As introduced in Section 2.2.2, the hydrogen mass flow rate is maintained no matter of the pressure inside the tank. Thus, more hydrogen can be filled into the tank, namely, the hydrogen capacity under different experimental setup might differ. However, the SOC and physical state of the charging process maintained in the same performance. The similar results of the P-C-T based SOC model under different experimental setup conditions further demonstrates the reliability of the proposed model.

6.3.2.2/ DISCHARGING CASE

From the database used to identify the P-C-T based SOC estimation model during discharging process only contains three different temperature, which is inadequate for analyses the variation of $K3$ and $K4$ like charging model. Therefore, test on large scale of temperature is performed. Figure 6.8 presents the P-C-T curves extracted from the recorded database on the test bench. As shown by each isotherm curve, the desorption reaction mainly happened during the pressure form 1.5 bar to 3 bar, which is lower than the charging condition under respectively temperature.

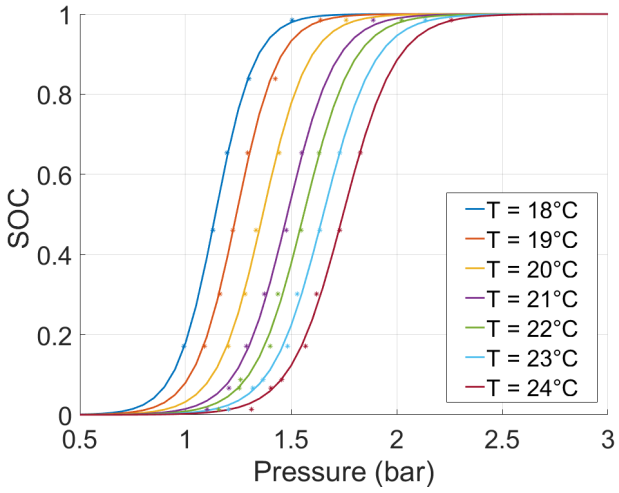

Figure 6.8: P-C-T curves of discharging process.

The identification results of the parameters are presented in Figure 6.9. With the isotherm curves under six different temperatures, the effect of temperature on equilibrium pressure can be fitted. The function of $K3$ and $K4$ are identified as follows:

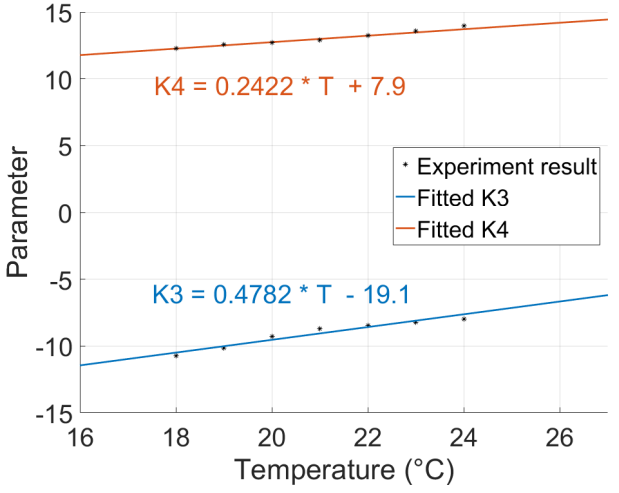

Figure 6.9: P-C-T based SOC model.

Figure 6.10 shows the integral model of the SOC model during discharging process. Similar to charging process model, this model determines the percentage of hydrogen remained in the tank, which is only affected by the physical state.

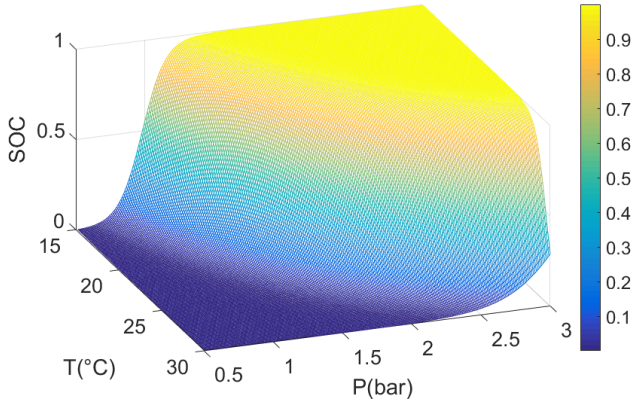

Figure 6.10: P-C-T based SOC model.

As mentioned above, one can see that the SOC of a MH hydrogen storage tank can be directly achieved by its physical performance. However, the hydrogen storage capacity is not only influenced by the ageing condition but also depending on the manually operation method. More hydrogen can be stored through appropriate setting.

6.3.2.3/ ONLINE SOC ESTIMATION DURING DISCHARGING PROCESS

As mentioned in Section 2.4, the online SOC estimation can now be tested with the complete P-C-T based model for discharging process. Thanks to the mathematical model presented in Figure 6.10, the SOC of the tank can be calculated by the data point recognized as second stage.

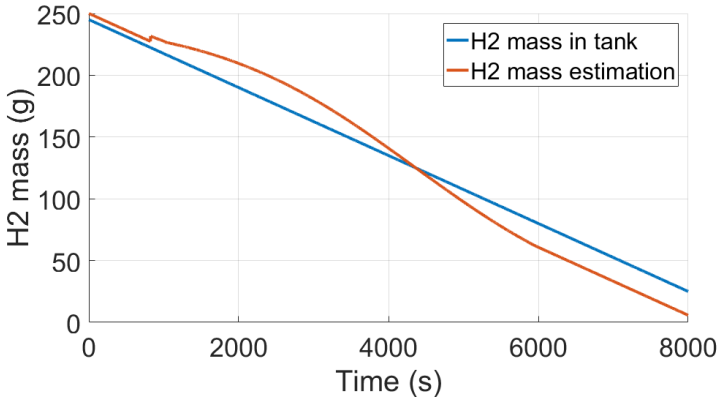

Figure 6.11: Online SOC estimation result during discharging process.

Figure 6.11 presents the online SOC estimation result during discharging process. Compared to the value of hydrogen mass in the tested database, the online SOC estimation

results shows a great agreement with the mean square error of 4.8%, which is acceptable. This SOC result is useful for the further strategic decision of driving and protection of the MH tank.

6.4/ VALIDATION OF THE PARAMETRIC STUDY OF THE DYNAMIC MODEL

6.4.1/ EXPERIMENT PROCESS

Chapter 4 presented the dynamic model of an embedded MH hydrogen storage tank and the parametric study. The parameters of the proposed model of the dynamic performance in discharging process are optimized by PSO method. In order to compare the simulations with experimental results using corresponding test condition, the following experimental setup is implemented.

Before testing, the MH hydrogen storage tanks on the test bench are fully charged, namely, under ambient temperature condition, no more hydrogen can be charged into the tank with the supplied pressure of laboratory. During the discharging process, the valve is completely turned on and the hydrogen flow rate is only dominated by the pressure difference between the test room and inside the tank. The generated hydrogen gas can be released freely. The circulation water is warmed by an extra heater, which is helpful for promoting the hydrogenation reaction. When the measured hydrogen releasing flow rate comes to zero, the test is stopped and the discharging process is regarded as completely finished.

The control and data acquisition system is programmed in $LabVIEW$. Through this experimental setup, temperatures at the surface of tanks, pressure at the outlet, input and output water temperatures and the released hydrogen flow rate are recorded and then used to calibrate the parameters of the computational simulation.

6.4.2/ RESULTS AND DISCUSSION

Figure 6.12 shows the dynamic performance of the hydrogen continuity during test. Since the MH tanks is a partial volume with a porosity, some gaseous hydrogen exists in the tank, which is discharged rapidly when the tank is open. In this test, the valve is completely opened without being controlled so that at beginning a significant decrease of hydrogen flow rate happened, as presented in Figure 6.12(a). As a result of the stable reaction, hydrogen is continuously desorped from the MH and released out of the tank. Until the hydrogen concentration inside the tank drops to a certain value, the hydrogen to metal ratio is too low to generate hydrogen in a high speed. The flow rate decreases to zero, which is considered as the end of discharging process. On the test bench, about 250 g of hydrogen can be discharged form two tested MH hydrogen storage tanks.

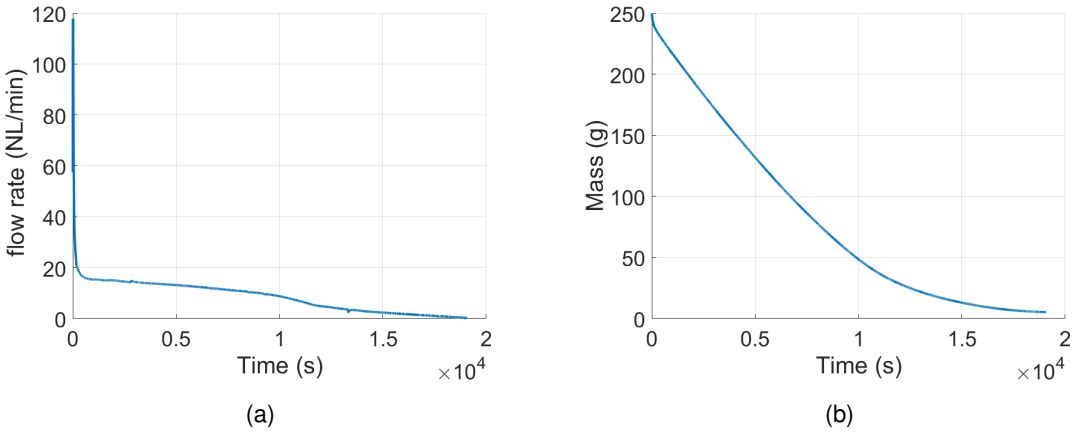

Figure 6.12: Time evolution of the hydrogen discharge characteristics form the MH tank on the test bench (a) Hydrogen releasing flow rate; (b) Hydrogen mass remaining in the tank.

Figure 6.13 and Figure 6.14 present the comparison of the results between experiment and simulation. In Figure 6.13, the experimental pressure is measured at the outlet of the tank while the simulation result is calculated by the inside pressure and equilibrium pressure model. For both of results, a sharp drop of pressure are observed at the beginning due to the rapid release of the gaseous hydrogen. Then the composed hydrogen in MH is desorped, which contributes to the pressure maintaining or increasing. With the discharging procedure, pressure drops with equilibrium pressure, which is leaded by the decreases of hydrogen to metal ratio. At the end, pressure is equal to equilibrium pressure, namely, the tank reaches balance condition and no more hydrogen can be desorped. The deviations are a consequence of the sensor location that pressure distributed inside the tank is not uniform like the assumptions on the simulated model.

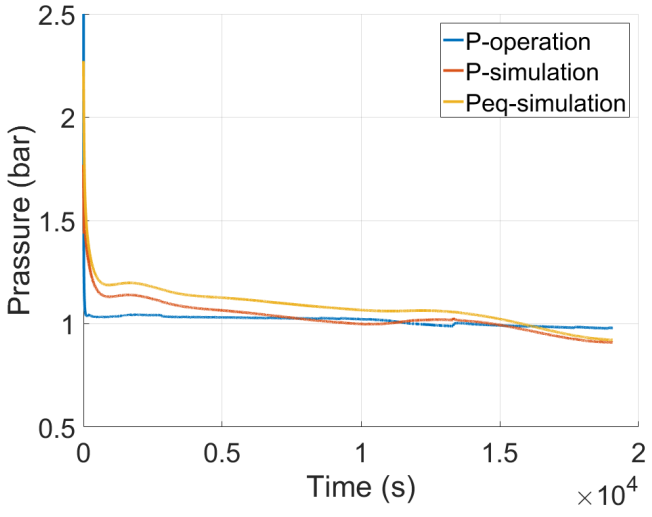

Figure 6.13: Pressure variation during discharging process.

Figure 6.14 depicts the comparison of temperature variation. The temperature of circulation water keeps raising thanks to the heater. The reason why the surface temperature of the tank drops at the beginning is composed of two parts. For one thing, based on the ideal state equation, the rapid pressure drop leads to the temperature decrease. For other, the heat supplied by the circulation water is not enough for the endothermic reaction. Then, they come to a kind of small slope region thanks to the adequate heat transfer rate between circulation water and MH material. Finally, the low reaction speed caused by low hydrogen to MH ratio reduced the heat requirement. Extra heat supplied by the circulation water leads to the raise of tank temperature.

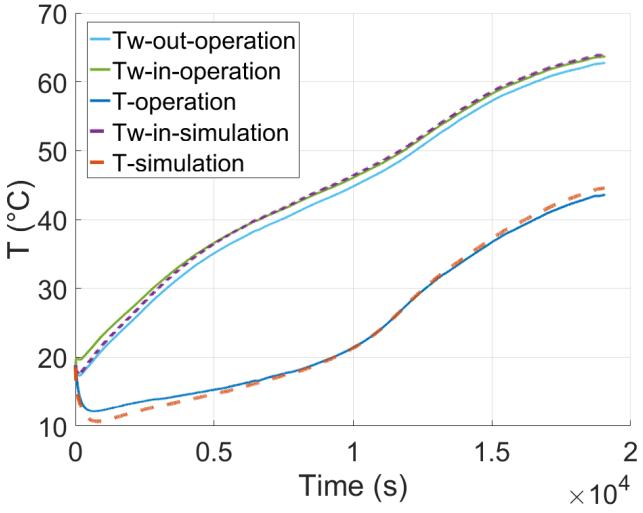

Figure 6.14: Temperature variation during discharging process.

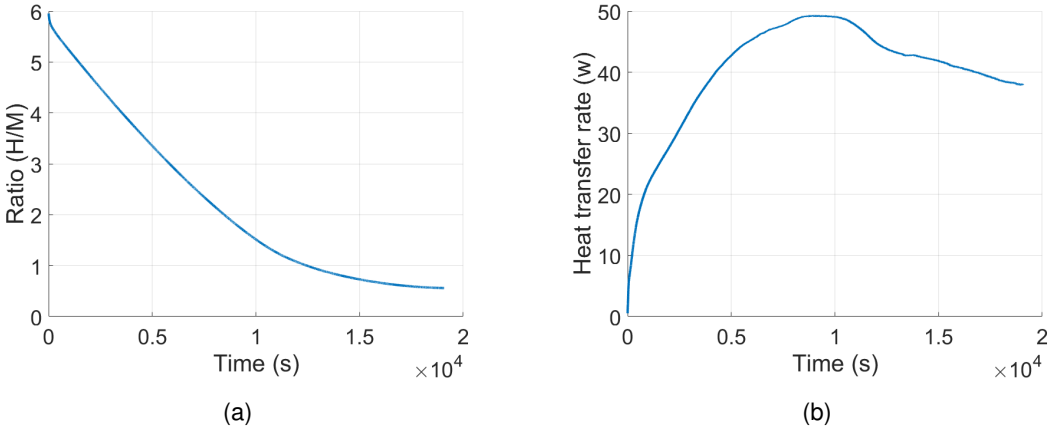

Figure 6.15: Time evolution of the hydrogen discharge characteristics form the MH tank on the test bench (a) Hydrogen to metal atomic ratio; (b) Heat transfer rate.

Figure 6.15 presents the evolution of the characteristics during test. The hydrogen to metal atomic ratio decreases with hydrogen desorption process. However, the gaseous hydrogen stored in the tank before discharging is not taken into consideration. The accu-

rate variation of this character should be analysed using other methods like nano microscope. The transferred heat from circulation water not only promotes the reaction speed but also increases the tank temperature.

6.5/ VALIDATION OF THE THERMAL COUPLING CONDITION

6.5.1/ EXPERIMENT PROCESS

Chapter 5 discussed the thermal coupling condition between the embedded fuel cell and MH hydrogen storage tank during vehicle operation. The heat generated by fuel cell is of significant effect on the dynamic performance of MH hydrogen storage tank. On the test bench, a modifiable radiator is used to simulate the heat supplied by fuel cell. Therefore, the influence of the extra heat on the hydrogen discharge characteristics can be observed.

Similar to the schematic presented in Figure 5.3, the radiator is located at the place of fuel cell. The maximum power can be provided by the radiator is 1800 W. Three group of test is designed that the radiator power is set as 0, 900 W and 1800 W separately. In each test, the discharging process starts from the same condition that the atmosphere temperature is 20$^{\circ}C$ and the tanks are fully charged. During two hours of discharging, the valve is fully opened and the hydrogen releasing flow rate is only influenced by the hydrogen generation rate.

6.5.2/ RESULTS AND DISCUSSION

Figure 6.16 presents the comparison of the experimental results under different power of radiator. As shown in Figure 6.16(a), the hydrogen discharging rate is sensitive to the supplied heat. As discussed before, high flow rate at the beginning is caused by the remaining gaseous hydrogen in MH tank before test. Then, the hydrogenation reaction speed lead the performance. Without extra heat supply, the speed of this endothermic reaction is slow, which results in a low hydrogen releasing flow rate. Meanwhile, no more energy is provided to circulation water and the reaction need to absorb heat from circulation water. Thus, the water temperature decreases follow the variation of tank temperature, as shown in Figure 6.16(b). The heat transfer rate is correspondingly slow, which can be seen in Figure 6.16(c). In level 1, the radiator power is 900W. With this extra heat supply, the hydrogenation speed is raised so that the flow rate is increased. As can be seen in Figure 6.16(b), the circulation water temperature almost unchanged, namely, a heat exchange balance is achieved between endothermic reaction and extra heat supplied by radiator. In level 2, 1800 W of heat is generated by radiator and supplied to the test bench. The hydrogen desorbed and released out rapidly. The circulation water and tank are both heated except for the effect of quick dropped pressure at the beginning. Figure 6.16(d) shows the hydrogen mass variation under these three test conditions. Obviously, extra heat is of great help to promote the hydrogen releasing speed.

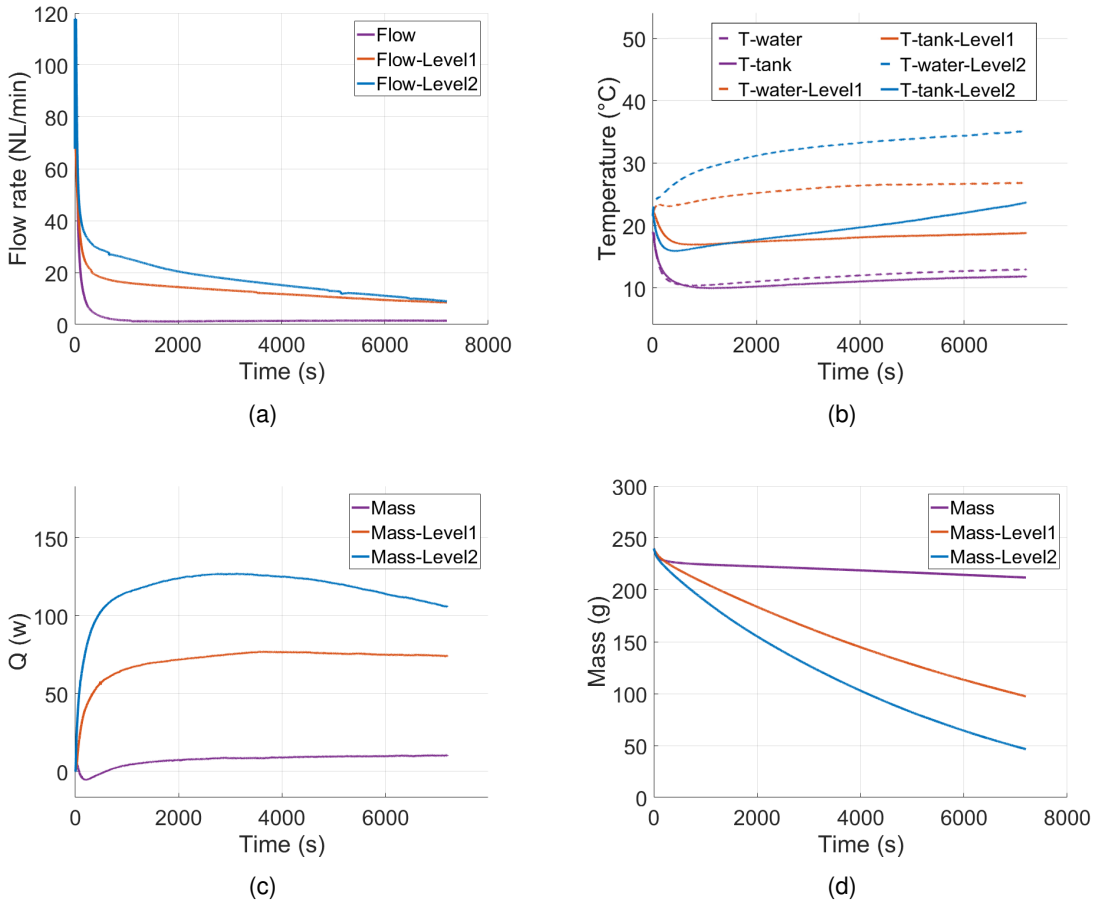

Figure 6.16: The effect of the supplied heat on the hydrogen discharge characteristics: (a) Hydrogen releasing flow rate; (b) Temperature variation; (c) Heat transfer rate; (d) Hydrogen mass remaining in the tank.

6.6/ CONCLUSION

This chapter has presented the test bench used to validate the theoretical research of MH hydrogen storage in previous chapters separately. In the test bench, the hardware system is composed by a MH reaction reactor and a heat exchange system, meanwhile, the software system is programmed by $LabVIEW$ for data acquisition.

On this test bench, three different experiment procedures are tested for validating corresponding models and strategies. The first experiment tested the characteristics of the used MH hydrogen storage tank. The results not only validate the proposed P-C-T based model for charging, but also supplement the discharging model with more experimental data. The online SOC estimation process during discharging the tank is also tested using real operation data based on the complete SOC model. The second experiment tested the dynamic performance during the whole discharging process. The evolution of temperature, pressure, hydrogen to metal ratio and heat transfer rate along with time are carefully recorded and studied, which show great agreement with the proposed model

simulation. In the third test, a radiator is added to simulate the function of fuel cell in thermal affection to hydrogen desorption. The results presented the close thermal coupling situation between fuel cell and MH tanks, which prove the possibility of an effective thermal control strategy for monitoring and optimizing the operation application.

7

GENERAL CONCLUSION

As a promising way to replace the fossil fuel and mitigating environmental problems, the main challenges hydrogen energy facing are production, storage, transportation and application. The works presented in this thesis are the contributions to the on-board hydrogen storage and application using MH tank. Combining the testing results from both laboratory experiments and real operational tests on FCEHVs equipped with MH hydrogen storage tanks, effective methods for online SOC estimation, dynamic modeling process and energy management strategy are proposed for optimizing the embedded hydrogen storage and application way.

Indeed, our research work concentrated on the analysis of the properties and performance of MH hydrogen storage system, the thermal exchange among hydrogen storage tank and fuel cell, the active management strategy of this coupling hydrogen system constituted of PEM fuel cell and MH tank. Firstly, in order to study the properties of MH reaction, statistical models are proposed through analyzing great number of data recorded from MH hydrogen storage tank charging and discharging tests. Combining with the characters of the reaction between hydrogen and MH material, a state classifier is designed through weighting the classify results of Naive Bayes classifier and Support Vector Machine classifier. The online state of charge estimation are therefore realized in both charging and discharging process. Then the performance of an embedded MH hydrogen storage tank are studied for the purpose of designing the dynamic model. Since the parameters of a commercial used MH tank are uncertain, particle swarm optimization algorithm has been used to identify these parameters of the model. In addition, the coupling PEMFC-MHT system is modeled to specify the thermal and heat exchange situation. An active thermal control strategy is proposed to optimize the operation mode of this system considering degradation, hydrogen consumption and power efficiency. Finally, a test bench is designed in laboratory and experiments are carried out to validate the proposed models and strategies.

Otherwise, the present research work opens several prospects for the future in the following aspects:

- In this study, the proposed dynamic models and validated using not only previous real operation FCEVs database, but also new designed test bench. However, the degradation model and thermal management strategy are just simulated through software. In the future, more test can be carried out on the test bench, such as MH hydrogen storage tank cycling test, thermal control test and energy management

test. By performing real experiment, the SOC model can be further supplemented and the control strategies can be validated in practical applications.

- For automobile application, the choice of the load power of PEM fuel cell and the number of the MH tank could be optimized for the purpose of extending the lifespan of PEM fuel cell, which could of great help in maintaining the output power, the fuel efficiency and fuel economy at the same time. Since the degradation mechanism of PEM fuel cell and MH tank are different, the synchronous of ageing degree has a great impact on the performance of the FCEHVs. This should be taken into consideration in fuel cell system sizing as well.
- Since the integration of MH tank and PEM fuel cell mainly relates to their thermal coupling, the effective thermal management strategy is of great importance to improve the efficiency. Except for optimizing the current heat exchange system like fan matrix and circulation water used in this thesis, other methods are worth to considering and designing.

BIBLIOGRAPHY

[1] DIEFENDERFER, J., ARORA, V., AND SINGER, L. **International energy outlook 2016 liquid fuels**. *Doe/Eia-0484* (2016), 202–586.

[2] BARTHELEMY, H., WEBER, M., AND BARBIER, F. **Hydrogen storage: Recent improvements and industrial perspectives**. *International Journal of Hydrogen Energy 42*, 11 (2017), 7254–7262.

[3] MAZZUCCO, A., DORNHEIM, M., SLOTH, M., JENSEN, T. R., JENSEN, J. O., AND ROKNI, M. **Bed geometries, fueling strategies and optimization of heat exchanger designs in metal hydride storage systems for automotive applications: A review**. *International Journal of Hydrogen Energy 39*, 30 (2014), 17054–17074.

[4] SATYAPAL, S. **U.s. department of energy hydrogen and fuel cells program 2016**.

[5] EDENHOFER, O. **Climate change 2014: mitigation of climate change**, vol. 3. Cambridge University Press, 2015.

[6] THE EUROPEAN COMMISSION, L. ., AND OTHERS. **Intended nationally determined contribution of the eu and its member states**.

[7] POUYANNÉ, P. **Integrating climate into our strategy**.

[8] SHIGENOBU WATANABE, N. **Hydrogne infrastruction in japan**.

[9] AHMADI, P., TORABI, S. H., AFSANEH, H., SADEGHEIH, Y., GANJEHSARABI, H., AND ASHJAEE, M. **The effects of driving patterns and pem fuel cell degradation on the lifecycle assessment of hydrogen fuel cell vehicles**. *International Journal of Hydrogen Energy* (2019).

[10] THOMAS, C. **Fuel cell and battery electric vehicles compared**. *international journal of hydrogen energy 34*, 15 (2009), 6005–6020.

[11] DAS, H. S., TAN, C. W., AND YATIM, A. **Fuel cell hybrid electric vehicles: A review on power conditioning units and topologies**. *Renewable and Sustainable Energy Reviews 76* (2017), 268–291.

[12] OF ENERGY, U. D. **The green hydrogen report**.

[13] VIVAS, F., DE LAS HERAS, A., SEGURA, F., AND ANDÚJAR, J. **A review of energy management strategies for renewable hybrid energy systems with hydrogen backup**. *Renewable and Sustainable Energy Reviews 82* (2018), 126–155.

[14] AHMADI, S., BATHAEE, S., AND HOSSEINPOUR, A. H. **Improving fuel economy and performance of a fuel-cell hybrid electric vehicle (fuel-cell, battery, and ultra-capacitor) using optimized energy management strategy**. *Energy conversion and management 160* (2018), 74–84.

[15] STAFFELL, I., SCAMMAN, D., ABAD, A. V., BALCOMBE, P., DODDS, P. E., EKINS, P., SHAH, N., AND WARD, K. R. **The role of hydrogen and fuel cells in the global energy system**. *Energy & Environmental Science 12*, 2 (2019), 463–491.

[16] (IEA), I. E. A. **International energy agency on fcv vehicles share in the market**.

[17] HU, X., JIANG, J., EGARDT, B., AND CAO, D. **Advanced power-source integration in hybrid electric vehicles: Multicriteria optimization approach**. *IEEE Transactions on Industrial Electronics 62*, 12 (2015), 7847–7858.

[18] LOTOTSKYY, M. V., TOLJ, I., PICKERING, L., SITA, C., BARBIR, F., AND YARTYS, V. **The use of metal hydrides in fuel cell applications**. *Progress in Natural Science: Materials International 27*, 1 (2017), 3–20.

[19] GODULA-JOPEK, A. **Hydrogen storage options including constraints and challenges**. *Hydrogen Production* (2015).

[20] KLEBANOFF, L. **Hydrogen storage technology: materials and applications**. CRC Press, 2012.

[21] SHABANI, B., AND ANDREWS, J. **An experimental investigation of a pem fuel cell to supply both heat and power in a solar-hydrogen raps system**. *International journal of hydrogen energy 36*, 9 (2011), 5442–5452.

[22] SOSSAN, F., BINDNER, H., MADSEN, H., TORREGROSSA, D., CHAMORRO, L. R., AND PAOLONE, M. **A model predictive control strategy for the space heating of a smart building including cogeneration of a fuel cell-electrolyzer system**. *International Journal of Electrical Power & Energy Systems 62* (2014), 879–889.

[23] NGUYEN, H. Q., ARIS, A. M., AND SHABANI, B. **Pem fuel cell heat recovery for preheating inlet air in standalone solar-hydrogen systems for telecommunication applications: An exergy analysis**. *International journal of hydrogen energy 41*, 4 (2016), 2987–3003.

[24] FAGHRI, A., AND GUO, Z. **Integration of heat pipe into fuel cell technology**. *Heat Transfer Engineering 29*, 3 (2008), 232–238.

[25] SILVA, A. P., GALANTE, R. M., PELIZZA, P. R., AND BAZZO, E. **A combined capillary cooling system for fuel cells**. *Applied Thermal Engineering 41* (2012), 104–110.

[26] SHABANI, B., ANDREWS, J., AND WATKINS, S. **Energy and cost analysis of a solar-hydrogen combined heat and power system for remote power supply using a computer simulation**. *Solar Energy 84*, 1 (2010), 144–155.

[27] SHABANI, B., ANDREWS, J., AND BADWAL, S. **Fuel cell heat recovery, electrical load management, and the economics of solar-hydrogen systems**. *International Journal of Power & Energy Systems 30*, 4 (2010), 256.

[28] ANSAREY, M., PANAHI, M. S., ZIARATI, H., AND MAHJOOB, M. **Optimal energy management in a dual-storage fuel-cell hybrid vehicle using multi-dimensional dynamic programming**. *Journal of Power Sources 250* (2014), 359–371.

[29] WANG, Y., MOURA, S. J., ADVANI, S. G., AND PRASAD, A. K. **Power management system for a fuel cell/battery hybrid vehicle incorporating fuel cell and battery degradation**. *International Journal of Hydrogen Energy 44*, 16 (2019), 8479–8492.

[30] LUNA, J., JEMEI, S., YOUSFI-STEINER, N., HUSAR, A., SERRA, M., AND HISSEL, D. **Nonlinear predictive control for durability enhancement and efficiency improvement in a fuel cell power system**. *Journal of Power Sources 328* (2016), 250–261.

[31] HUANG, Y., WANG, H., KHAJEPOUR, A., HE, H., AND JI, J. **Model predictive control power management strategies for hevs: A review**. *Journal of Power Sources 341* (2017), 91–106.

[32] HU, X., MOURA, S. J., MURGOVSKI, N., EGARDT, B., AND CAO, D. **Integrated optimization of battery sizing, charging, and power management in plug-in hybrid electric vehicles**. *IEEE Transactions on Control Systems Technology 24*, 3 (2015), 1036–1043.

[33] CHAN, C. C. **The state of the art of electric, hybrid, and fuel cell vehicles**. *Proceedings of the IEEE 95*, 4 (2007), 704–718.

[34] CELL TODAY, F. **Fuel cell electric vehicles: The road ahead**.

[35] TOYOTA. **https://www.toyota.co.uk/world-of-toyota/environment/fuel-cell-vehicle**.

[36] CAPROS, P., DE VITA, A., TASIOS, N., SISKOS, P., KANNAVOU, M., PETROPOULOS, A., EVANGELOPOULOU, S., ZAMPARA, M., PAPADOPOULOS, D., NAKOS, C., AND OTHERS. **Eu reference scenario 2016-energy, transport and ghg emissions trends to 2050.**

[37] ARVIND NOEL XAVIER LEO, A. H. K. **Fuel cell electric vehicles: The genesis of a new era or myth-busting vehicle technology?** *Open Access Government* (2018).

[38] DELUCCHI, M., YANG, C., BURKE, A., OGDEN, J., KURANI, K., KESSLER, J., AND SPERLING, D. **An assessment of electric vehicles: technology, infrastructure requirements, greenhouse-gas emissions, petroleum use, material use, lifetime cost, consumer acceptance and policy initiatives**. *Philosophical Transactions of the Royal Society A: Mathematical, Physical and Engineering Sciences 372*, 2006 (2014), 20120325.

[39] BURKE, A., ZHAO, H., AND MILLER, M. **Comparing fuel economies and costs of advanced vs. conventional vehicles**. *Sustainable transportation energy pathways: a research summary for decisionmakers* (2011), 97–120.

[40] GIELEN, D., GORINI, R., WAGNER, N., LEME, R., GUTIERREZ, L., AND PRAKASH, G. **Global energy transformation: A roadmap to 2050**. *International Renewable Energy Agency: Abu Dhabi, Vereinigte Arabische Emirate* (2018), 76.

[41] BUBNA, P., BRUNNER, D., GANGLOFF JR, J. J., ADVANI, S. G., AND PRASAD, A. K. **Analysis, operation and maintenance of a fuel cell/battery series-hybrid bus for urban transit applications**. *Journal of Power Sources 195*, 12 (2010), 3939–3949.

[42] ZHAO, H., AND BURKE, A. **Effects of different powertrain configurations and control strategies on fuel economy of fuel cell vehicles**. In *The 25th World Battery, Hybrid and Fuel Cell Electric Vehicle Symposium and Exhibition* (2010).

[43] ANDREASEN, S. J., ASHWORTH, L., SAHLIN, S., JENSEN, H.-C. B., AND KÆR, S. K. **Test of hybrid power system for electrical vehicles using a lithium-ion battery pack and a reformed methanol fuel cell range extender**. *International journal of hydrogen energy 39*, 4 (2014), 1856–1863.

[44] KELOUWANI, S., AGBOSSOU, K., AND DUBÉ, Y. **Impacts of blended mode and charge-sustaining mode on the battery efficiency for a serial fc-phev**. In *2013 IEEE International Symposium on Industrial Electronics* (2013), IEEE, pp. 1–5.

[45] HOOGERS, G. **Fuel cell technology handbook**. CRC press, 2002.

[46] PEIGHAMBARDOUST, S. J., ROWSHANZAMIR, S., AND AMJADI, M. **Review of the proton exchange membranes for fuel cell applications**. *International journal of hydrogen energy 35*, 17 (2010), 9349–9384.

[47] MERLE, G., WESSLING, M., AND NIJMEIJER, K. **Anion exchange membranes for alkaline fuel cells: A review**. *Journal of Membrane Science 377*, 1-2 (2011), 1–35.

[48] BLOMEN, L. J., AND MUGERWA, M. N. **Fuel cell systems**. Springer Science & Business Media, 2013.

[49] WANG, M., CHEN, M., YANG, Z., WANG, Y., WANG, Y., LIU, G., LEE, J. K., AND WANG, X. **A study on fuel additive of methanol for room temperature direct methanol fuel cells**. *Energy Conversion and Management 168* (2018), 270–275.

[50] GALVEZ, J. M., AND ORDONEZ, M. **Swinging bus operation of inverters for fuel cell applications with small dc-link capacitance**. *IEEE Transactions on Power Electronics 30*, 2 (2014), 1064–1075.

[51] MCLEAN, G., NIET, T., PRINCE-RICHARD, S., AND DJILALI, N. **An assessment of alkaline fuel cell technology**. *International Journal of Hydrogen Energy 27*, 5 (2002), 507–526.

[52] KIRUBAKARAN, A., JAIN, S., AND NEMA, R. **A review on fuel cell technologies and power electronic interface**. *Renewable and Sustainable Energy Reviews 13*, 9 (2009), 2430–2440.

[53] QINGFENG, L., HJULER, H. A., AND BJERRUM, N. **Phosphoric acid doped polybenzimidazole membranes: physiochemical characterization and fuel cell applications**. *Journal of Applied Electrochemistry 31*, 7 (2001), 773–779.

[54] DICKS, A. L. **Molten carbonate fuel cells**. *Current Opinion in Solid State and Materials Science 8*, 5 (2004), 379–383.

[55] SINGHAL, S. C., AND KENDALL, K. **High-temperature solid oxide fuel cells: fundamentals, design and applications**. Elsevier, 2003.

[56] LIU, H., SONG, C., ZHANG, L., ZHANG, J., WANG, H., AND WILKINSON, D. P. **A review of anode catalysis in the direct methanol fuel cell**. *Journal of Power Sources 155*, 2 (2006), 95–110.

[57] BARBIR, F. **PEM fuel cells: theory and practice**. Academic Press, 2012.

[58] ZHOU, D., GAO, F., BREAZ, E., RAVEY, A., MIRAOUI, A., AND ZHANG, K. **Dynamic phenomena coupling analysis and modeling of proton exchange membrane fuel cells**. *IEEE Transactions on Energy Conversion 31*, 4 (2016), 1399–1412.

[59] DAS, V., PADMANABAN, S., VENKITUSAMY, K., SELVAMUTHUKUMARAN, R., BLAABJERG, F., AND SIANO, P. **Recent advances and challenges of fuel cell based power system architectures and control–a review**. *Renewable and Sustainable Energy Reviews 73* (2017), 10–18.

[60] ZHAO, J., JIAN, Q., LUO, L., HUANG, B., CAO, S., AND HUANG, Z. **Dynamic behavior study on voltage and temperature of proton exchange membrane fuel cells**. *Applied Thermal Engineering 145* (2018), 343–351.

[61] CHEN, F., SU, Y.-G., SOONG, C.-Y., YAN, W.-M., AND CHU, H.-S. **Transient behavior of water transport in the membrane of a pem fuel cell**. *Journal of Electroanalytical Chemistry 566*, 1 (2004), 85–93.

[62] KIM, H.-I., CHO, C. Y., NAM, J. H., SHIN, D., AND CHUNG, T.-Y. **A simple dynamic model for polymer electrolyte membrane fuel cell (pemfc) power modules: Parameter estimation and model prediction**. *International journal of hydrogen energy 35*, 8 (2010), 3656–3663.

[63] WU, H., BERG, P., AND LI, X. **Non-isothermal transient modeling of water transport in pem fuel cells**. *Journal of Power Sources 165*, 1 (2007), 232–243.

[64] RAGA, C., BARRADO, A., LAZARO, A., FERNANDEZ, C., VALDIVIA, V., AND QUESADA, I. **Black-box model and identification methodology for pem fuel cell with overshooted transient response**. In *2012 IEEE Energy Conversion Congress and Exposition (ECCE)* (2012), IEEE, pp. 3168–3174.

[65] HOU, Y., SHEN, C., HAO, D., LIU, Y., AND WANG, H. **A dynamic model for hydrogen consumption of fuel cell stacks considering the effects of hydrogen purge operation**. *Renewable energy 62* (2014), 672–678.

[66] SOLTANI, M., AND BATHAEE, S. M. T. **Development of an empirical dynamic model for a nexa pem fuel cell power module**. *Energy Conversion and Management 51*, 12 (2010), 2492–2500.

[67] MOCOTEGUY, P., DRUART, F., BULTEL, Y., BESSE, S., AND RAKOTONDRAINIBE, A. **Monodimensional modeling and experimental study of the dynamic behavior of proton exchange membrane fuel cell stack operating in dead-end mode**. *Journal of Power Sources 167*, 2 (2007), 349–357.

[68] TANG, Y., YUAN, W., PAN, M., LI, Z., CHEN, G., AND LI, Y. **Experimental investigation of dynamic performance and transient responses of a kw-class pem fuel cell stack under various load changes**. *Applied Energy 87*, 4 (2010), 1410–1417.

[69] JIA, F., GUO, L., AND LIU, H. **A study on current overshoot during start-ups and optimal start-up strategy of proton exchange membrane fuel cells**. *International Journal of Hydrogen Energy 40*, 24 (2015), 7754–7761.

[70] JANG, J.-H., YAN, W.-M., CHIU, H.-C., AND LUI, J.-Y. **Dynamic cell performance of kw-grade proton exchange membrane fuel cell stack with dead-ended anode**. *Applied energy 142* (2015), 108–114.

[71] LARMINIE, J., DICKS, A., AND MCDONALD, M. S. **Fuel cell systems explained**, vol. 2. J. Wiley Chichester, UK, 2003.

[72] BUSQUET, S., HUBERT, C.-E., LABBE, J., MAYER, D., AND METKEMEIJER, R. **A new approach to empirical electrical modelling of a fuel cell, an electrolyser or a regenerative fuel cell**. *Journal of Power Sources 134*, 1 (2004), 41–48.

[73] PRIYA, K., SATHISHKUMAR, K., AND RAJASEKAR, N. **A comprehensive review on parameter estimation techniques for proton exchange membrane fuel cell modelling**. *Renewable and Sustainable Energy Reviews 93* (2018), 121–144.

[74] MANN, R. F., AMPHLETT, J. C., HOOPER, M. A., JENSEN, H. M., PEPPLEY, B. A., AND ROBERGE, P. R. **Development and application of a generalised steady-state electrochemical model for a pem fuel cell**. *Journal of power sources 86*, 1-2 (2000), 173–180.

[75] YAN, Q., TOGHIANI, H., AND CAUSEY, H. **Steady state and dynamic performance of proton exchange membrane fuel cells (pemfcs) under various operating conditions and load changes**. *Journal of Power Sources 161*, 1 (2006), 492–502.

[76] RIASCOS, L. A. M., AND PEREIRA, D. D. **Controlling operating temperature in pem fuel cells**. In *ABCM Symposium Series in Mechatronics* (2010), vol. 4, pp. 137–146.

[77] WU, J., YUAN, X. Z., MARTIN, J. J., WANG, H., ZHANG, J., SHEN, J., WU, S., AND MERIDA, W. **A review of pem fuel cell durability: Degradation mechanisms and mitigation strategies**. *Journal of Power Sources 184*, 1 (2008), 104–119.

[78] GITTLEMAN, C. S., COMS, F. D., AND LAI, Y.-H. **Membrane durability: physical and chemical degradation**. *Polymer electrolyte fuel cell degradation* (2012), 15–88.

[79] JOUIN, M., GOURIVEAU, R., HISSEL, D., PÉRA, M.-C., AND ZERHOUNI, N. **Degradations analysis and aging modeling for health assessment and prognostics of pemfc**. *Reliability Engineering & System Safety 148* (2016), 78–95.

[80] BRESSEL, M., HILAIRET, M., HISSEL, D., AND BOUAMAMA, B. O. **Extended kalman filter for prognostic of proton exchange membrane fuel cell**. *Applied Energy 164* (2016), 220–227.

[81] LIU, D., AND CASE, S. **Durability study of proton exchange membrane fuel cells under dynamic testing conditions with cyclic current profile**. *Journal of Power Sources 162*, 1 (2006), 521–531.

[82] YAN, X., HOU, M., SUN, L., CHENG, H., HONG, Y., LIANG, D., SHEN, Q., MING, P., AND YI, B. **The study on transient characteristic of proton exchange membrane fuel cell stack during dynamic loading**. *Journal of Power Sources 163*, 2 (2007), 966–970.

[83] LIN, R., LI, B., HOU, Y., AND MA, J. **Investigation of dynamic driving cycle effect on performance degradation and micro-structure change of pem fuel cell**. *International Journal of Hydrogen Energy 34*, 5 (2009), 2369–2376.

[84] DE BERNARDINIS, A., AND COQUERY, G. **First approach for a fault tolerant power converter interface for multi-stack pem fuel cell generator in transportation systems**. In *2008 13th International Power Electronics and Motion Control Conference* (2008), IEEE, pp. 2192–2199.

[85] CANDUSSO, D., DE BERNARDINIS, A., PÉRA, M.-C., HAREL, F., FRANÇOIS, X., HISSEL, D., COQUERY, G., AND KAUFFMANN, J.-M. **Fuel cell operation under degraded working modes and study of diode by-pass circuit dedicated to multi-stack association**. *Energy Conversion and Management 49*, 4 (2008), 880–895.

[86] SOMAIAH, B., AND AGARWAL, V. **Distributed maximum power extraction from fuel cell stack arrays using dedicated power converters in series and parallel configuration**. *IEEE Transactions on Energy Conversion 31*, 4 (2016), 1442–1451.

[87] STEELE, B. C., AND HEINZEL, A. **Materials for fuel-cell technologies**. In *Materials For Sustainable Energy: A Collection of Peer-Reviewed Research and Review Articles from Nature Publishing Group*. World Scientific, 2011, pp. 224–231.

[88] LI, Q., CHEN, W., LIU, Z., HUANG, J., AND MA, L. **Net power control based on linear matrix inequality for proton exchange membrane fuel cell system**. *IEEE Transactions on Energy Conversion 29*, 1 (2013), 1–8.

[89] ZHANG, T., WANG, P., CHEN, H., AND PEI, P. **A review of automotive proton exchange membrane fuel cell degradation under start-stop operating condition**. *Applied energy 223* (2018), 249–262.

[90] STETSON, N. **An overview of u.s. doe's activities for hydrogen fuel cell technologies**. *U.S.Department of Energy* (2017).

[91] LIDE, D. R. **CRC handbook of chemistry and physics**, vol. 85. CRC press, 2004.

[92] WHITE, C., STEEPER, R., AND LUTZ, A. **The hydrogen-fueled internal combustion engine: a technical review**. *International journal of hydrogen energy 31*, 10 (2006), 1292–1305.

[93] ENERGY.GOV. **Doe technical targets for onboard hydrogen storage for light-duty vehicles**.

[94] NIAZ, S., MANZOOR, T., AND PANDITH, A. H. **Hydrogen storage: Materials, methods and perspectives**. *Renewable and Sustainable Energy Reviews 50* (2015), 457–469.

[95] ABDALLA, A. M., HOSSAIN, S., NISFINDY, O. B., AZAD, A. T., DAWOOD, M., AND AZAD, A. K. **Hydrogen production, storage, transportation and key challenges with applications: a review**. *Energy conversion and management 165* (2018), 602–627.

[96] BOGDANOVIĆ, B., AND SANDROCK, G. **Catalyzed complex metal hydrides**. *MRS bulletin 27*, 9 (2002), 712–716.

[97] SANDÍ, G. **Hydrogen storage and its limitations**. *Interface 13*, 3 (2004), 40–44.

[98] MIDILLI, A., AY, M., DINCER, I., AND ROSEN, M. **On hydrogen and hydrogen energy strategies: I: current status and needs**. *Renewable and sustainable energy reviews 9*, 3 (2005), 255–271.

[99] CRABTREE, G. W., DRESSELHAUS, M. S., AND BUCHANAN, M. V. **The hydrogen economy**. *Physics today 57*, 12 (2004), 39–44.

[100] PETITPAS, G., AND ACEVES, S. **Modeling of sudden hydrogen expansion from cryogenic pressure vessel failure**. *International Journal of Hydrogen Energy 38*, 19 (2013), 8190–8198.

[101] KAWASAKI. **Kawasaki hydrogen road**.

[102] CHAMOUN, R., DEMIRCI, U. B., AND MIELE, P. **Cyclic dehydrogenation–(re) hydrogenation with hydrogen-storage materials: An overview**. *Energy Technology 3*, 2 (2015), 100–117.

[103] PRABHUKHOT PRACHI, R., WAGH MAHESH, M., AND OTHERS. **A review on solid state hydrogen storage material**. *Advances in Energy and Power 4*, 2 (2016), 11–22.

[104] ZHANG, Y.-H., JIA, Z.-C., YUAN, Z.-M., YANG, T., QI, Y., AND ZHAO, D.-L. **Development and application of hydrogen storage**. *Journal of Iron and Steel Research International 22*, 9 (2015), 757–770.

[105] JIA, Y., SUN, C., SHEN, S., ZOU, J., MAO, S. S., AND YAO, X. **Combination of nanosizing and interfacial effect: future perspective for designing mg-based nanomaterials for hydrogen storage**. *Renewable and Sustainable Energy Reviews 44* (2015), 289–303.

[106] ZÜTTEL, A. **Hydrogen storage methods**. *Naturwissenschaften 91*, 4 (2004), 157–172.

[107] ABE, J., AJENIFUJA, E., AND POPOOLA, O. **Hydrogen energy, economy and storage: Review and recommendation**. *International Journal of Hydrogen Energy* (2019).

[108] RUSMAN, N., AND DAHARI, M. **A review on the current progress of metal hydrides material for solid-state hydrogen storage applications**. *International Journal of Hydrogen Energy 41*, 28 (2016), 12108–12126.

[109] SCHLAPBACH, L., AND ZÜTTEL, A. **Hydrogen-storage materials for mobile applications**. In *Materials for sustainable energy: a collection of peer-reviewed research and review articles from nature publishing group*. World Scientific, 2011, pp. 265–270.

[110] **http://hydrogenmaterialssearch.govtools.us/**.

[111] HOFFMAN, K., REILLY, J., SALZANO, F., WAIDE, C., WISWALL, R., AND WINSCHE, W. **Metal hydride storage for mobile and stationary applications**. Tech. rep., SAE Technical Paper, 1976.

[112] RUEDA, M., SANZ-MORAL, L. M., AND MARTÍN, Á. **Innovative methods to enhance the properties of solid hydrogen storage materials based on hydrides through nanoconfinement: A review**. *The Journal of Supercritical Fluids* (2018).

[113] VAJO, J. J., AND OLSON, G. L. **Hydrogen storage in destabilized chemical systems**. *Scripta Materialia 56*, 10 (2007), 829–834.

[114] LIU, J., HAN, Y., AND GE, Q. **Effect of doped transition metal on reversible hydrogen release/uptake from naalh4**. *Chemistry–A European Journal 15*, 7 (2009), 1685–1695.

[115] WANG, Y., AND WANG, Y. **Recent advances in additive-enhanced magnesium hydride for hydrogen storage**. *Progress in Natural Science: Materials International 27*, 1 (2017), 41–49.

[116] FANG, Z.-Z., KANG, X.-D., LUO, J.-H., WANG, P., LI, H.-W., AND ORIMO, S.-I. **Formation and hydrogen storage properties of dual-cation (li, ca) borohydride**. *The Journal of Physical Chemistry C 114*, 51 (2010), 22736–22741.

[117] MIWA, K., OHBA, N., TOWATA, S.-I., NAKAMORI, Y., AND ORIMO, S.-I. **First-principles study on copper-substituted lithium borohydride,(li1- xcux) bh4**. *Journal of alloys and compounds 404* (2005), 140–143.

[118] NAKANO, A., MAEDA, T., ITO, H., MOTYKA, T., PEREZ-BERRIOS, J. M., AND GREENWAY, S. **Experimental study on a metal hydride tank for the totalized hydrogen energy utilization system**. *Energy Procedia 29* (2012), 463–468.

[119] MINKO, K., ARTEMOV, V., AND YAN'KOV, G. **Numerical simulation of sorption/desorption processes in metal-hydride systems for hydrogen storage and purification. part i: development of a mathematical model**. *International Journal of Heat and Mass Transfer 68* (2014), 683–692.

[120] BOUKHARI, A., AND BESSAIH, R. **Numerical heat and mass transfer investigation of hydrogen absorption in an annulus-disc reactor**. *International Journal of Hydrogen Energy 40*, 39 (2015), 13708–13717.

[121] MAEDA, T., NISHIDA, K., TANGE, M., TAKAHASHI, T., NAKANO, A., ITO, H., HASEGAWA, Y., MASUDA, M., AND KAWAKAMI, Y. **Numerical simulation of the hydrogen storage with reaction heat recovery using metal hydride in the totalized hydrogen energy utilization system**. *international journal of hydrogen energy 36*, 17 (2011), 10845–10854.

[122] MOMEN, G., HERMOSILLA, G., MICHAU, A., PONS, M., FIRDAOUS, M., MARTY, P., AND HASSOUNI, K. **Experimental and numerical investigation of the thermal effects during hydrogen charging in packed bed storage tank**. *International Journal of Heat and Mass Transfer 52*, 5-6 (2009), 1495–1503.

[123] NAM, J., KO, J., AND JU, H. **Three-dimensional modeling and simulation of hydrogen absorption in metal hydride hydrogen storage vessels**. *Applied energy 89*, 1 (2012), 164–175.

[124] MUTHUKUMAR, P., SINGHAL, A., AND BANSAL, G. **Thermal modeling and performance analysis of industrial-scale metal hydride based hydrogen storage container**. *International journal of hydrogen energy 37*, 19 (2012), 14351–14364.

[125] JEMNI, A., AND NASRALLAH, S. B. **Study of two-dimensional heat and mass transfer during absorption in a metal-hydrogen reactor**. *International Journal of Hydrogen Energy 20*, 1 (1995), 43–52.

[126] AKANJI, O. L., AND KOLESNIKOV, A. V. **Modeling of heat and mass transfer in lani5 matrix during hydrogen absorption-desorption cycle**. *Polish Journal of Chemical Technology 14*, 3 (2012), 71–76.

[127] FRENI, A., CIPITI, F., AND CACCIOLA, G. **Finite element-based simulation of a metal hydride-based hydrogen storage tank**. *International Journal of Hydrogen Energy 34*, 20 (2009), 8574–8582.

[128] JEMNI, A., NASRALLAH, S. B., AND LAMLOUMI, J. **Experimental and theoretical study of ametal–hydrogen reactor**. *International Journal of Hydrogen Energy 24*, 7 (1999), 631–644.

[129] BUSQUÉ, R., TORRES, R., GRAU, J., RODA, V., AND HUSAR, A. **Mathematical modeling, numerical simulation and experimental comparison of the desorption process in a metal hydride hydrogen storage system**. *International Journal of Hydrogen Energy 43*, 35 (2018), 16929–16940.

[130] MINKO, K. B., BOCHARNIKOV, M. S., YANENKO, Y. B., LOTOTSKYY, M. V., KOLESNIKOV, A., AND TARASOV, B. P. **Numerical and experimental study of heat-and-mass transfer processes in two-stage metal hydride hydrogen compressor**. *International Journal of Hydrogen Energy 43*, 48 (2018), 21874–21885.

[131] SOUAHLIA, A., DHAOU, H., ASKRI, F., SOFIENE, M., JEMNI, A., AND NASRALLAH, S. B. **Experimental and comparative study of metal hydride hydrogen tanks**. *international journal of hydrogen energy 36*, 20 (2011), 12918–12922.

[132] CHIBANI, A., BOUGRIOU, C., AND MEROUANI, S. **Simulation of hydrogen absorption/desorption on metal hydride lani5-h2: Mass and heat transfer**. *Applied Thermal Engineering 142* (2018), 110–117.

[133] GUPTA, R. B. **Hydrogen fuel: production, transport, and storage**. CRC press, 2008.

[134] DAVID, E. **An overview of advanced materials for hydrogen storage**. *Journal of materials processing technology 162* (2005), 169–177.

[135] HIROSE, K. **Handbook of hydrogen storage: new materials for future energy storage**. John Wiley & Sons, 2010.

[136] ZÜTTEL, A., REMHOF, A., BORGSCHULTE, A., AND FRIEDRICHS, O. **Hydrogen: the future energy carrier**. *Philosophical Transactions of the Royal Society A: Mathematical, Physical and Engineering Sciences 368*, 1923 (2010), 3329–3342.

[137] WEI, T., LIM, K. L., TSENG, Y., AND CHAN, S. **A review on the characterization of hydrogen in hydrogen storage materials**. *Renewable and Sustainable Energy Reviews 79* (2017), 1122–1133.

[138] WEBB, C., AND GRAY, E. M. **Analysis of uncertainties in gas uptake measurements using the gravimetric method**. *International Journal of Hydrogen Energy 39*, 13 (2014), 7158–7164.

[139] BLACH, T., AND GRAY, E. M. **Sieverts apparatus and methodology for accurate determination of hydrogen uptake by light-atom hosts**. *Journal of Alloys and Compounds 446* (2007), 692–697.

[140] SANDROCK, G. **A panoramic overview of hydrogen storage alloys from a gas reaction point of view**. *Journal of alloys and compounds 293* (1999), 877–888.

[141] GNASER, H. **Sims detection in the 1012 atoms cm-3 range**. *Surface and Interface Analysis: An International Journal devoted to the development and application of techniques for the analysis of surfaces, interfaces and thin films 25*, 10 (1997), 737–740.

[142] LIU, J., ZHENG, Z., CHENG, H., LI, K., YAN, K., HAN, X., WANG, Y., AND LIU, Y. **Long-term hydrogen storage performance and structural evolution of lani4al alloy**. *Journal of Alloys and Compounds 731* (2018), 172–180.

[143] SUZUKI, K., ISHIKAWA, K., AND AOKI, K. **Degradation of lani5 and lani4. 7al0. 3 hydrogen-absorbing alloys by cycling**. *Materials Transactions, JIM 41*, 5 (2000), 581–584.

[144] LOTOTSKYY, M., YARTYS, V., POLLET, B., AND BOWMAN JR, R. **Metal hydride hydrogen compressors: a review**. *International journal of hydrogen energy 39*, 11 (2014), 5818–5851.

[145] WANNER, M., FRIEDLMEIER, G., HOFFMANN, G., AND GROLL, M. **Thermodynamic and structural changes of various intermetallic compounds during extended cycling in closed systems**. *Journal of alloys and compounds 253* (1997), 692–697.

[146] BOWMAN JR, R. C., PAYZANT, E. A., WILSON, P. R., PEARSON, D. P., LEDOVSKIKH, A., DANILOV, D., NOTTEN, P., AN, K., SKORPENSKE, H. D., AND WOOD, D. **Characterization and analyses of degradation and recovery of lani4. 78sn0. 22 hydrides following thermal aging**. *Journal of Alloys and Compounds 580* (2013), S207–S210.

[147] PARK, J.-G., KIM, D.-M., JANG, K.-J., HAN, J.-S., CHO, K., AND LEE, J.-Y. **The intrinsic degradation behavior of (v0. 53ti0. 47) 0.925 fe0. 075 alloy during temperature-induced hydrogen absorption-desorption cycling**. *Journal of alloys and compounds 293* (1999), 150–155.

[148] LIU, J., LI, K., CHENG, H., YAN, K., WANG, Y., LIU, Y., JIN, H., AND ZHENG, Z. **New insights into the hydrogen storage performance degradation and al functioning mechanism of lani5-xalx alloys**. *international journal of hydrogen energy 42*, 39 (2017), 24904–24914.

[149] GOLBEN, M., AND DACOSTA, D. H. **Disproportionation resistant alloy development for hydride hydrogen compression**. In *Proc* (2002), Citeseer.

[150] REITER, J., KARLMANN, P., BOWMAN JR, R., AND PRINA, M. **Performance and degradation of gas-gap heat switches in hydride compressor beds**. *Journal of Alloys and Compounds 446* (2007), 713–717.

[151] LAURENCELLE, F., DEHOUCHE, Z., AND GOYETTE, J. **Hydrogen sorption cycling performance of lani4. 8sn0. 2**. *Journal of alloys and compounds 424*, 1-2 (2006), 266–271.

[152] CHENG, H., YANG, H., LI, S., DENG, X., CHEN, D., AND YANG, K. **Effect of hydrogen absorption/desorption cycling on hydrogen storage performance of lani4. 25al0. 75**. *Journal of Alloys and Compounds 453*, 1-2 (2008), 448–452.

[153] CRIVELLO, J.-C., AND GUPTA, M. **Electronic properties of lani4. 75sn0. 25, lani4. 5m0. 5 (m= si, ge, sn), lani4. 5sn0. 5h5**. *Journal of alloys and compounds 356* (2003), 151–155.

[154] MORADI, R., AND GROTH, K. M. **Hydrogen storage and delivery: review of the state of the art technologies and risk and reliability analysis**. *International Journal of Hydrogen Energy* (2019).

[155] MOHAMMADSHAHI, S., GRAY, E. M., AND WEBB, C. **A review of mathematical modelling of metal-hydride systems for hydrogen storage applications**. *International Journal of Hydrogen Energy 41*, 5 (2016), 3470–3484.

[156] YANG, F., WANG, G., ZHANG, Z., MENG, X., AND RUDOLPH, V. **Design of the metal hydride reactors–a review on the key technical issues**. *International Journal of Hydrogen Energy 35*, 8 (2010), 3832–3840.

[157] TETUKO, A. P., SHABANI, B., OMRANI, R., PAUL, B., AND ANDREWS, J. **Study of a thermal bridging approach using heat pipes for simultaneous fuel cell cooling and metal hydride hydrogen discharge rate enhancement**. *Journal of Power Sources 397* (2018), 177–188.

[158] CHABANE, D., HAREL, F., DJERDIR, A., CANDUSSO, D., ELKEDIM, O., AND FENINECHE, N. **A new method for the characterization of hydrides hydrogen tanks dedicated to automotive applications**. *international journal of hydrogen energy 41*, 27 (2016), 11682–11691.

[159] **http://mobypost-project.eu**.

[160] ZHANG, Y.-C., AND SAKHANENKO, L. **The naive bayes classifier for functional data**. *Statistics & Probability Letters 152* (2019), 137–146.

[161] BAESENS, B., VAN GESTEL, T., VIAENE, S., STEPANOVA, M., SUYKENS, J., AND VANTHIENEN, J. **Benchmarking state-of-the-art classification algorithms for credit scoring**. *Journal of the operational research society 54*, 6 (2003), 627–635.

[162] VAPNIK, V. **The nature of statistical learning theory**. Springer science & business media, 2013.

[163] WIJAYANTA, A. T., NAKASO, K., AOKI, T., KITAZATO, Y., AND FUKAI, J. **Effect of pressure, composition and temperature characteristics on thermal response and overall reaction rates in a metal hydride tank**. *international journal of hydrogen energy 36*, 5 (2011), 3529–3536.

[164] BRIKI, C., BELKHIRIA, S., DHAOU, M. H., ASKRI, F., AND JEMNI, A. **Dynamic study of a new design of a tanks based on metallic hydrides**. *International Journal of Hydrogen Energy 43*, 3 (2018), 1566–1576.

[165] BAO, Z., WU, Z., NYAMSI, S. N., YANG, F., AND ZHANG, Z. **Three-dimensional modeling and sensitivity analysis of multi-tubular metal hydride reactors**. *Applied Thermal Engineering 52*, 1 (2013), 97–108.

[166] CHO, J.-H., YU, S.-S., KIM, M.-Y., KANG, S.-G., LEE, Y.-D., AHN, K.-Y., AND JI, H.-J. **Dynamic modeling and simulation of hydrogen supply capacity from a metal hydride tank**. *international journal of hydrogen energy 38*, 21 (2013), 8813–8828.

[167] KYOUNG, S., FEREKH, S., GWAK, G., JO, A., AND JU, H. **Three-dimensional modeling and simulation of hydrogen desorption in metal hydride hydrogen storage vessels**. *international journal of hydrogen energy 40*, 41 (2015), 14322–14330.

[168] CHABANE, D., HAREL, F., DJERDIR, A., CANDUSSO, D., ELKEDIM, O., AND FENINECHE, N. **Energetic modeling, simulation and experimental of hydrogen desorption in a hydride tank**. *International Journal of Hydrogen Energy 44*, 2 (2019), 1034–1046.

[169] DHAOU, H., ASKRI, F., SALAH, M. B., JEMNI, A., NASRALLAH, S. B., AND LAMLOUMI, J. **Measurement and modelling of kinetics of hydrogen sorption by lani5 and two related pseudobinary compounds**. *International Journal of Hydrogen Energy 32*, 5 (2007), 576–587.

[170] YANG, F., WANG, G., ZHANG, Z., AND RUDOLPH, V. **Investigation on the influences of heat transfer enhancement measures in a thermally driven metal hydride heat pump**. *international journal of hydrogen energy 35*, 18 (2010), 9725–9735.

[171] SHI, Y. **Particle swarm optimization**. *IEEE connections 2*, 1 (2004), 8–13.

[172] MATLAB. **version 9.0 (R2016a)**. The MathWorks Inc., Natick, Massachusetts, 2016.

[173] DEVARAKONDA, M., BROOKS, K., RÖNNEBRO, E., AND RASSAT, S. **Systems modeling, simulation and material operating requirements for chemical hydride based hydrogen storage**. *international journal of hydrogen energy 37*, 3 (2012), 2779–2793.

[174] GAMBINI, M. **Metal hydride energy systems performance evaluation. part a: dynamic analysis model of heat and mass transfer**. *International journal of hydrogen energy 19*, 1 (1994), 67–80.

[175] ASKRI, F., JEMNI, A., AND NASRALLAH, S. B. **Prediction of transient heat and mass transfer in a closed metal–hydrogen reactor**. *International Journal of Hydrogen Energy 29*, 2 (2004), 195–208.

[176] NYAMSI, S. N., YANG, F., AND ZHANG, Z. **An optimization study on the finned tube heat exchanger used in hydride hydrogen storage system–analytical method and numerical simulation**. *international journal of hydrogen energy 37*, 21 (2012), 16078–16092.

[177] SUDA, S., KOBAYASHI, N., AND YOSHIDA, K. **Reaction kinetics of metal hydrides and their mixtures**. *Journal of the Less Common Metals 73*, 1 (1980), 119–126.

[178] LÜ, X., QU, Y., WANG, Y., QIN, C., AND LIU, G. **A comprehensive review on hybrid power system for pemfc-hev: Issues and strategies**. *Energy conversion and management 171* (2018), 1273–1291.

[179] AHMED, N. A. **On-grid hybrid wind/photovoltaic/fuel cell energy system**. In *IPEC, 2012 Conference on Power & Energy* (2012), IEEE, pp. 104–109.

[180] CHAUHAN, A., AND SAINI, R. **A review on integrated renewable energy system based power generation for stand-alone applications: configurations, storage options, sizing methodologies and control**. *Renewable and Sustainable Energy Reviews 38* (2014), 99–120.

[181] MACDONALD, B. D., AND ROWE, A. M. **Impacts of external heat transfer enhancements on metal hydride storage tanks**. *International Journal of Hydrogen Energy 31*, 12 (2006), 1721–1731.

[182] MUTHUKUMAR, P., KUMAR, A., RAJU, N. N., MALLESWARARAO, K., AND RAHMAN, M. M. **A critical review on design aspects and developmental status of metal hydride based thermal machines**. *International Journal of Hydrogen Energy* (2018).

[183] MacDonald, B. D., and Rowe, A. M. **A thermally coupled metal hydride hydrogen storage and fuel cell system**. *Journal of power sources 161*, 1 (2006), 346–355.

[184] Garrier, S., Chaise, A., De Rango, P., Marty, P., Delhomme, B., Fruchart, D., and Miraglia, S. **Mgh2 intermediate scale tank tests under various experimental conditions**. *International Journal of Hydrogen Energy 36*, 16 (2011), 9719–9726.

[185] Lozano, G. A., Ranong, C. N., von Colbe, J. M. B., Bormann, R., Hapke, J., Fieg, G., Klassen, T., and Dornheim, M. **Optimization of hydrogen storage tubular tanks based on light weight hydrides**. *international journal of hydrogen energy 37*, 3 (2012), 2825–2834.

[186] Delhomme, B., De Rango, P., Marty, P., Bacia, M., Zawilski, B., Raufast, C., Miraglia, S., and Fruchart, D. **Large scale magnesium hydride tank coupled with an external heat source**. *International journal of hydrogen energy 37*, 11 (2012), 9103–9111.

[187] Ferekh, S., Gwak, G., Kyoung, S., Kang, H.-g., Chang, M.-h., Yun, S.-h., Oh, Y.-h., Kim, W., Kim, D., Hong, T., and others. **Numerical comparison of heat-fin-and metal-foam-based hydrogen storage beds during hydrogen charging process**. *International Journal of Hydrogen Energy 40*, 42 (2015), 14540–14550.

[188] Anbarasu, S., Muthukumar, P., and Mishra, S. C. **Tests on lmni4. 91sn0. 15 based solid state hydrogen storage device with embedded cooling tubes–part a: Absorption process**. *International Journal of Hydrogen Energy 39*, 7 (2014), 3342–3351.

[189] Ma, J., Wang, Y., Shi, S., Yang, F., Bao, Z., and Zhang, Z. **Optimization of heat transfer device and analysis of heat & mass transfer on the finned multi-tubular metal hydride tank**. *International journal of hydrogen energy 39*, 25 (2014), 13583–13595.

[190] Afzal, M., and Sharma, P. **Design of a large-scale metal hydride based hydrogen storage reactor: Simulation and heat transfer optimization**. *International Journal of Hydrogen Energy 43*, 29 (2018), 13356–13372.

[191] Garrison, S. L., Hardy, B. J., Gorbounov, M. B., Tamburello, D. A., Corgnale, C., Mosher, D. A., Anton, D. L., and others. **Optimization of internal heat exchangers for hydrogen storage tanks utilizing metal hydrides**. *International Journal of Hydrogen Energy 37*, 3 (2012), 2850–2861.

[192] Jiang, Z., Dougal, R. A., Liu, S., Gadre, S. A., Ebner, A. D., and Ritter, J. A. **Simulation of a thermally coupled metal-hydride hydrogen storage and fuel cell system**. *Journal of Power Sources 142*, 1-2 (2005), 92–102.

[193] Tetuko, A. P., Shabani, B., and Andrews, J. **Thermal coupling of pem fuel cell and metal hydride hydrogen storage using heat pipes**. *international journal of hydrogen energy 41*, 7 (2016), 4264–4277.

[194] DHAOU, H., KHEDHER, N. B., MELLOULI, S., SOUAHLIA, A., ASKRI, F., JEMNI, A., AND NASRALLAH, S. B. **Improvement of thermal performance of spiral heat exchanger on hydrogen storage by adding copper fins**. *International Journal of Thermal Sciences 50*, 12 (2011), 2536–2542.

[195] LIU, Z., LI, Y., BU, Q., GUZY, C. J., LI, Q., CHEN, W., AND WANG, C. **Novel fuel cell stack with coupled metal hydride containers**. *Journal of Power Sources 328* (2016), 329–335.

[196] MILED, A., MELLOULI, S., MAAD, H. B., AND ASKRI, F. **Improvement of the performance of metal hydride pump by using phase change heat exchanger**. *International Journal of Hydrogen Energy 42*, 42 (2017), 26343–26361.

[197] ZHOU, D., RAVEY, A., AL-DURRA, A., AND GAO, F. **A comparative study of extremum seeking methods applied to online energy management strategy of fuel cell hybrid electric vehicles**. *Energy conversion and management 151* (2017), 778–790.

[198] LV, C., ZHANG, J., LI, Y., AND YUAN, Y. **Novel control algorithm of braking energy regeneration system for an electric vehicle during safety–critical driving maneuvers**. *Energy conversion and management 106* (2015), 520–529.

[199] KAYA, K., AND HAMES, Y. **Two new control strategies: For hydrogen fuel saving and extend the life cycle in the hydrogen fuel cell vehicles**. *International Journal of Hydrogen Energy* (2019).

[200] (ED.), C. S. **Chapter 3-fuel cell electrochemistry**. *PEM fuel cell modeling and simulation using Matlab* (Academic Press, Burlington (2008)), 49–76.

[201] LI, H., RAVEY, A., N'DIAYE, A., AND DJERDIR, A. **Online adaptive equivalent consumption minimization strategy for fuel cell hybrid electric vehicle considering power sources degradation**. *Energy Conversion and Management 192* (2019), 133–149.

[202] ZHENG, C., OH, C., PARK, Y., AND CHA, S. **Fuel economy evaluation of fuel cell hybrid vehicles based on equivalent fuel consumption**. *International Journal of Hydrogen Energy 37*, 2 (2012), 1790–1796.

[203] LELKES, A., AND BUFE, M. **Bldc motor for fan application with automatically optimized commutation angle**. In *2004 IEEE 35th Annual Power Electronics Specialists Conference (IEEE Cat. No. 04CH37551)* (2004), vol. 3, IEEE, pp. 2277–2281.

[204] SPODARYK, M., SHCHERBAKOVA, L., SAMELJUK, A., WICHSER, A., ZAKAZNOVA-HERZOG, V., HOLZER, M., BRAEM, B., KHYZHUN, O., MAURON, P., REMHOF, A., AND OTHERS. **Description of the capacity degradation mechanism in lani5-based alloy electrodes**. *Journal of Alloys and Compounds 621* (2015), 225–231.

[205] MORDKOVICH, V., KOROSTYSHEVSKY, N., BAYCHTOK, Y. K., MAZUS, E., DUDAKOVA, N., AND MORDOVIN, V. **Degradation of lani5 by thermobaric cycling in hydrogen and hydrogen-nitrogen mixture**. *International Journal of Hydrogen Energy 15*, 10 (1990), 723–726.

[206] USDRIVE. **Fuel cell technical team road map**. *technical document* (2017).

[207] YADAV, M., SAHU, B., GUPTA, B., AND BHATT, S. **Effect of mass flow rate and temperature on the performance of pem fuel cell: an experimental study**. *Int J Curr Eng Technol 3*, 3 (2013), 950.

[208] BASUALDO, M., FEROLDI, D., AND OUTBIB, R. **Pem fuel cells with bio-ethanol processor systems**. *Springer 10* (2011), 978–1.

[209] KLEBANOFF, L., AND KELLER, J. **Final report for the doe metal hydride center of excellence**. *Sandia National Laboratories, Albuquerque, NM, Report No. SAND2012-0786* (2012).

[210] DEPATURE, C., JEMEI, S., BOULON, L., BOUSCAYROL, A., MARX, N., MORANDO, S., AND CASTAINGS, A. **Ieee vts motor vehicles challenge 2017-energy management of a fuel cell/battery vehicle**. In *2016 IEEE Vehicle Power and Propulsion Conference (VPPC)* (2016), IEEE, pp. 1–6.

List of Figures

List of Tables

List of Definitions

Acronyms

EV	Electric vehicle
FCV	Fuel cell vehicle
FCHEV	Fuel cell hybrid electrical vehicle
AFC	Alkaline fuel cell
PAFC	Phosphoric acid fuel cell
MCFC	Molten carbonate fuel cell
SOFC	Solid oxide fuel cell
DMFC	Direct methanol fuel cell
GDL	Gas diffusion layer
IEO	International energy outlook
MOF	Metal organic framework
COF	Covalent organic framework
DOE	Department of energy
PCT	Pressure composition isotherm
SOC	State of charge
SIMS	Secondary ion mass spectrometry
TDS	Thermal desorption spectroscopy
MH	Metal hydride
MHT	Metal hydride tank
PEMFC	Proton exchange membrane fuel cell
NB	Naive Bayes
SVM	Support vector machine
PSO	Practical swarm optimization
LTOC	Long-term operation controller
ECCE	Electrical chain component
FCS	Fuel cell system
ICE	Internal combustion engine
UCS	Ultra capacitor system
FWS	Flywheel system
EMS	Energy management system

ECCE	Electrical chain component
ICE	Internal combustion engine
UCS	Ultra capacitor system
EMS	Energy management system
Symbols	
E_{nernst}	Nernst voltage of fuel cell (V)
F	Faraday constant
α	Change transfer coefficient
R_u	Universal gas constant $(J/molk)$
I_{FC}	Fuel cell current (A)
V_{FC}	Fuel cell voltage (V)
Q_{FC}	Fuel cell heat (w)
P	Pressure (P_a)
ρ^g	Density of gaseous hydrogen (kg/m^3)
ρ_0^s	Density of empty MH (kg/m^3)
ρ_s^s	Density of saturated MH (kg/m^3)
m_w	Circulation water mass flow rate (kg/s)
ε	Porosity of MH
M_{MH}	Molecular weight of MH (g/mol)
C_{ps}	Specific heat of MH $(J/kg/K)$
ΔH	Enthalpy of reaction (J/kg_{H_2})
C_d	Hydrogen desorption rate constant $(1/s)$
E_d	Activation energy for desorption (J/mol)
m_{MH}	Hydrogen Mass flow rate desorbed/absorbed from MH (kg/s)
C_{pw}	Specific heat of circulation water $(J/kg/K)$
M_{MH}	Molecular weight of MH (g/mol)
M_{O_2}	Molecular weight of oxygen (g/mol)
C_{pg}	Specific heat of gaseous hydrogen $(J/kg/K)$
M_{H_2}	Molecular weight of hydrogen (g/mol)
C_{pair}	Specific heat of air $(J/kg/K)$
Subscripts	
eq	Equilibrium
$tank$	MH tank
w	Circulation water
$blower$	Air blower
exc	Heat ex-changer
r	Reference

I

ANNEXES

A

List of publications by the author

Journal:

- Zhu D, Ait-Amirat Y, N'Diaye A, Djerdir A. New dynamic modeling of a real embedded metal hydride hydrogen storage system. International Journal of Hydrogen Energy. 2019 Nov 8; 44(55): 29203-211.
- Zhu D, Ait-Amirat Y, N'Diaye A, Djerdir A. Active thermal management between proton exchange membrane fuel cell and metal hydride hydrogen storage tank considering long-term operation. Energy Conversion and Management. 2019 Dec 15; 202:112187.

International conference:

- D. Zhu, D. Chabane, Y. Ait Amirat, A. N'diaye, A. Djerdir. Estimation of the state of charge of a hydride hydrogen tank for vehicle applications, Vehicle Power and Propulsion Conference (VPPC), 2017 IEEE.
- D. Zhu, Y. Ait Amirat, A. N'diaye, A. Djerdir, Numerical Study of a Metal Hydride Hydrogen Tank Based on Real Operating Data, International Conference on Emerging and Renewable Energy: Generation and Automation (ICEREGA), 2018.
- D. Zhu, Y. Ait Amirat, A. N'diaye, A. Djerdir, Parametric studies of the on board metal hydride hydrogen storage system based on real operating data , 16th International Symposium on Metal-Hydrogen Systems (MH2018), 2018.

Document generated with LaTeX and:
the LaTeX style for PhD Thesis created by S. Galland — http://www.multiagent.fr/ThesisStyle
the tex-upmethodology package suite — http://www.arakhne.org/tex-upmethodology/